Process-based modelling of regional water and energy fluxes taking into account measured neutron intensities by cosmic-ray probes

Roland Baatz

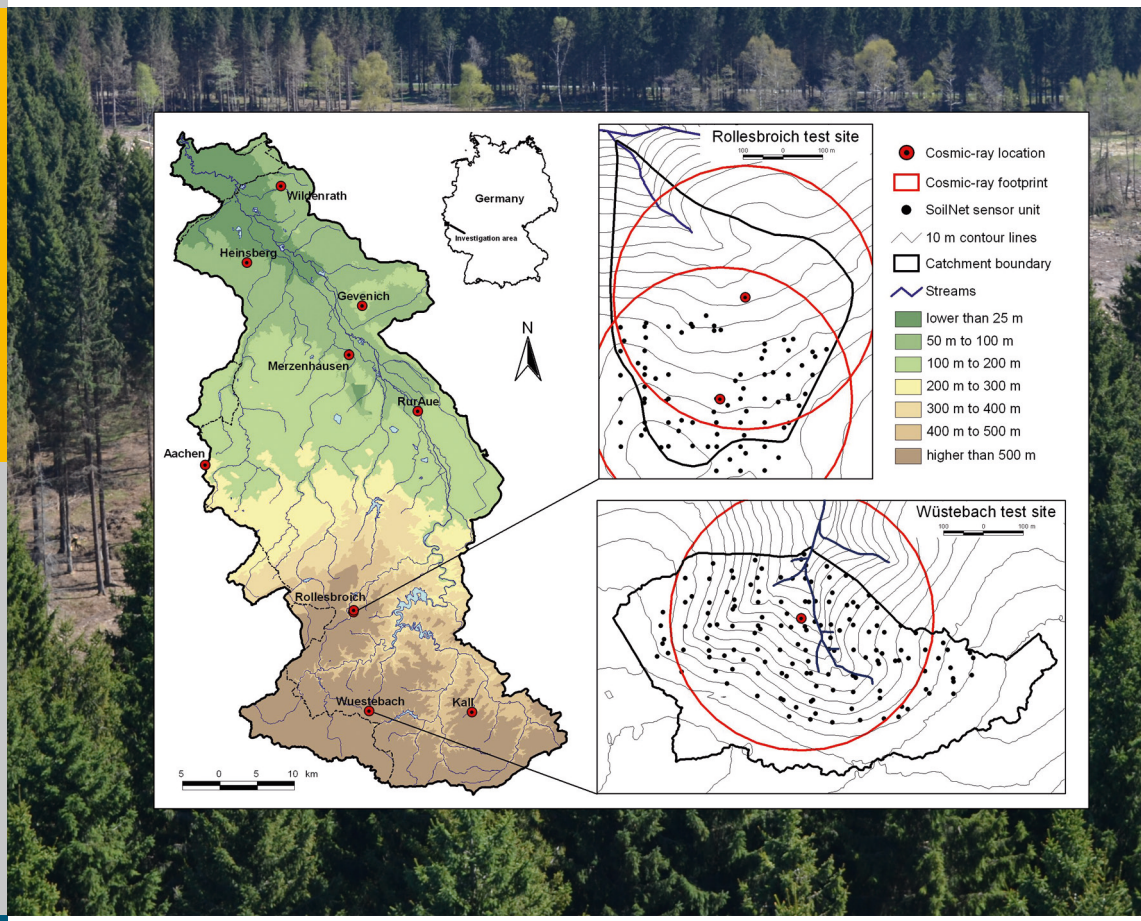

Member of the Helmholtz Association

Energie & Umwelt / Energy & Environment
Band / Volume 362
ISBN 978-3-95806-211-5

JÜLICH FORSCHUNGSZENTRUM

Schriften des Forschungszentrums Jülich
Reihe Energie & Umwelt / Energy & Environment Band / Volume 362

Forschungszentrum Jülich GmbH
Institute of Bio- and Geosciences
Agrosphere (IBG-3)

Process-based modelling of regional water and energy fluxes taking into account measured neutron intensities by cosmic-ray probes

Roland Baatz

Schriften des Forschungszentrums Jülich
Reihe Energie & Umwelt / Energy & Environment Band / Volume 362

ISSN 1866-1793 ISBN 978-3-95806-211-5

Bibliographic information published by the Deutsche Nationalbibliothek.
The Deutsche Nationalbibliothek lists this publication in the Deutsche
Nationalbibliografie; detailed bibliographic data are available in the
Internet at http://dnb.d-nb.de.

Publisher and Distributor: Forschungszentrum Jülich GmbH
Zentralbibliothek
52425 Jülich
Tel: +49 2461 61-5368
Fax: +49 2461 61-6103
Email: zb-publikation@fz-juelich.de
www.fz-juelich.de/zb

Cover Design: Grafische Medien, Forschungszentrum Jülich GmbH

Printer: Grafische Medien, Forschungszentrum Jülich GmbH

Schriften des Forschungszentrums Jülich
Reihe Energie & Umwelt / Energy & Environment, Band / Volume 362

D 82 (Diss. RWTH Aachen University, 2016)

ISSN 1866-1793
ISBN 978-3-95806-211-5

The complete volume is freely available on the Internet on the Jülicher Open Access Server (JuSER)
at www.fz-juelich.de/zb/openaccess.

Contents

Abstract

At the land surface, the hydrologic cycle is strongly linked to soil water content (SWC). Land surface models describe the mass and energy fluxes at the land surface and to the atmosphere with a spatial resolution of a few km^2 at the catchment scale. The calibration and evaluation of land surface models requests observation data, ideally at the same spatial resolution. SWC characterization by model prediction and observation remains a challenge in land surface hydrology. Recently, cosmic-ray probes (CRPs) were developed for continuous passive SWC estimation from neutron flux measurements at a scale relevant for land surface models. One objective of this work was to set up a network of ten CRPs and to evaluate SWC estimates by CRPs. For evaluation, the footprint average SWC of the CRPs was compared to the horizontally and vertically weighted signal of two distributed networks of in-situ SWC sensors. Three different parameterization methods to estimate SWC from neutron flux were compared. Numerical complexity and potential applications distinguish the three parameterization methods. The three parameterization methods resulted in close SWC estimates at the ten study sites although the neutron flux – SWC relationships were slightly different amongst the parameterization methods. SWC estimated by the calibrated CRPs was very close to SWC measured by alternative SWC measurements. Root mean square errors (RMSEs) of the SWC were 0.031 cm^3/cm^3 at the distributed in-situ SWC sensor networks.

The second part of this dissertation focuses on empirically quantifying the impact of aboveground biomass on SWC estimates by CRPs. The footprint average aboveground biomass was estimated for ten calibrated CRPs. The calibration data set of the ten calibrated CRPs was used to derive an empirical correction for the influence of vegetation on neutron flux. The vegetation correction is applied directly on measured neutron flux. Additional field measurements along a strong gradient in biomass were done to evaluate the empirical vegetation correction method. Sensor specific counting efficiency was determined for each CRP and the CRPs were normalized to a standard efficiency. The study found a reduction of 0.9% in fast neutrons per kg of dry above ground biomass per m^2. The empirical vegetation correction was applied successfully to the *hmf*-method and the COSMIC operator, two measurement operators to determine SWC from neutron flux and vice versa. Including the vegetation correction for CRP-based SWC estimates could explain 95% of the measured neutron flux variability compared to 76% if vegetation correction was not included. In future work, the

empirical vegetation correction should be tested also at other CRP networks but sensor specific counting efficiencies needs to be taken into account if more than one individual CRP is used.

In the third part of this dissertation, the benefit of a CRP network for improving the characterization of states and parameters of a land surface model was analyzed. The Community Land Model (CLM) was set up with a regional high resolution (~1km^2) surface and subsurface parameterization. Two soil maps, a regional and a biased soil map were used for the soil texture. The uncertainty of forcing data, soil texture, and organic matter content was characterized by perturbing these input data. CLM was coupled to the COSMIC operator and the Local Ensemble Transform Kalman Filter (LETKF), a sequential data assimilation algorithm. Over a two year period (2011-2012), data of the CRPs were assimilated daily if available for either only state updates or joint state-parameter updates. The third year (2013) served as verification period and no data assimilation was done. Modeled SWC was evaluated against SWC measured by CRPs. Modeled SWC with the regional soil map was already close to observed SWC (RMSE=0.04 cm^3/cm^3). Data assimilation even improved these results in the assimilation period for state (RMSE=0.028 cm^3/cm^3) and joint state-parameter (RMSE=0.028 cm^3/cm^3) updates. Modeled SWC with the biased soil map resulted in higher RMSEs on average. If only states were updated with the biased soil map, SWC characterization improved significantly during the assimilation period (open loop: 0.109 cm^3/cm^3; update: 0.03 cm^3/cm^3), which was also the case for joint state-parameter estimation (update: 0.03 cm^3). During the verification period, joint state-parameter estimation improved SWC if the biased soil map was used as prior information (open loop: 0.115 cm^3/cm^3; update: 0.044 cm^3/cm^3), but not if the regional soil map was used (open loop: 0.041 cm^3/cm^3; update: 0.047 cm^3/cm^3). A second jackknife evaluation was done by assimilating eight CRPs with joint state-parameter updates and using the ninth CRP observations for evaluation. In the evaluation period 2013, eight out of nine CRPs showed improved SWC in case of the biased soil map. In case of the regional soil map, seven out of nine CRPs showed improved SWC compared to open loop SWC. In conclusion, the results suggest that the network of CRPs was suited for improving the characterization of states and parameters of a land surface model by data assimilation, but not in case of a good quality soil map as prior information.

Zusammenfassung

Der hydrologische Kreislauf an der Landoberfläche ist eng mit der Bodenfeuchte (BF) verknüpft. Landoberflächenmodelle (LOM) modellieren die Masse und Energieflüsse an der Landoberfläche mit einer räumlichen Auflösung von wenigen km^2 auf regionaler Ebene. Deren Kalibrierung und Bewertung erfordert Beobachtungsdaten idealerweise in einer ähnlichen räumlichen Auflösung. In dieser Auflösung bleibt Modellierung und Beobachtung von BF eine Herausforderung. Für diesen Zweck wurden vor kurzem Cosmic-Ray Sensoren (CRS) entwickelt, um invers BF auf Basis detektierter Neutronendichte zu bestimmen. Ein Ziel der vorliegenden Arbeit war es ein Netzwerk von CRS aufzubauen und die Messgenauigkeit zu bestimmen. Hierzu wurde an zwei CRS Standorten die gewichtete mittlere BF über die CRS Messfläche (~30 ha) mit Hilfe eines verteilten Bodenfeuchtesensornetzwerkes bestimmt. Die gemittelten BF ergaben eine gute Übereinstimmung zu denen der CRS (mittlere quadratische Abweichung (MQA)=0.030 cm^3/cm^3) an beiden Standorten. Es wurde weiterhin die Güte von drei verschiedenen Parametrisierungen zur Bodenfeuchtebestimmung mit CRS verglichen. Die Methoden unterschieden sich in der numerischen Komplexität und künftige Anwendungsmöglichkeiten. Diese drei Methoden resultierten in leicht unterschiedliche Kalibrierungskurven, welche jedoch den MQA nicht beeinflussten.

Der zweite Teil dieser Arbeit war auf die Ermittlung einer empirischen Korrektur für oberirdische Biomasse fokussiert. Für die zehn kalibrierten CRS wurde die oberirdische Biomasse ermittelt, um den Einfluss von Biomasse auf gemessene Neutronendichte zu quantifizieren und dafür eine geeignete Korrekturmethode zu entwickeln. Zur Evaluierung der Korrektur wurden zusätzliche Messungen mit CRS und einem Bodenfeuchtesensornetzwerk entlang eines starken Biomassegradienten durchgeführt. Es wurde eine Reduktion um 0.9% der Neutronendichte pro kg überirdische Biomasse pro m^2 ermittelt. Weiterhin wurde die Vegetationskorrektur erfolgreich auf die *hmf*-Methode und den COSMIC Operator angewendet, zwei Messoperatoren zur Berechnung von BF von Neutronendichte und vice versa. Unter Einbeziehung der Vegetationskorrektur konnte BF 95% der Variabilität in bemessener Neutronendichte erklären, im Gegensatz zu 76% wenn die Vegetationskorrektur nicht angewendet wurde. In künftigen Projekten könnte die Vegetationskorrektur auch auf andere CRS Netzwerke angewendet werden. Wie diese Studie gezeigt hat ist es hierfür unabdingbar, dass für den sensorabhängigen Zählwirkungsgrad korrigiert wird.

Im dritten Teil dieser Dissertation, wurden die Möglichkeiten untersucht, Zustandsvariablen und Parameter in einem LOM mit der Assimilierung von realen CRS Messdaten zu verbessern. Für das hydrologische Rureinzugsgebiet wurde das Community Land Model (CLM) in einer Auflösung von ~1km^2 aufgesetzt und parametrisiert. Die Bodentextur wurde mit einer regionalen und einer polarisierten Bodenkarte initialisiert. Unsicherheiten in atmosphärischem Antrieb, Bodentextur und Organischem Bodenanteil wurden durch Perturbierung der Eingabedaten charakterisiert. CLM wurde mit dem COSMIC Operator und dem Local Ensemble Transform Kalman Filter (LETKF), einem sequentiellen Datenassimilierungsverfahren, gekoppelt. Es wurden in einigen Experimenten lediglich Zustandsvariablen, in andern zusätzlich Bodenparameter aktualisiert. Daten von CRS wurden über einen Zeitraum von zwei Jahren assimiliert (2011-2012). Anschließend wurde ein drittes Jahr (2013) zur Evaluierung der Parameterabschätzung ohne Assimilierung modelliert. Die modellierte bzw. assimilierte BF wurde mit gemessenen CRS BF (Referenz) verglichen. Die anhand der regionalen Bodenkarte modellierte BF stimmte bereits im Leerlauf (LL) gut mit den beobachteten BF überein (MQF=0.04 cm^3/cm^3). Während der Assimilierungsperiode konnte diese Übereinstimmung noch verbessert werden, sowohl für die Aktualisierung von Zustandsvariablen, als auch für die kombinierte Aktualisierung von Zustandsvariablen und Parametern (beide MQF=0.028 cm^3/cm^3). Der LL mit polarisierter Bodenkarte resultierte in wesentlich höhere Fehlerwerte. Auch diese konnten mit der Aktualisierung von Zustandsvariablen und Parametern (MQF=0.03 cm^3/cm^3) im Vergleich zum Leerlauf (MQF=0.109 cm^3/cm^3) wesentlich verbessert werden. Parameterabschätzung führte auch zu starken Verbesserungen im Evaluierungszeitraum im Falle der polarisierten Bodenkarte (MQF=0.072 cm^3/cm^3 Verbesserung), nicht jedoch im Falle der regionalen Bodenkarte (MQF=-0.006 cm^3/cm^3 Verbesserung). Es wurden weitere 18 Jackknife Evaluierungsläufe durchgeführt, in welcher für beide Bodenkarten jeweils Daten von acht CRS assimiliert wurden und der jeweils neunte CRS zur Evaluierung genutzt wurde. In dem Evaluierungsjahr 2013 zeigten acht von neun Läufen verbesserte BF im Falle der polarisierten Bodenkarte, und sieben von neun Läufen verbesserte BF im Falle der regionalen Bodenkarte. Insgesamt konnte anhand dieser Beispiele gezeigt werden, dass CRS Netzwerke die Verbesserung von Bodenparametern mit Hilfe des LETKF Datenassimilierungsverfahrens ermöglichen. Die Verbesserung wurde nicht nur an den Beobachteten Gitterzellen erbracht, es wurde mit der Jackknife Methode auch gezeigt, dass an unbeobachteten Gitterzellen des Modelles Verbesserungen erreicht werden können. Der LETKF zeigte sich somit geeignet, die Beobachtungen an den einzelnen Punkten auch in den Raum zu übertragen.

List of Figures

List of Tables

List of Acronyms

AGB	Aboveground biomass
BWE	Biomass water equivalent
CLM	Community land mode
COSMIC	Cosmic ray soil moisture interaction code
CRP	Cosmic-ray probe
DREAM	Differential evolution adaptive Metroplois
EMI	Electromagnetic induction
EnKF	Ensemble Kalman filter
ERT	Electrical resisitivity tomography
GPR	Ground penetrating radar
hmf	Hydrogen molar fraction
JULES	Joint UK environment simulator
LETKF	Local ensemble transform Kalman filter
LSM	Land surface model
MAE	Mean absolute error
MCMC	Markov chain monte carlo
MCNPx	Monte carlo neutron particle model
NMDB	Neutron monitor database
PEST	Parameter estimation software
PFT	Plant functional types
RMSE	Root mean squared error
SCE	Shuffled complex evolution
SCE-UA	Shuffled complex evolution Metropolis
SMAP	Soil moisture active passive mission
SWC	Soil water content
TDT	Time domain transmission
VWC	Volumetric water content

1 Introduction

1.1 General context

The global hydrologic cycle is of unchallenged importance to sustain life on Earth and the well-being of mankind. Presently, it is estimated that a total of 73 x 10^3 km^3 water per year is given back to the atmosphere through evapotranspiration over the land surface, 40 x 10^3 km^3 per year runoff is generated while 413 x 10^3 km^3 water per year evaporates from oceans from a total of 486 x 10^3 km^3 precipitation over land and ocean (Dingman 2008). From this quantitative point of view the contribution of soil moisture, the soil water content in the unsaturated zone, is small (<0.009 %) compared to the global water resources (Dingman 2008). Nevertheless, soil moisture is a major variable in the global hydrological cycle governing the link at the land surface between aquifers, vegetation, ecology, and the atmosphere. Amongst other processes, root zone soil moisture controls groundwater recharge (Brutsaert 2005), partitioning of net radiation into latent and sensible heat fluxes (Shukla and Mintz 1982), runoff generation processes after precipitation events (Robinson et al. 2008a; Vereecken et al. 2008), and evapotranspiration during periods of limited soil moisture availability (Denmead and Shaw 1962; Jung et al. 2010). Hence, an improved understanding of the role of soil moisture is compulsory to better quantify hydrologic processes at the land surface. Land Surface Models (LSM) describe the coupled water, energy and bio-geochemical cycles at the land surface and to the atmosphere. Modeling the land surface resolves transport processes of water and energy within soils, the ecosystem and between the land and the atmosphere. Soil water content is an important state variable of LSMs. LSMs can represent the lower boundary condition of atmospheric circulation models and therefore allow estimating for example the intensity of soil moisture-precipitation feedbacks (Eltahir 1998; Koster et al. 2004), and summer climate variability and drought (Oglesby and Erickson 1989; Seneviratne et al. 2006; Sheffield and Wood 2008). Increasing computational capacities lead to higher model resolution of LSMs. In addition, novel emerging observation technologies and increasing amounts of observation data allow for a more precise calibration and evaluation of land surface processes posing new challenges to land surface modeling itself. In this respect, computational parameter estimation techniques that consider observation uncertainties and model uncertainties experience an increasing research interest for model calibration and state estimation. Amongst other observations, soil moisture observations are of

high relevance as a source for hydrologic LSM calibration and validation (Brocca et al. 2012; Koster et al. 2004). Common scales of soil moisture measurements are local scale (several dm^3), field scale (from several tens of m^2 to ha) and regional scale (several km^2) soil moisture observations. The intrinsic characteristic of each method is that the large scale observations ideally represent spatial averages of small scale soil water content while neglecting sub-scale variability. However, the spatial and temporal structure of soil moisture is highly heterogeneous (Vereecken et al. 2014). This poses a challenge to measure soil moisture at the field scale which is the scale relevant for high resolution LSMs. In the following subchapters of the introduction, the most important soil moisture measurements across scales that prevailed cosmic ray soil moisture estimation are briefly outlined. The state of the art of soil moisture measurements is followed by a brief description of the community land model, a LSM, and an introduction to ensemble Kalman filtering. The dissertation's introduction is finalized with naming the research objectives and stating the outline of the dissertation.

1.2 State of the art

1.2.1 Soil water content measurements

The most exact method to determine soil water content of a small sample is gravimetric soil sampling and determining the weight difference between wet and dry soil. For the gravimetric sampling a fixed volume of soil is extracted from the ground, weighed to determine the wet weight, and oven-dried at a fixed temperature of at least 70 degree Celsius for at least 48 hours. When several weighing repetitions show no further weight reduction, the dry weight can be determined. Soil water content can be expressed now as gravimetric soil water content θ_{grav} in g/g:

$$\theta_{grav} = \left(m_{wet} - m_{dry}\right)/m_{dry} \quad (1)$$

where m_{wet} and m_{dry} are the wet and dry mass of soil, respectively, in g. Alternatively, soil water content is expressed as volumetric soil water content θ_{vol} in cm^3/cm^3:

$$\theta_{vol} = \frac{V_{water}}{V_{total}} = \frac{m_{wet} - m_{dry}}{m_{dry}} \times \frac{\rho_{bd}}{\rho_{water}} \quad (2)$$

where V_{water} is the volume occupied by water in cm^3 with respect to the total volume of the sample V_{total} in cm^3, ρ_{water} is the density of water in g/cm^3 and ρ_{bd} is the density of soil in

g/cm^3. Since gravimetric soil sampling is very time consuming, a range of sensors has been developed within the last four decades to measure soil moisture continuously.

1.2.1.1 Local Scale Soil Moisture Measurements

Topp et al. (1980) were pioneers in geophysical soil moisture determination by relating the dielectric conductivity of wet soil to soil water content using time domain reflectometry (TDR) probes. TDR probes use the contrasting high dielectric conductivity of water to the low dielectric conductivity of dry soil to estimate soil water content from empirical equations. TDR probes have a length of several cm and determine soil water content in a volume of a few dm^3. They can be installed at a fixed location in the field or can be used as mobile invasive sensors (Robinson et al. 2003). For these point measurements, alternative sensors were developed which use the surrounding soil as sensor capacitor (Kelleners et al. 2005) or electromagnetic time domain transmission (TDT) sensors which use the water-affected time of an electromagnetic wave to travel a certain soil domain (Blonquist et al. 2005). A large number of point measurements interconnected to a sensor network is able to monitor soil moisture at the field scale or the scale of a small watershed (Robinson et al. 2008a; Rosenbaum et al. 2012). Local soil moisture measurements are advantageous for continuous monitoring of soil moisture in space and time at a high resolution but they are invasive and require considerable maintenance and investment costs (Bogena et al. 2010; Brocca et al. 2012).

1.2.1.2 Field Scale Hydro-geophysical Soil Moisture Measurements

Research interest and advances in hydro-geophysical methods to characterize field scale soil water content (several tens of m^2 or ha) increased in recent years (Robinson et al. 2008b). The three main principles are electromagnetic induction (EMI) (Mcneill 1980), electrical resistivity tomography (ERT) (Kemna et al. 2000) and ground penetrating radar (GPR) (Eppstein and Dougherty 1998). These three techniques have the potential to measure soil moisture on the field scale with a resolution up to several meters (Vereecken et al. 2014). EMI systems use a transmitter to induce a current into the soil which generates two electromagnetic fields in the sub-surface. A receiver measures the electromagnet field as a response showing the apparent

electrical conductivity distribution of the soil. ERT systems consist of at least two electrodes to inject an electric current into the soil (transmitter) and two electrodes to measure the potential difference (receivers). This potential difference represents the apparent electrical conductivity distribution of the soil between transmitter and receiver. Generally, ERT systems consist of several tens of electrodes that are used to measure apparent electric conductivity of a cross section. However, the apparent electrical conductivity does not only depend on soil moisture but also on other soil properties such as clay content, salinity and temperature and their spatial structure (Abdu et al. 2008). High heterogeneity of soil properties makes it challenging to infer soil water content from EMI or ERT measurements alone, because apparent electrical conductivity is a combined signal mainly of these four soil properties (Loke et al. 2013). Similar to TDR, GPR is founded on the electromagnetic wave propagation of soils that is used to determine the dielectric permittivity of the soil. In contrast to TDR, GPR is non-invasive like EMI and GPR. Electromagnetic waves are emitted into the sub-surface by a transmitter and their signal is received by a receiver several meters apart. However, GPR faces several limitations that limit the applicability of GPR for soil moisture estimation on the field scale such as surface roughness, vegetation scattering and elevated clay content (Lambot et al. 2006; Vereecken et al. 2014).

1.2.1.3 Regional scale soil moisture remote sensing

On the regional scale (several km^2) surface soil moisture is frequently estimated by active or passive microwave remote sensing techniques from space. These techniques can determine soil water content for the upper few centimeters of soil. Passive remote sensing instruments are receivers that measure electromagnetic waves emitted by the earth surface. These radiometers can either be mounted on ground, or on vehicles, or can be airborne or satellite based. The spatial resolution of the radiometer increases depending on the sensor mounting height from several m^2 (ground based) to several km^2 (space). The frequency of emitted waves is between 1 and 12 GHz and relates to the backscattering behavior of the dielectric soil properties (Njoku 1977). Under bare or cropped soil conditions it was shown that passive microwave remote sensing can map soil moisture accurately (e.g. Jonard et al. 2011; Wigneron et al. 1995).

However, the emitted signal is strongly influenced by surface roughness, roughness distribution and vegetation. These limitations also exist for soil moisture estimation with active microwave remote sensing techniques (Satalino et al. 2002). Active remote sensing or radar uses an airborne or space borne transmitter that emits an electromagnetic pulse and an antenna to capture the backscattering signal. The backscattering signal relates to the soil roughness and to the dielectric soil permittivity which is linked to soil moisture (Altese et al. 1996; Satalino et al. 2002). Soil roughness varies under bare soil conditions and needs to be determined accurately for soil moisture estimation with radar (Verhoest et al. 2008). Soil moisture determination with radar under vegetation cover is potentially also possible if biomass water content and plant structure is accounted for (Ulaby et al. 1996; Vereecken et al. 2012). The contributions of the different factors soil roughness, vegetation and soil moisture can be decomposed by expensive modeling approaches (e.g. Jagdhuber et al. 2013). Additionally, common single frequency based approaches are being expanded by multi-frequency techniques and show promising results (Reigber et al. 2013).

1.2.1.4 Soil moisture determination with cosmic-ray probes

While a large number of local scale soil moisture measurements may be adequate to represent field scale soil moisture measurements, they are linked to high investment and maintenance cost. In contrast, regional scale soil moisture measurements by remote sensing are too coarse for representing soil moisture at the scale of high resolution LSMs and are prone to vegetation effects. Hydro-geophysical methods were developed for measuring field scale soil water content, but these methods are limited by soil surface roughness, vegetation effects and variable soil texture. A recently emerging observation technology for non-invasive soil moisture estimation is the cosmic-ray probe (CRP) (Desilets et al. 2010; Zreda et al. 2008). CRPs bridge the gap between point scale soil moisture measurements and regional scale remote sensing soil moisture measurements. One advantage of CRPs compared to other hydro-geophysical methods is a higher sensitivity to soil water content but low sensitivity to soil properties of secondary interest while measuring soil water content continuously (resolution of 1 hour or more). The measurement principle of CRPs is based on neutron particle physics. High energetic

primary cosmic rays, mainly protons, enter the Earth's atmosphere from space and are moderated on their trajectory through the atmosphere by terrestrial particles and become high energetic neutrons. At the soil surface, neutrons are moderated to lower energetic neutrons primarily by the presence of water. Hydrogen acts as the most effective neutron moderator amongst all chemical elements because the mass of its atomic nuclei is closest to the mass of a neutron. Hence, the presence of water in the top soil causes the formation of a homogeneous layer of neutrons in the first few meters above the soil surface. The horizontal footprint for soil moisture measurements of a CRP ranges between 130 and 240 meter, and vertically between 15 and 83 cm into the soil depending on soil water content, air humidity, and biomass (Kohli et al. 2015). The setup and footprint of a CRP is illustrated in Figure 1. CRPs continuously measure neutron flux and allow inferring the integral areal average soil water content over the footprint from a single measurement. Temporal resolution (~1 hour or longer) and measurement noise depend on sensor location and sensor size.

Research on the use and accuracy of CRPs increased in recent years. Results of simulations with the extended Monte Carlo Neutron Particle Model (MCNPx) (Pelowitz 2005) suggested that the passive measurement of neutron flux above the soil surface shows a good correlation with soil water content (Zreda et al. 2008). This led to first measurements to test the performance and design of CRPs on a high altitude test site with a dry climate in Tucson, Arizona. It was found that soil water content can be measured with CRPs (Zreda et al. 2008) and a simple shape defining function, the N_0-function, could relate gravimetric soil water content θ_{grav} to corrected neutron flux N in neutrons per hour measured by a CRP (Desilets et al. 2010):

$$\theta_{grav} = 0.0808 \times (N/N_0 - 0.372)^{-1} - 0.115 \quad (3)$$

where N_0 is a site specific time-constant calibration parameter in neutrons per hour under dry soil conditions. However, neutron flux strongly varies also by other factors that need to be corrected for. Correction methods were developed for incoming cosmic ray intensity (Desilets et al. 2006), air pressure (Desilets and Zreda 2003), and air humidity (Rosolem et al. 2013). These first advances were followed by a number of evaluation studies initiated in Germany on a crop field (Villarreyes et al. 2011), in North America on an arid grass land (Franz et al. 2012b) and again in Germany in a dense spruce forest (Bogena et al. 2013), in which CRPs were found to be

capable of monitoring soil water content using the N_0-method. However, evaluation sites were few and two new methods were developed based on simulations with MCNPx, the hydrogen molar fraction method (*hmf*-method) (Franz et al. 2013a) and the COsmic ray Soil Moisture Interaction code (COSMIC) (Shuttleworth et al. 2013). The advances in soil moisture estimation with CRPs lead to the financing and realization of networks of CRPs in North America (Zreda et al. 2012), Germany (Baatz et al. 2014) and Australia (Hawdon et al. 2014). At the beginning of this dissertation, the evaluation of CRP measurement accuracy and the choice of the soil moisture estimation method were questions that needed to be addressed. Further research aimed to quantify the impact of above ground biomass on neutron counts and soil water content, which was first included in the *hmf*-method (Franz et al. 2013a). Franz et al. (2013a) illustrated the beneficial impact of including biomass in the calibration of CRPs using MCNPx simulations, but also pointed out that vegetation distribution is of major importance for parameterizing the impact on expected neutron flux. It was also shown that continuous soil moisture measurements are affected by above ground biomass for maize fields (Franz et al. 2013c). In the context of this dissertation, (Baatz et al. 2015) developed an empirical vegetation correction method for high biomass stands (e.g. forests). However, the quantification of the biomass effects on neutron flux and soil moisture estimates from CRPs are under ongoing investigation.

The advances and accuracy in soil moisture estimation using CRPs led to the application of CRPs in hydrologic models. Shuttleworth et al. (2013) developed the COSMIC operator for reproducing measured neutron flux from modeled vertical soil water content profiles in hydrologic data assimilation frameworks. COSMIC was applied with the Data Assimilation Research Testbed DART (Anderson et al. 2009) for improving soil moisture states in the Noah LSM (Shuttleworth et al. 2013). In addition, the COSMIC operator was applied to inversely determine soil moisture from measured neutron flux (Baatz et al. 2014; Rosolem et al. 2014). Villarreyes et al. (2014) used a Parameter ESTimation software (PEST) for estimating soil hydraulic parameters in the HYDRUS-1D model using CRP soil moisture measurements and the N_0-method. Han et al. (2015) used CRP measurements and the N_0-method in a data assimilation framework for estimating a systematic model forcing bias of the Community Land Model (CLM).

At the moment, applications of CRP measurements to hydrologic models are rare and constrained to single CRPs only. While many hydrologic models and LSMs operate on regional and global scale, the potential of CRP networks for improving spatially distributed LSM states and parameters remains a question for research. The present dissertation addresses this question by assimilating measured CRP data in the community land model, a LSM of the most recent generation.

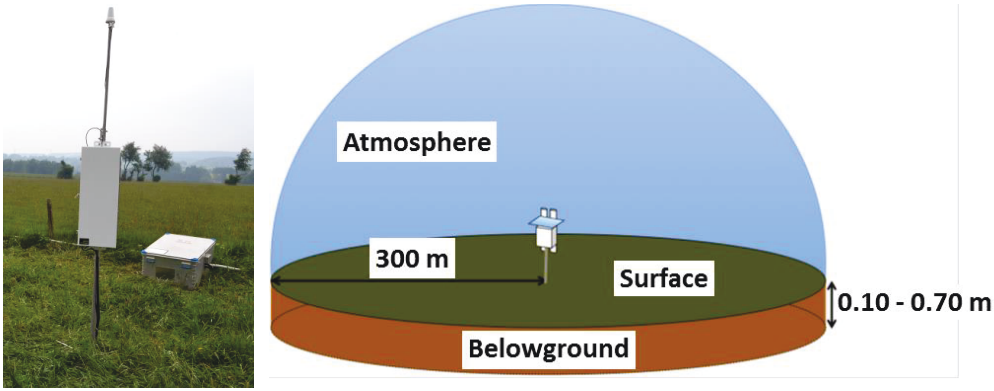

Figure 1: CRP set up at a pole at the Rollesbroich pasture test site (left side), and schematic diagram illustrating a CRP on a pasture, the horizontal footprint in the atmosphere and the vertical footprint in soil (right side, adapted from (Rosolem et al. 2014)).

1.2.2 Community land model

In this dissertation, the Land Surface Model (LSM) of choice is the Community Land Model version 4.5 (CLM). CLM is the land component of the community earth system model (CESM) and the community atmosphere model (CAM) (Oleson et al. 2013). The land component supplies the CESM and the CAM with mass and energy fluxes to the atmospheric component. A first version of a common land model CLM Version 2 was released in 2003 (Dai et al. 2003). From then onwards CLM has improved and expanded its modelling capabilities. It includes biogeophysical and biogeochemical processes, the hydrologic cycle and a dynamic vegetation component (Figure 2). There are a number of LSMs of different complexity: the Noah LSM (Niu et al. 2011; Yang et al. 2011) or the Joint UK Land Environment Simulator (JULES) (Best et al.

2011; Clark et al. 2011) to name a few. Like CLM, these two LSM also include strong capabilities in modeling bio-geochemical processes, mass and energy fluxes within soils as well as to and from the atmosphere. However, one of the differences amongst LSMs is soil depth parameterization. In CLM, Noah and JULES, the depth of the uppermost soil layer in default configuration is 0.7 cm, 10 cm and 30 cm, respectively. CRPs are highly sensitive to surface soil water content distribution of the first few centimeters. Therefore the high resolution of surface soil water content distribution could turn out as a key advantage of CLM when using CLM for assimilating CRP measurements.

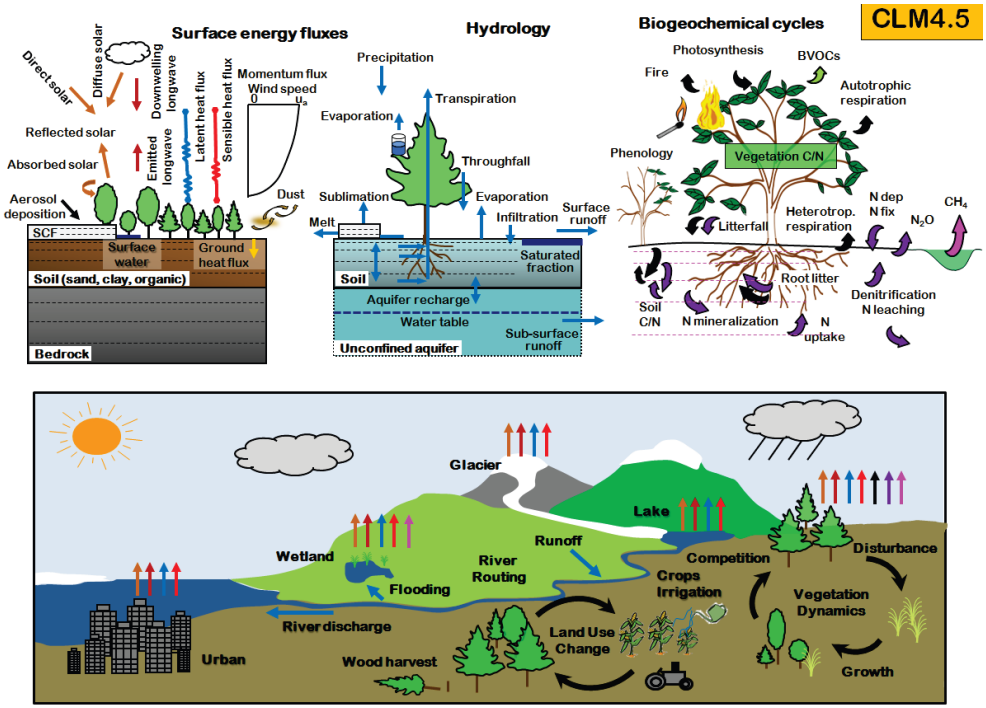

Figure 2: The biogeophysical, biogeochemical, hydrologic and land surface processes modeled by the community land model version 4.5 (adapted from (Oleson et al. 2013)).

In CLM, the land surface of a grid cell is covered by one or more of five major land cover types: vegetated, glacier, lake, urban and wetland. Each of the land cover types possesses its own parameterization scheme. The vegetated land unit is used exclusively in this dissertation

therefore it is described solely here. The vegetated fraction of a grid cell consists of one or more plant functional types (PFTs) (Oleson and Bonan 2000). PFTs are essentially biomes that may co-exist within a single grid cell. There are in total 16 PFTs in CLM plus bare soil: eleven PFTs for different forests, three PFTs for grass lands and two PFTs for crops. PFTs are distinguished by PFT specific physiological and structural parameters: root distribution parameters, optical-, radiation specific-, aerodynamic- and photosynthetic properties. Soil surface mass and energy transport processes to and from the atmosphere are moderated on the PFT level.

The grid cell's sub-surface is modeled by one vertical soil column. The soil columns surface and sub-surface is parameterized by a set of hard coded parameters in the CLM source files and a set of input data. Some relevant input data are: sand and clay content (soil texture), organic matter content, soil color, and maximum fractional saturated area. Some relevant hard coded sub-surface parameters are: max sub-surface drainage, sub-surface drainage decay factor, and overland flow decay factor. The vertical soil column is partitioned into ten permeable soil layers and five impermeable bed rock layers. Layer thickness is calculated by an exponential function and increases from 0.7 cm (layer one) to 2.8 m (layer ten) and even thicker for bed rock. Individual grid cell processes are modeled one-dimensionally in the vertical direction and are unconnected in the horizontal direction.

At the surface, the total net radiation is the sum of incoming shortwave radiation minus outgoing shortwave radiation (reflected solar radiation related to the albedo factor) plus incoming longwave radiation (mainly from water vapor and atmospheric CO_2) minus outgoing shortwave radiation (emitting land according Stefan Boltzmann´s law). The amount of incoming shortwave radiation depends on radiation transport processes such as ground and canopy absorption, reflectance and emittance, and canopy transmittance. Momentum, sensible heat and latent heat fluxes are calculated at the reference height of the atmospheric forcing data based on Monin-Obukhov similarity theory for vegetation and soil surface. At vegetated surfaces, momentum, sensible heat and latent heat fluxes depend on gradients in air temperature and humidity close to the land surface as well as the roughness coefficient. The coupling of vegetation temperature and sensible heat fluxes is solved with Newton-Raphson

iteration. Resulting updates of energy and water states of the upper soil layer are propagated as forcing to the soil for the next time step.

The heat transport in CLM is based on heat conduction in the vertical direction (1D). The heat conducted depends on the spatial temperature gradient times the thermal conductivity of the medium. Based on the law of energy conservation, the 1D continuity equation is solved numerically for the fifteen soil layers with a zero-flux lower boundary condition. The energy transport to and from the atmosphere form the upper boundary condition.

For hydrology, atmospheric precipitation is separated at the top of the canopy into canopy interception and throughfall depending on canopy storage capacity, canopy surface, current canopy water storage, and water fluxes to and from the canopy. Canopy water evaporates or drips onto the soil during the next time step. The grid cell's precipitation on the soil includes the sum of drip water and throughfall of the current time step. Precipitation can result in runoff, surface water storage and infiltration. Grid cell surface runoff is calculated by the fractional saturated area, the overland flow decay factor and water table depth. If the maximum infiltration capacity is exceeded infiltration excess runoff is generated. Infiltration into the soil surface layer forms the upper boundary condition for sub-surface water transport processes. The lower boundary condition depends on the water table depth. Water flow follows the mass conservation principle:

$$\frac{\partial \theta_{vol}}{\partial t} = \frac{\partial q}{\partial z} - Q \qquad 4$$

where the change in volumetric soil water content θ_{vol} in mm^3/mm^3 by time *t* (s) is described as the change of soil water flux *q* in mm/s by soil layer depth *z* in mm. *Q* is a soil water content sink term in s^{-1} (e.g. evapotranspiration by plants through root water update). In CLM, Darcy's law describes the soil water flux *q* by:

$$q = -k \frac{\partial (\psi + z)}{\partial z} \qquad 5$$

where *k* is the hydraulic conductivity in mm/s and ψ is the hydraulic potential in mm. Replacing Darcy's law into equation 4 and assuming *Q* = 0 yields the 1D Richards equation:

$$\frac{\partial \theta_{vol}}{\partial t} = \frac{\partial}{\partial z}\left[k\left(\frac{\partial \theta_{vol}}{\partial z}\frac{\partial \psi}{\partial \theta_{vol}}\right)\right] + 1 \quad 6$$

A slightly modified form of the Richards equation (Zeng and Decker 2009) is solved numerically with a finite-difference scheme. Chapter 4 of this dissertation describes how the soil hydraulic properties like hydraulic conductivity, soil matric potential, the exponent B and porosity are derived from soil texture and organic matter content. Grid cell drainage is calculated by layer from the variable water table depth, the sub-surface drainage decay factor and maximum sub-surface drainage. For a complete technical description of CLM the technical manual of CLM can be consulted (Oleson et al. 2013).

1.2.3 Data assimilation with the ensemble Kalman filter

A general formulation for parameter estimation problems is Bayes Theorem stating that the posterior probability distribution of model states and parameters is proportional to the prior probability distribution of states and parameters times the conditional probability of the measurement data given the prior states and parameters. Growing computational resources allow solving Bayes Theorem by estimating the posterior pdf with Monte Carlo based methods. The Markov Chain Monte Carlo methods (MCMC) (Hastings 1970; Kuczera and Parent 1998; Metropolis et al. 1953) generate a large random sampling space to solve Bayes Theorem without simplifying assumptions. Recently, some efficient MCMC variants were developed: the Shuffled Complex Evolution (SCE) algorithm (Duan et al. 1992), the Shuffled Complex Evolution Metropolis (SCE-UA) algorithm (Vrugt et al. 2003), and the Differential Evolution Adaptive Metropolis (DREAM) algorithm (Vrugt et al. 2009). These methods need a large number of model runs to find optimal parameter sets and to estimate model uncertainty. They are not suited for problems with many unknown parameters like a distributed LSM. A further disadvantage is that they often neglect the uncertainty in model forcing and initial conditions which impact model state and parameter estimates. In contrast, the ensemble Kalman filter propagates a model in time with an ensemble of forcing data from an ensemble of initial conditions of a previous forecast step (Kurtz et al. 2012).

Assuming a normally distributed model and observation error, the Ensemble Kalman Filter (EnKF) (Evensen 1994) is a sequential filter which estimates optimal model states from an ensemble of model runs taking into account parameter uncertainty, forcing uncertainty and measurement uncertainty. Optimal means the minimization of the difference between model states and observations under consideration of both being uncertain and at exactly one point in time. Sequential means that the optimization is done at each succeeding assimilation time step. The EnKF was developed as extension to the Kalman Filter which solves a linear problem based on the assumption of Gaussian distributed process noise (model uncertainty) and observation noise (measurement uncertainty) (Kalman 1960). The EnKF is robust for non-linear model dynamics and quantifies model uncertainty by an ensemble of model realizations with uncertain inputs (Burgers et al. 1998). A state augmentation approach allows the EnKF to update model states and model parameters simultaneously. According to Hendricks Franssen and Kinzelbach (2008), there are at least three approaches to propagate an update from an augmented state vector to the analysis: by a non-iterative (e.g. Chen and Zhang 2006), an iterative (Wen and Chen 2006) and a restart approach (e.g. Gu and Oliver 2007). Alternative techniques for joint state-parameter estimation are particle filters (Montzka et al. 2011; Moradkhani et al. 2005a), and simultaneous optimization and data assimilation (Vrugt et al. 2005).

An EnKF cycle consists of a forecast step and an analysis step which are repeated sequentially each time observations become available. The dimensions that play a role for the EnKF are the number of observations (*nobs*), the ensemble size (*N*), the number of model states (*m*) and the number of parameters updated (*p*). In the forecast step, the model *M* is propagated from time step *t*-1 to timestep *t* when observations become available for assimilation

$$\mathbf{x}_i^t = M(\mathbf{x}_i^{t-1}) \quad 7$$

where $\mathbf{x}_i^t \in \mathbb{R}^m$ is the model state vector for the realization *i* at the time of assimilation and $\mathbf{x}_i^{t-1} \in \mathbb{R}^m$ the model state vector at the previous time step. At the timestep *t*, the model covariance $\mathbf{P}^f \in \mathbb{R}^{m \times N}$ is determined from the ensemble of model state vectors

$$\mathbf{P}^f = \frac{1}{N-1}\sum_{i=1}^{N}(\mathbf{x}_i^t - \bar{\mathbf{x}}^t)(\mathbf{x}_i^t - \bar{\mathbf{x}}^t)^T \quad 8$$

where *f* marks the prior, forecasted, model covariance matrix $\mathbf{P}^f$, $\mathbf{x}_i^t$ the model state of a single realization and $\bar{\mathbf{x}}^t \in \mathbb{R}^m$ is the mean of the model states over all realizations. This equation stresses the importance of a good prior ensemble model state estimate, as the successive calculations depend on the spread of model realizations and the mean of model state realizations as best prior estimate. The model states are related or mapped to the available observations at time *t* using the measurement matrix **H** $\in \mathbb{R}^{nobs \times m}$

$$\hat{\mathbf{x}}_i^t = \mathbf{H}\mathbf{x}_i^t \tag{9}$$

where $\hat{\mathbf{x}}_i^t$ is the mapped model state vector. The observation error ε is specified by the modeler, and used to perturb the observations with Gaussian random noise $\varepsilon = N(0, \sigma)$ with mean zero and the measurement standard deviation σ:

$$\mathbf{y}_i^t = \mathbf{y}^t + \boldsymbol{\varepsilon}_i \tag{10}$$

Where $\mathbf{y}^t \in \mathbb{R}^{nobs}$ is the vector containing the observations, $\boldsymbol{\varepsilon}_i \in \mathbb{R}^{nobs}$ is the vector with perturbations for each observation, and $\mathbf{y}_i^t$ is the perturbed observation for realization *i*. The observation error covariance matrix $\mathbf{R}^t \in \mathbb{R}^{nobs \times nobs}$ is calculated analogue to (8) with

$$\mathbf{R}^t = \frac{1}{N-1}\sum_{i=1}^{N} \boldsymbol{\varepsilon}_i \boldsymbol{\varepsilon}_i^T \tag{11}$$

This allows to deduce the Kalman gain **K** $\in \mathbb{R}^{m \times nobs}$ from model forecast error covariance $\mathbf{P}^f$, measurement error covariance **R** and the measurement matrix **H** with

$$\mathbf{K} = \mathbf{P}^f\mathbf{H}^{\mathrm{T}}(\mathbf{H}\mathbf{P}^f\mathbf{H}^{\mathrm{T}} + \mathbf{R}^t)^{-\mathbf{1}} \tag{12}$$

where $^{-1}$ indicates the inversion of a matrix and $^{\mathrm{T}}$ indicates matrix transposition. Consequently, the Kalman gain accounts for the weighting of model errors versus observation errors, taking into account the spatial correlation of model states and therefore the spatial influence function of observations. The Kalman gain $\mathbf{K}$ is used in the analysis step to calculate the state analysis by weighting the observations $\mathbf{y}_i^t$ and the model state forecast $\mathbf{x}_i^f$ for each realization *i* as in

$$\mathbf{x}_i^a = \mathbf{x}_i^f + \mathbf{K}\left(\mathbf{y}_i^t - \mathbf{H}\mathbf{x}_i^f\right) \tag{13}$$

which can be rewritten as

$$\mathbf{x}_i^a = (1 - \mathbf{K}\mathbf{H})\mathbf{x}_i^f + \mathbf{K}(\mathbf{y}_i^t) \tag{14}$$

where the model state analysis $\mathbf{x}_i^a \in \mathbb{R}^m$ is more clearly expressed as weighted average of model state forecast and observation. The difference between state analysis and model state

forecast is called increment and the difference between observation and model state forecast is called innovation. The model *M* is propagated forward in time with the model state analysis $\mathbf{x}_i^a$ until the next observation becomes available.

Parameters can be optimally updated with the EnKF using a state augmentation approach (e.g. Annan and Hargreaves 2004; Chen and Zhang 2006; Hendricks Franssen and Kinzelbach 2008; Zupanski and Zupanski 2006). For state augmentation, the model state forecast vector is extended by the parameter vector to form a new augmented state vector $\mathbf{x}_i^t$

$$\mathbf{x}_i^t = \begin{Bmatrix} \mathbf{x}_s^t \\ \mathbf{x}_p^t \end{Bmatrix} \quad 15$$

where $\mathbf{x}_s^t \in \mathbb{R}^m$ is the model state vector and $\mathbf{x}_p^t \in \mathbb{R}^p$ is the parameter vector. Equations 7-14 need to be modified accordingly to include model parameters in calculation of the model error covariance matrix $\mathbf{P}^f$, the measurement matrix **H**, the Kalman gain **K** and finally the updated state-parameter vector $\mathbf{x}_i^a$. The Kalman gain than weights also the parameter space vector so that the augmented analysis includes model states and model parameters. Studies on joint state-parameter estimation in LSMs with an EnKF variant are limited, particularly with real data. This dissertation presents a study on the potential of the local ensemble transform Kalman filter, an EnKF variant, in improving sub-surface states and parameters of a regional high resolution LSM using real data of a novel cosmic-ray soil moisture observation network.

1.3 Research objectives

Cosmic-ray probes (CRPs) are particularly promising for updating soil moisture states and sub-surface parameters of the Community Land Model (CLM). Yet, CRPs are a novel observation technology that was tested at few locations only. The first research objective is therefore to evaluate CRP measurements against alternative soil moisture measurements. It is tested whether the promising characteristics of CRPs documented in earlier studies are also valid for field experiments in the moist temperate climate of Central Europe, Germany. The pre-installed distributed soil moisture sensor networks at Wuestebach (Rosenbaum et al. 2012) and Rollesbroich (Qu et al. 2014) are used for evaluation and validation of the CRP footprint and measurement accuracy. Hydrogen in biomass can have a significant contribution to the total

signal of a CRP. A second challenge facing the application of CRPs and a second objective of this work is to determine the influence of biomass on the CRP signal. Biomass changes within a CRP footprint occur on pasture land with regular mowing and hay extraction activities, at agricultural sites with crop cycling, and where woody biomass is removed. Therefore the quantification of the contribution that biomass may have to the CRP signal and to soil moisture estimation by CRPs is of high importance. Once the accuracy of soil moisture estimates from CRPs has been evaluated, and sources of errors such as biomass changes are quantified, CRP measurements are ready to be used in CLM for data assimilation experiments. The third objective of this work is to investigate the potential of CRPs for improving model state estimation and sub-surface parameter characterization of a LSM. The study is carried out with real data. The measurement operator is to be evaluated with alternative soil moisture measurements and against other possible measurement operators. A regional LSM of the Rur catchment is set up with regional model parameterization and real atmospheric high resolution forcing data. A data assimilation framework that has been developed, and tested previously in synthetic test cases (Han et al. 2014; Han et al. 2015) is then applied with real measurements to evaluate how real CRP measurements can improve model states and model parameters in a data assimilation framework. Regarding LSMs, the results of this study point to opportunities, limitations and challenges for the use of CRPs as a new measurement device for providing data to condition LSMs.

1.4 Outline

The dissertation is structured in five chapters. In Chapter 2, the measurement accuracy of soil moisture estimates from cosmic-ray probes (CRPs) is evaluated. The setup of a network of ten CRPs in the Rur catchment in western Germany is outlined. Soil moisture is determined at all sites continuously in time from corrected neutron flux measurements using three different parameterization methods. Soil water content from CRP measurements is evaluated at two sites against soil water content measurements made by a distributed sensor network. Further evaluation measurements were made at five sites. In Chapter 3, the impact of biomass within the CRP footprint on neutron flux and soil water content estimation is quantified empirically. Calibration results of sixteen CRP calibration campaigns are analyzed towards the influence of

biomass on the neutron flux signal. An empirical correction method is developed that allows to correct CRP measurements for changes of biomass within the CRP footprint. Changes of biomass may occur in case of moving CRPs over large areas for areal soil water content quantification or in case of calibrated CRPs when biomass is removed from or added to the footprint. The empirical vegetation correction aims for high biomass stands where biomass impacts are most prominent. The vegetation correction can be applied with either of the three available soil moisture estimation methods known for CRPs. In Chapter 4, the value of CRPs for improving soil moisture states and parameter estimation in the community land model version 4.5 (CLM), a LSM, is explored. The regional CLM is set up with regional parameterization and high resolution atmospheric forcing data. Data of nine CRPs are assimilated over a period of almost two years, followed by a one year evaluation period. Soil moisture states and parameters are evaluated over the total simulation period at the nine CRP sites. Spatial parameter estimation is evaluated with additional simulations where data of eight CRPs are assimilated and the data of the ninth CRP are used for evaluation. In the last Chapter, the results of this dissertation are summarized and perspectives are drawn towards future research directions.

2 Calibration and evaluation of a cosmic-ray probe network*

2.1 Introduction

Soil water content is a key variable in the global hydrologic cycle. Important hydrologic processes such as evapotranspiration are controlled by root zone soil water content in case of water limitation (Denmead and Shaw 1962; Jung et al. 2010). This is generally the case in (semi-)arid environments and may also occur in temperate regions during summer time. Therefore, agricultural production can be limited by soil water availability, which raises the need for irrigation in large parts of the world to sustain food supply (Siebert et al. 2005). Furthermore, climate and weather conditions are influenced by mass and energy fluxes between the land surface and the atmosphere (Shukla and Mintz 1982). To better understand hydrologic processes on relevant scales, soil water content measurements are important for validating and calibrating hydrologic models (Brocca et al. 2012), and land surface and climate models (Koster et al. 2004). Recent publications emphasize the need for soil water content measurements at the field scale to derive process variables and parameters (Crow et al. 2012; Vereecken et al. 2008). However, high spatial variability and temporal dynamics of soil water content pose a challenge for soil water content measurements at relevant scales.

Current state-of-the-art methods for soil water content measurements include point measurements using electromagnetic sensors or gravimetric sampling, sensor networks, geophysical measurements, and air- and space-borne remote sensing (Vereecken et al. 2008). The main limitation of electromagnetic soil water content sensors and gravimetric sampling is that they only provide information for a small volume of soil (~ 10^{-3} m^3). Given the high spatial variability of soil water content, a large number of point measurements is required to provide wireless sensor networks were developed that allow continuous monitoring of soil water adequate information on soil water content at larger scales (Crow et al. 2012). Therefore, content at a large number of locations (Bogena et al. 2010; Dorigo et al. 2011; Schaefer et al. 2007). Although sensor networks achieve a high temporal resolution, the spatial extent of sensor networks is still relatively small (< 1 km^2).

*adapted from: Baatz, R., Bogena, H.R., Hendricks Franssen, H.-J., Huisman, J.A., Qu, W., Montzka, C., and Vereecken, H. (2014), Calibration of a catchment scale cosmic-ray probe network: A comparison of three parameterization methods. Journal of Hydrology, doi:10.1016/j.jhydrol.2014.02.026.

Soil water content derived from space-borne remote sensing techniques is based on the use of active and passive microwave sensors with the advantage of global coverage (Kerr 2007). However, L-band passive microwave sensors (e.g. Soil Moisture and Ocean Salinity satellite (SMOS)) are only sensitive to soil water content of the upper few cm of the soil, and additional information on vegetation characteristics and surface roughness is needed to estimate soil water content from measured brightness temperature (Kerr et al. 2012). C-band active microwave measurements have an even smaller penetration depth and are strongly affected by vegetation and surface roughness (Jackson and Schmugge 1989). The accuracy of future soil water content products of the upcoming Soil Moisture Active Passive Mission (SMAP) will also be limited by vegetation cover, and may also suffer from radio frequency interference (Entekhabi et al. 2010).

Geophysical techniques, such as ground penetrating radar (Eppstein and Dougherty 1998; Huisman et al. 2003) and electromagnetic induction (Akbar et al. 2005; Sheets and Hendrickx 1995), show promising results to overcome the existing gap between continuous point measurements in time and temporally sparse but global remote sensing data (Robinson et al. 2008b), although they are labor-intensive when large-scale surveys (> 1 km^2) are required.

Recently, passive neutron sensors, so called cosmic-ray probes (CRP), were proposed to measure soil water content at the field scale (Zreda et al. 2008). The general measurement principle is similar to that of active neutron probes. Soil water content monitoring using passive neutron probes relies on the determination of the time-variable fast neutron flux near the earth surface. High energy protons from space, or primary cosmic rays, serve as natural radiation source. Proton interaction in the Earth's atmosphere with terrestrial atoms produces high energy neutrons, so called secondary cosmic rays. Subsequent collision and moderation of secondary cosmic rays with terrestrial nuclei produces fast neutrons in the atmosphere. Only fast neutrons are then effectively moderated and absorbed by hydrogen. Therefore, the fast neutron flux shows a strong inverse correlation with the abundance of hydrogen atoms in the upper soil layer and thus can be used to determine soil water content (Zreda et al., 2008). The most attractive feature of the CRP is the relatively large measurement volume. Because of the

large mean free path in air traveled by fast neutrons before collisions, the horizontal footprint has an approximate radius of about 300 meters around the CRP at sea level or somewhat less depending on air density (Desilets and Zreda 2013). The effective measurement depth varies as a function of soil water content between ~12 cm for moist soils up to 70 cm for dry soils (Franz et al. 2012b).

Recently, the use of CRPs for soil water content sensing has increased considerably. Several methods are now available to estimate soil water content from the fast neutron flux: i) a site-specific shape-defining function (N_0-method) (Desilets et al. 2010), ii) a universal calibration function (*hmf*-method) (Franz et al. 2013a) and iii) a COsmic-ray Soil Moisture Interaction Code (COSMIC operator) (Shuttleworth et al. 2013). All three parameterization methods were calibrated with the Monte Carlo Neutron-Particle eXtended model (MCNPx) (Pelowitz 2005). The MCNPx model is a state-of-the-art particle transport model developed mainly at the Los Alamos National Laboratory. The site-specific N_0-method is the computationally simplest method requiring only one parameter for soil water content estimation. However, it requires intensive soil sampling for the parameter estimation. The universal calibration function was developed to overcome the necessity of local calibration campaigns in case of logistic or practical difficulties. However, bulk density, lattice water and aboveground biomass need to be measured or derived from maps, if these variables cannot be measured directly within the footprint. The COSMIC operator was developed to reproduce the time-costly modeling of neutron soil water interaction processes with the MCNPx code. The COSMIC code also requires site-specific calibration of three parameters. Inputs and calibration are therefore similar to the N_0-method.

All three methods are parameterized based on an imperfect representation of reality in the MCNPx model, and are, therefore, subject to uncertainties in user-defined model parameterization, initial and boundary conditions. It has also been reported that the three methods differ in how neutron detection by the CRP is modelled. Initial modelling work assumed that only fast neutrons are detected by the polyethylene-shielded detector. However, very recently it was realized that a larger part of the detected neutrons (about 30 %) may also

come from the thermal energy range (D. Desilets and T.E. Franz, personal communication). Documentation of these aspects is limited in previous publications and can therefore not be analyzed in further detail in this paper. Clearly, the availability of three different methods to estimate soil water content from cosmic-ray probe (CRP) measurements raises the question how well each of the three parameterization methods performs under various soil, meteorological, and vegetation conditions.

Within this context, the main objective of this study is to compare the three available methods of soil water content determination from CRP measurements at several test sites against independent in-situ soil water content measurements. The test sites are located in the Rur catchment in western Germany and are part of the Terrestrial Environmental Observatories (TERENO) infrastructure (Zacharias et al. 2011). The test sites are particularly well suited for an inter-comparison study because of their low altitude and the fact that they are located close together within 0.63 degree latitude. Additionally, the test sites have different types of vegetation cover, a wide range in mean annual precipitation (from 743 to 1401 mm), and two of the test sites are equipped with distributed in-situ soil water content sensor networks. Two of the parameterization methods (*hmf*-method and the COSMIC operator) were developed to reproduce measured neutron flux data from measured soil water content (Franz et al. 2013a; Shuttleworth et al. 2013). In this study, these two methods are used inversely for soil water content determination along with the N_0-method. Repeated gravimetric in-situ sampling campaigns and the two distributed sensor networks are used to evaluate the reliability of the three methods.

2.2 Materials and methods

2.2.1 Site description and instrumentation

The Rur catchment is situated in western Germany and covers an area of 2354 km² (Figure 3). It is part of the TERENO project that established four terrestrial observatories in Germany (Bogena et al. 2012; Zacharias et al. 2011). The Rur catchment exhibits distinct gradients in topography, land use, and climate. The elevation ranges from 15 m in the lowland region in the North up to 690 m in the hilly region in the South. The lowland region is characterized by intensive

agriculture, whereas the southern part is mainly covered by forest and grassland. The total land use distribution in the catchment is 14% coniferous forest, 17% deciduous forest, 32% grassland, and 34% crop land (mainly wheat, maize, sugar beet and barley). In the northern part of the Rur catchment, the mean annual precipitation and potential evapotranspiration are about 700 mm and 600 mm, respectively. At the higher altitudes in the southern part of the catchment, mean annual precipitation increases to 1200 mm and the potential evapotranspiration decreases to less than 500 mm (Bogena et al. 2005).

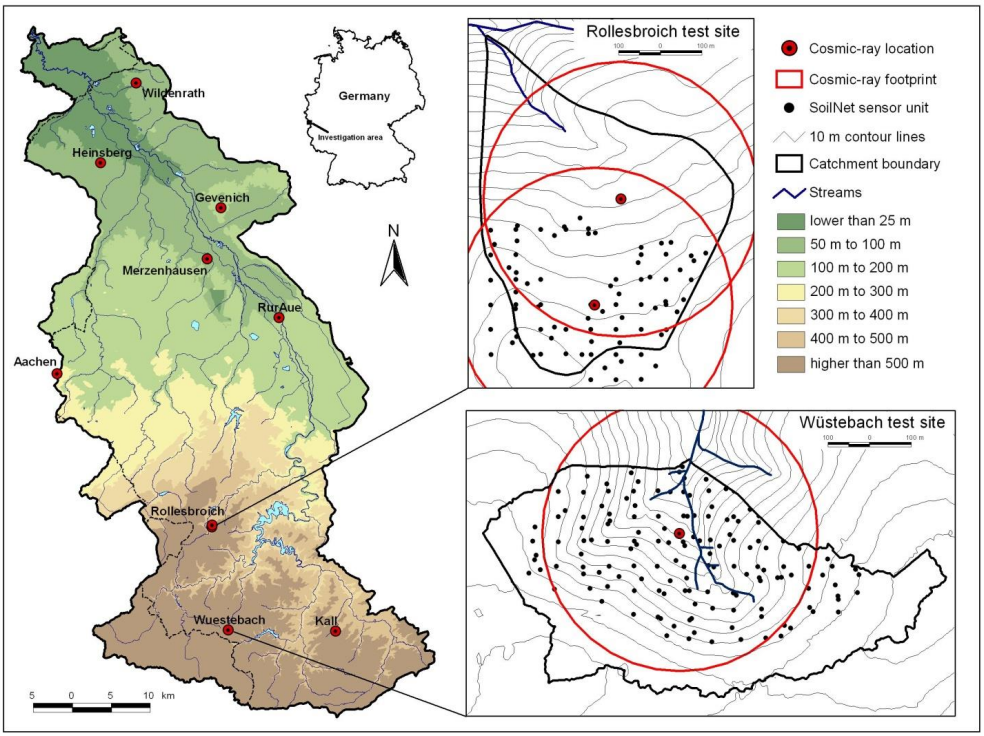

Figure 3: Locations of the ten CRPs installed in the Rur catchment (left), setup of the Rollesbroich test site (upper right) and the Wuestebach test site (lower right panel) with the SoilNet sensor units.

Ten cosmic-ray probes (type CRS1000, HydroInnova LLC, 2009) were installed in the Rur catchment at a height of 1.5 meters (Figure 4). Five probes are equipped with two neutron detectors to measure neutron flux at two different energy levels (epithermal and fast neutron

counters), whereas the other CRPs solely measure fast neutrons. Neutrons are detected by ^{3}He filled tubes (diameter = 3 cm; length = 30 cm). A neutron colliding with ^{3}He in these tubes produces charged particles that trigger ionization processes and electronic pulses that can be detected by a connected pulse module. Pulses are counted over an hourly interval and sent remotely to a database (Zreda et al. 2012).

Figure 4: Cosmic-ray probe located at the test site Rollesbroich is shown with the slow (white, dashed) and fast (white) neutron counter with the pulse modules on top.

The CRPs were installed between February 1st, 2011 and May 22nd, 2012. Altitudes of the measurement sites range between 51 and 627 m asl. The sites Gevenich, Merzenhausen,

Rollesbroich, RollesbroichN, Rur Aue, Wildenrath and Wuestebach are additionally equipped with a Vaisala Weather Transmitter WXT520 (Vaisala, 2010) to monitor air humidity, air temperature and air pressure at 2.0 m height. Table 1 provides more information on the different locations. All land use types within the catchment are represented by the CRP network. Table 2 lists the main land use fractions within the CRP footprints. The land use fractions were determined from a 15 m resolution land use map (Waldhoff 2012) assuming a horizontal footprint with a radius of 300 m for the CRP.

Table 1: Site characteristics of the ten CRPs installed in the Rur catchment (annual average temperature (T_{AV}) and annual average precipitation (P_{AV})).

	Latitude	Longitude	Start of	Altitude	T_{AV}	P_{AV}
			measurement	m asl	°C	m
Aachen	50.798550 N	6.024716 E	13/01/2012	232	9.94	952
Gevenich	50.989220 N	6.323550 E	07/07/2011	108	10.16	884
Heinsberg	51.041104 N	6.104238 E	09/09/2011	57	10.25	814
Kall	50.501332 N	6.526450 E	15/09/2011	504	7.71	935
Merzenhausen	50.930325 N	6.297468 E	19/05/2011	94	10.22	825
Rollesbroich	50.621911 N	6.304241 E	19/05/2011	515	7.88	1307
RollesbroichN	50.624190 N	6.305142 E	22/05/2012	506	7.91	1309
RurAue	50.862329 N	6.427335 E	08/11/2011	102	10.13	743
Wildenrath	51.132744 N	6.169175 E	07/05/2012	76	10.28	856
Wuestebach	50.503487 N	6.333017 E	01/02/2011	605	7.47	1401

Table 2: Land use fractions at the ten sites within the CRP footprint.

	Grassland [%]	Crops [%]	Coniferous forest [%]	Deciduous forest [%]	Water body [%]	Urban [%]
Aachen	19	72	0	0	0	9
Gevenich	0	85	0	0	0	15
Heinsberg	35	39	0	2	0	24
Kall	72	11	0	0	0	17
Merzenhausen	1	82	0	0	0	16
Rollesbroich	92	0	0	0	0	8
RollesbroichN	87	0	0	0	0	12
RurAue	58	25	0	10	1	6
Wildenrath	3	7	54	34	0	2
Wuestebach	7	0	92	1	0	0

The grassland test site Rollesbroich and the forest test site Wuestebach are equipped with in-situ distributed soil water content sensor networks (SoilNet) developed at the Forschungszentrum Jülich GmbH. At Wuestebach (Figure 3), the SoilNet consists of 600 ECHO2O EC-5 and 300 ECHO2O 5TE sensors at depths of 5, 20 and 50 cm and installation was completed in August 2009 (Bogena et al. 2010). These sensors were evaluated and calibrated in earlier studies and the accuracy of the sensors was quantified with a RMSE of ≤ 0.02 cm^3 cm^{-3} (Rosenbaum et al. 2010; Rosenbaum et al. 2012). Dry aboveground biomass at the Wuestebach site was estimated using allometric functions by Etmann (2009). She found a dry above ground biomass of 30 kg m^{-2}, which consisted mainly of Norway Spruce (Picea abies L.) with an age of more than 60 years. Precipitation is monitored at the nearby weather station Kalterherberg by the German Weather Service. In contrast to the previous study on the Wuestebach catchment by Bogena et al. (2013), we neglect the presence of the litter layer in the analysis. In our approach, we used only in-situ calibration by gravimetric samples while in the paper of Bogena et al. (2013) a one-dimensional soil hydraulic model was used to account for the influence of water dynamics in the litter layer on neutron count rates. At Rollesbroich (Figure 3), 504 SPADE sensors were installed in May 2011 to measure soil water content at depths of 5, 20 and 50 cm (Qu et al. 2013). The sensors were calibrated using laboratory measurements (Qu et al. 2013). The grassland fields belong to several farmers and are mowed two or three times per year

between May and November. Precipitation is measured on site by tipping buckets operated in the vicinity of the CRP.

2.2.2 Corrections of neutron counts

Neutron flux was corrected for each sensor to account for environmental and technical issues that are independent from the hydrogen content within the footprint. Measurements acquired with voltages below 11 V were also removed to maintain a stable sensor counting efficiency. Neutron flux is strongly dependent on atmospheric pressure (Desilets et al. 2006). Therefore, neutron count rates in the Rur catchment were normalized to standard atmospheric pressure at sea level P_{ref} = 1013.25 hPa using:

$$N_p = N_{raw} \times exp\left[\beta \times (P - P_{ref})\right] \quad 16$$

where pressure-corrected neutron flux N_p was calculated from measured uncorrected neutron flux N_{raw}, measured atmospheric pressure P [hPa], and the barometric pressure coefficient β = 0.0076 hPa^{-1}.

The secondary cosmic ray intensity at the earth surface also depends on incoming primary cosmic ray intensity (Desilets and Zreda 2001). Therefore, pressure and efficiency corrected incoming primary cosmic ray intensity provided by the Neutron Monitor Database (NMDB) was used to correct for this effect. The stations Kiel (KIEL) located in northern Germany and Jungfraujoch (JUNG) located in Switzerland were used to normalize all CRPs to a reference incoming cosmic ray intensity I_{ref} as follows (Zreda et al. 2012):

$$N_{pi} = N_p \times \left(I_{ref}/I\right) \quad 17$$

where I is incoming cosmic ray intensity, N_p is pressure corrected neutron flux, and N_{pi} is pressure and incoming cosmic ray intensity corrected neutron flux. Both stations have data gaps for our study period, and relative differences of both stations match closely. Therefore, we decided to use the average of both stations to correct neutron flux using Eq. 17.

Measured neutron flux is also affected by absolute atmospheric water vapor content (Rosolem et al. 2013). Neutron flux is normalized to fixed reference water vapor content with:

$$N_{pih} = N_{pi} \times \left[1.0 + 0.0054 \times \left(\rho_{wv} - \rho_{ref}\right)\right] \quad 18$$

where N_{pih} is neutron flux corrected for pressure, incoming cosmic ray intensity and water vapor, ρ_{wv} is measured water vapor content [g m^{-3}] and $\rho_{ref} = 0$ g m^{-3} is reference water vapor content. Water vapor content is measured at all locations and was interpolated for times when no data was available. Hereafter, the terminology "measured neutron flux" refers to the neutron flux that was corrected for pressure, incoming cosmic ray and air humidity.

2.2.3 Measurement support volume

The effective measurement support volume is defined as the volume from where 86% of the detected neutrons originate (Zreda et al., 2008). For this study, we assume a horizontal footprint with a radius of 300 m around the CRP (Desilets and Zreda 2013). The effective sensor depth is the vertical extent of the measurement support volume, and was characterized by Franz et al. (2012b) as:

$$z^* = 5.8 \times (\rho_{bd} \times \tau + \theta_{vol} + 0.0829)^{-1} \quad 19$$

where z^* is the effective measurement depth [cm], ρ_{bd} is mean soil bulk density [g cm^{-3}], τ is the lattice water content [g g^{-1}] and θ_{vol} is soil water content [cm^3 cm^{-3}]. Horizontally and vertically homogeneous distribution of soil water content, lattice water, and bulk density were assumed when using this equation. Effects of horizontal soil water content heterogeneity on neutron flux were reported to be small (Franz et al. 2013b).

In case of vertically heterogeneous soil water content, vertical weights for individual soil layers were calculated and assigned to calculate vertical weighted soil water content using the method of Bogena et al. (2013). Weights ($CFoC_z$) were iteratively determined for each layer with Eq. 20 depending on the depth z [cm] of the layer i and the sum of hydrogen pools H_p in g cm^{-3} (i.e. lattice water and soil water content):

$$CFoC_i = 1 - exp(-z/\gamma) \quad 20$$

with

$$\gamma = -5.8 \times \left(ln(0.14)\right)^{-1} \times \left(H_p + 0.0829\right)^{-1} \quad 21$$

At first, the weight for the first layer $CFoC_1$ is determined with Eq. 20 and 21 using the arithmetic mean of the measured hydrogen pools. Subsequently, the weights of the layers below are determined with $CFoC_i = CFoC_i - CFoC_{i-1}$. The weight of the deepest layer is calculated by assigning a residual weight equal to 100% minus the sum of all other weights. The weighted mean soil water content is calculated with these weights and the procedure is repeated with the weighted mean soil water content until the change in weighted mean soil water content is negligible (<0.0001 cm cm^{-3}). We used the arithmetic mean of bulk density and lattice water measurements of the top soil (see Section 2.2.4.2).

2.2.4 Quantification of hydrogen pools

2.2.4.1 Hydrogen pools

Hydrogen pools within the effective measurement volume include subsurface hydrogen sources (soil water content, lattice water, belowground biomass), aboveground biomass, snow, and intercepted and ponded water. Bogena et al. (2013) showed that even in a forested site the hydrogen pool of intercepted water is relatively small compared to other hydrogen pools. For this reason and because ponded water only has a short-term effect on neutron count rates, ponded water and intercepted water were excluded from the analysis. Bogena et al. (2013) also showed that during days with snow cover, the estimated soil water content can exceed the expected values by more than 0.5 cm^3 cm^{-3}. Since an appropriate method to estimate snow water equivalent from neutron flux is not available, we excluded days with significant snow cover from the analysis.

2.2.4.2 Soil sampling for calibration of CRPs

Several soil sampling campaigns were conducted in 2012 and 2013 to quantify above and below ground hydrogen pools. A HUMAX soil corer (Martin Burch AG, Switzerland) with a diameter of 50.8 mm and a length of 30 cm was used to extract soil samples. In radii of 25, 75 and 175 m around the CRP, six soil samples were collected on each radius with an approximate radial distance of 60 degree between samples. This resulted in 18 sampling locations for each CRP. For

exact dates and calibration results, we refer to Table 3. Each 30-cm long soil sample was split into six sub-samples of 5 cm length. Soil water content and dry bulk density (ρ_{bd}) were determined by drying the samples at 105 °C for 48 hours. Subsequently, the soil samples were sieved and merged to generate a mixed sample for each depth. Three 15 mg aliquots were taken from these bulk samples and burned at 1000°C. For lattice water determination, hydrogen atoms were detected through a heat conductivity detector. The total organic carbon was measured using a Vario EL Cube (Elementar Analysensysteme GmbH). The arithmetic mean of the three samples was used to calculate average values of the soil properties for each depth. In July 2013, a 20x20 cm sample of wet aboveground biomass was taken at each soil sampling location for the sites Merzenhausen, Gevenich and Aachen. Wet biomass samples were weighted before and after drying at 105 °C for 2 days according to ASTM E-1756 to determine total solids in biomass. The water lost by drying is hereafter called vegetation water.

Table 3: Results from the 16 calibration campaigns (IDs) carried out in 2012 and 2013 at the ten sites in the Rur catchment, corresponding soil properties and calibration parameters (mean bulk density (bd), lattice water (lw), soil water content (θ_{vol}), wet aboveground biomass (AGB_{wet}), measured corrected neutron flux, hydrogen molar fraction (*hmf*) and the calibration parameters N_0, N_S and N_{COSMIC}).

IDs	Location	Date of	ρ_{bd}	lw	θ_{vol}	AGB_{wet}	Neutron flux	hmf	N_0	N_S	N_{COSMIC}
		calibration	g cm^{-3}	cm^3 cm^{-3}	cm^3 cm^{-3}	kg m^{-2}	cph	moles $moles^{-1}$	cph	cph	cph
1	Wuestebach	23/08/2012	0.83	0.067	0.35	68.2	472	0.30	936	699	166
2	RollesbroichN	18/07/2012	1.09	0.072	0.56	0.8	526	0.20	1081	435	192
3	Rollesbroich	18/07/2012	1.09	0.068	0.46	0.7	613	0.19	1208	479	213
4	Merzenhausen	10/08/2012	1.39	0.039	0.19	4.3	798	0.14	1202	452	194
5	Gevenich	19/10/2012	1.31	0.034	0.26	4.4	759	0.16	1242	485	207
6	Heinsberg	19/10/2012	1.27	0.039	0.34	3.3	705	0.17	1242	492	213
7	Kall	10/08/2012	1.31	0.086	0.33	1.2	705	0.18	1268	497	219
8	RurAue	12/09/2012	1.11	0.046	0.28	6.1	641	0.17	1109	447	188
9	Wildenrath	12/09/2012	1.21	0.027	0.14	37.3	699	0.18	1014	517	158
10	Aachen	18/10/2012	1.12	0.058	0.38	3.9	620	0.19	1169	477	203
11	Merzenhausen	19/11/2012	1.27	0.035	0.27	4.3	728	0.16	1212	476	203
12	RurAue	23/11/2012	1.12	0.047	0.35	6.1	603	0.19	1109	456	191
13	Wildenrath	16/11/2012	1.15	0.026	0.19	37.3	628	0.20	988	526	160
14	Merzenhausen	18/07/2013	1.34	0.037	0.12	4.3	875	0.12	1212	432	185
15	Gevenich	19/07/2013	1.42	0.037	0.15	4.4	846	0.13	1206	440	189
16	Aachen	18/07/2013	1.20	0.063	0.27	3.9	680	0.17	1174	466	199

2.2.4.3 Above ground biomass estimation

Total aboveground biomass for each sensor was calculated based on the fractions of land use types in each CRP footprint (Waldhoff 2012) and was assumed to be constant in time. For the spruce forest of the Wuestebach site, dry aboveground biomass was assumed to be 30 kg m^{-2} (Etmann 2009). For other locations, a dry aboveground forest biomass of 18.4 kg m^{-2} was assumed (Oehmichen et al. 2011). Vegetation water in forest was assumed to be 56 % of the total aboveground forest biomass (Nurmi 1999). Grassland and crop biomass were sampled in July 2013 at Merzenhausen, Gevenich and Aachen. The resulting average dry aboveground biomass and vegetation water for grassland and crops were assigned to the respective land use fractions given in Table 2. Urban fractions and water bodies were not considered. Belowground

biomass is not estimated separately, because the samples taken with the HUMAX soil corer included medium and fine root biomass.

2.2.5 Cosmic-ray probe soil water content determination

Results of the soil sampling campaigns were used for calibration of the ten CRPs using three different parameterization methods (i.e. the N_0-method, the hydrogen molar fraction based (*hmf*) method and the COSMIC operator). The three methods are outlined in the following three sections. The main differences amongst the methods are the complexity of the applied parameterizations, and whether the methods include above ground biomass explicitly in the parameterization (i.e. *hmf*-method) or not (i.e. N_0-method and COSMIC operator). All methods use a single calibration parameter N_X.

2.2.5.1 N_0-method

Desilets et al. (2010) developed a shape-defining function, hereafter called N_0-method, to determine volumetric soil water content θ_{vol} [cm^3 cm^{-3}] directly from corrected neutron flux:

$$\theta_{vol} = (a_0 \times \rho_{bd}) \times \left(N_{pih}/N_0 - a_1\right)^{-1} - (a_2 \times \rho_{bd}) \quad 22$$

where the parameters a_0 = 0.0808, a_1 = 0.372, a_2 = 0.115 are dimensionless and N_0 is a site specific calibration parameter. It is assumed that the parameters a_0, a_1 and a_2 are constant in time and independent of soil chemical composition (Zreda et al, 2008; Desilets et al., 2010). N_0 is a time-constant site-specific calibration parameter that depends mainly on the site-specific environment and reference conditions. Following Zreda et al. (2012), lattice water [cm^3 cm^{-3}] is added to the left side of Eq. 22 to acknowledge the presence of additional hydrogen pools that are not removed during the oven drying process. N_0 is then calibrated by fitting measured neutron flux over a 12 hour time interval at the time of calibration to vertically weighted soil water content, taking into account bulk density and lattice water as detailed in Bogena et al. (2013).

2.2.5.2 Molar fraction based method (*hmf*-method)

The universal calibration function was developed by Franz et al. (2013a) to provide reasonable estimates of soil water content on the basis of measurements of neutron flux in combination with other measurable hydrogen pools (water vapor content of air, soil lattice water, soil carbon, and aboveground biomass) without the need of a site-specific calibration using in-situ soil water content measurements. It assumes a monotonic relationship between the amount of hydrogen present in the CRP support volume and neutron flux (Franz et al. 2013a). The total moles in the cosmic-ray support volume and the hydrogen molar fraction are calculated using average soil properties and average aboveground biomass. The hydrogen molar fraction is the fraction of all hydrogen moles within the sensor footprint $\sum H$ [mol/mol] divided by the sum of all moles of all elements $\sum E_{all}$ [mol/mol] including air (NO), (vegetation) water (H_2O), dry soil (SiO_2), dry aboveground vegetation ($C_6H_{12}O_6$), carbon (C):

$$hmf = \sum H / \sum E_{all} \quad 23$$

For simplicity, air and soil elements are reduced to nitrogen (N), oxygen (O), silicate (Si), hydrogen (H) and carbon (C). Vegetation is assumed to consist of a wet part and a dry part as outlined in Section 2.2.4. According to Franz et al. (2013), the relationship between hydrogen molar fraction (*hmf*) and neutron flux can be approximated with:

$$N_{pih}/N_s = 4.486\exp(-48.1 \times hmf) + 4.195\exp(-6.181 \times hmf) \quad 24$$

where N_S is a time-constant site-specific calibration parameter [cph] and N_{pih} is the neutron flux corrected for pressure, incoming cosmic ray and air humidity. N_S is calibrated for each probe with the average measured neutron flux N_{pih} of a 12 hour time window at the time of calibration and the calculated hydrogen molar fraction based on the sampling campaign results. The fully calibrated *hmf*-method is then used to inversely derive the hydrogen molar fraction and soil water content from measured neutron flux using a one-dimensional optimization scheme (Brent 1973). For this, we minimized the squared difference between modeled and measured neutron flux to an accuracy of 10^{-5} cph.

2.2.5.3 COSMIC operator

The COSMIC operator was developed to represent a simplified interaction of cosmic-rays with the subsurface for use in data assimilation (Shuttleworth et al. 2013). The main processes represented in the COSMIC operator are i) an exponential reduction of *high* energy neutron flux towards deeper soil layers, ii) the generation of *fast* neutrons from *high* energy neutrons at different depths, and iii) an additional depth-dependent reduction of lower energy neutrons before they are detected at the surface. The code requires parameterization of several site-specific time-constant parameters. The COSMIC-specific parameters L_1 = 162.0 g cm^{-2}, L_2 = 129.1 g cm^{-2} and L_4 = 3.16 g cm^{-2} were found to be constant for all locations through calibration with the MCNPx code (Shuttleworth et al., 2013). The parameters L_3 [g cm^{-2}] and α [cm^3 g^{-1}] are calculated using mean soil bulk density (0-30 cm) according to:

$$L_3 = -31.65 + 99.29 \times \rho_{bd} \quad 25$$

$$\alpha = 0.404 - 0.101 \times \rho_{bd} \quad 26$$

Additionally, the site-specific time-constant calibration parameter N_{COSMIC} is required to run the COSMIC operator. We derived N_{COSMIC} by one-dimensional optimization (Brent 1973) of measured neutron flux (12 hour average at the time of calibration) and reproduced neutron flux by the COSMIC operator given measured soil water content, bulk density and lattice water. The fully calibrated COSMIC operator can then be used to inversely determine soil water content from measured neutron flux N_{pih} at each site. A detailed description of the COSMIC code is given in Shuttleworth et al. (2013).

2.2.6 Evaluation of soil water content estimated with CRP

The soil sampling for CRP calibration was repeated for several locations during November 2012 and July 2013. This was done to compare site-specific time-constant calibration parameters of the first campaign (N_{X1}) to calibration parameters of the second campaign (N_{X2}). Also in-situ measured soil water content during the second campaign ($VWC_{grav.-2}$) was compared to soil water content determined from the CRP ($VWC_{cosmic-ray-2}$) using calibration parameters of the first campaign.

In order to compare soil water content measurements of the SoilNet in Rollesbroich and Wuestebach with soil water content measurements of the CRPs, a horizontally and vertically weighted average of the soil water content measurements with SoilNet is required. For this, we first averaged the SoilNet measurements horizontally for each layer as described in Bogena et al. (2013). The area around the CRP was split into seven annular segments with radii to the CRP of 50 to 350 meters. Horizontal weights were assigned according to the relative cumulative fraction of neutron counts detected by the sensor following Zreda et al. (2008). Vertical weights were assigned to each layer as described in Section 2.3. Days with snow or soil temperatures below 0 °C were removed from the time-series. To reduce noise, soil water content determined from CRP and SoilNet were averaged over one day.

The correspondence between the two time series ($x_{t,1}$ and $x_{t,2}$, measured and predicted) was quantified using the Mean Absolute Error (MAE) and Root Mean Square Error (RMSE):

$$MAE = \frac{1}{n}\sum_{t=1}^{n}\left(x_{t,1} - x_{t,2}\right) \quad 27$$

$$RMSE = \sqrt{\frac{\sum_{t=1}^{n}\left(x_{t,1} - x_{t,2}\right)^2}{n}} \quad 28$$

where n is the total number of time steps.

2.3 Results

2.3.1 Measured neutron flux

Average corrected neutron fluxes were derived for all ten CRP sites. Average incoming cosmic ray intensity was 156.94 neutrons per second at KIEL and 166.95 neutrons per second at JUNG in 2012. These values were taken as reference incoming cosmic ray intensity at both locations. Minimum and maximum incoming cosmic ray intensity were 137.84 neutrons per second and 175.37 neutrons per second, respectively. The correction for incoming cosmic ray intensity ranged from 0.95 to 1.13 in 2012. Maximum air humidity in 2012 was 17.86 g m^{-3} corresponding to a maximum correction factor for air humidity of 1.099. The pressure correction factor ranged between 0.4786 and 1.244 for the ten stations. After correction, average corrected daily

neutron flux varied between 463 neutron counts per hour (cph) at the forested site Wuestebach and 794 cph at the agricultural site Gevenich during the second half of 2012 when all CRP were operational.

Figure 5 shows the temporal evolution in neutron flux. Drying periods in summer led to an increase in neutron flux, whereas intensive rain events and days of consecutive rain led to a decrease in neutron flux. Absolute fluctuations in neutron flux are larger for sensors with high count rates than for sensors with low count rates. Overall, Figure 5 shows strong correlations in neutron flux amongst the sites because they were subject to the same regional weather events. However, the neutron flux data also show that high precipitation and low evapotranspiration and the associated higher average soil water content and high amounts of aboveground biomass were factors that reduced neutron flux. For example, locations at higher altitude with high average soil water content generally showed lower neutron fluxes (e.g. Wuestebach, Rollesbroich, RollesbroichN and Kall). Of these high-altitude locations, Wuestebach had the lowest neutron flux at a given water content because it additionally had a high aboveground biomass. Wildenrath had very low average soil water content, but due to the high amount of aboveground biomass the measured neutron flux is equally low as at the wet grassland site Kall.

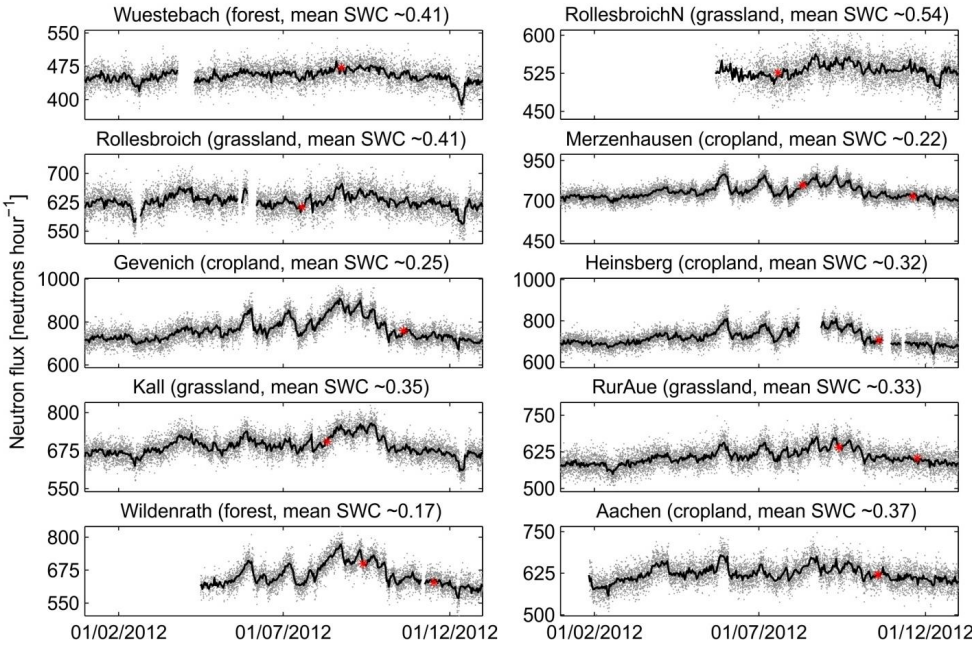

Figure 5: Hourly measured and corrected neutron flux (grey dots), daily average measured corrected neutron flux (black line) and calibration points (red dots) for the ten CRPs installed in the area. Main land use and average soil water content derived with the COSMIC operator during the measurement period in 2012 at the ten locations are also indicated.

2.3.2 Calibration results

Results of the calibration campaigns are summarized in Table 3. Mean bulk densities ranged between 0.83 g cm^{-3} at the forest site Wuestebach to 1.42 g cm^{-3} at the agricultural site Gevenich. Mean lattice water ranged from 0.026 cm^3 cm^{-3} to 0.086 cm^3 cm^{-3}. Weighted mean soil water content at times of calibration ranged between 0.12 cm^3 cm^{-3} and 0.56 cm^3 cm^{-3}. The sites with highest wet aboveground biomass were Wuestebach (68.2 kg m^{-2}) and Wildenrath (38.0 kg m^{-2}) due to the high proportion of forest within the CRP footprint (Table 2). Correspondingly, the lowest values for the calibration parameter N_0 were found for both forest sites (936 and 988 for Wuestebach and Wildenrath, respectively). Also the COSMIC calibration parameter N_{COSMIC} was lowest at these locations (166 and 160 for Wuestebach and Wildenrath,

respectively). N_{COSMIC} and N_0 showed a high positive linear correlation (R^2 = 0.76) for the 16 calibration data sets (Figure 6). However, we found less correlation between N_S and N_0 (R^2 = 0.38), and N_S and N_{COSMIC} (R^2 = 0.18). The calibration parameters N_0, N_{COSMIC} and N_S correlate well with wet above ground biomass with R^2 = 0.72, R^2 = 0.62 and R^2 = 0.79, respectively. The hydrogen molar fractions calculated from measured variables ranged from 0.12 at a soil water content value of 0.12 cm^3 cm^{-3} in Merzenhausen at July 18th, 2013 to 0.30 at a soil water content value of 0.35 cm^3 cm^{-3} in Wuestebach at August 10th, 2012 (Table 3). The high *hmf* in Wuestebach is mainly caused by high amounts of aboveground biomass in the form of trees within the footprint.

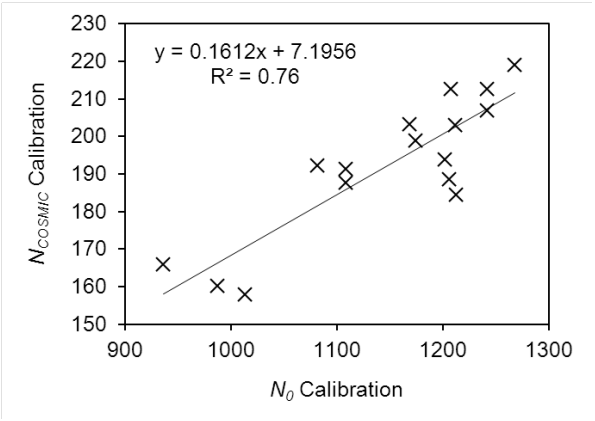

Figure 6: Correlation between N_0 and N_{COSMIC} derived from measured neutron flux and in-situ calibration.

Figure 7 shows the site-specific and method-specific CRP calibration curves for all three methods. For each calibration, we used in-situ data of the first calibration campaign performed at each site. The calibration curves of the COSMIC and *hmf*-methods were similar, although only the *hmf*-method considered aboveground biomass. The N_0-method deviated from the other two parameterization methods and showed stronger changes in estimated soil water content for a given change in neutron flux rate, particularly for low water content. In the remainder of this paper, we focus on the results of the N_0-method and the COSMIC operator because the *hmf*

derived neutron flux – soil water content relationships were very close to the ones of the COSMIC operator.

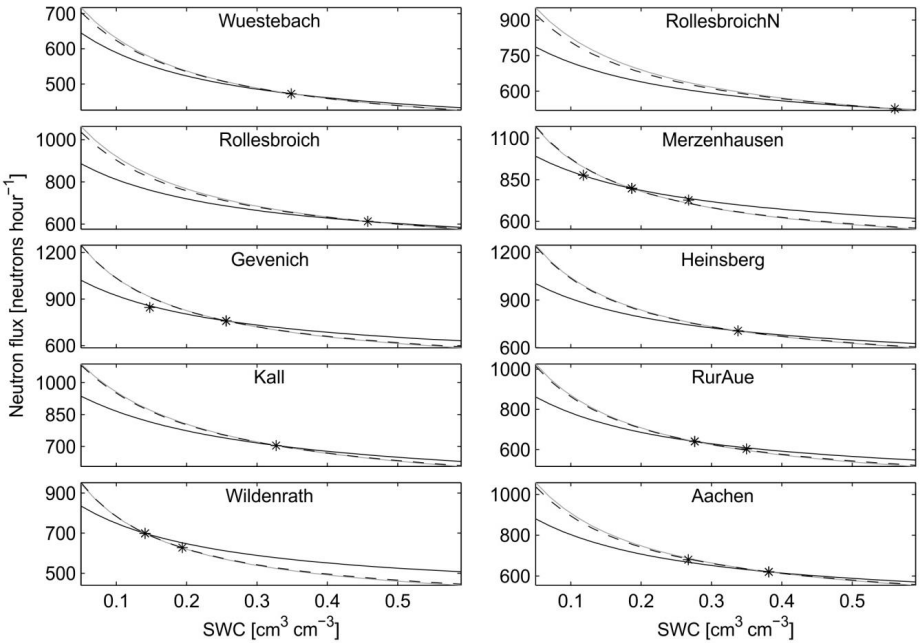

Figure 7: Calibration curves showing site-specific and method-dependent relationships between neutron flux and soil water content. The black asterisks indicate the calibration measurements. The methods shown are the N_0-method (black), the COSMIC operator (dashed) and the *hmf*-method (gray).

2.3.3 Comparison of soil water content results from N_0-method and COSMIC operator

Soil water content determined from CRP measurements using the N_0-method and the COSMIC operator is shown in Figure 8 for four selected locations. The results show that different calibration methods yield soil water content deviations up to 0.06 cm^3 cm^{-3}. The drier locations (Merzenhausen and Wildenrath) showed larger deviations than the wetter locations (Wuestebach and Rollesbroich). The range of COSMIC-derived soil water content is smaller than

that of the N_0-method for all four sites. Therefore, dry periods were interpreted drier and wet periods were interpreted wetter with the N_0-method than with the COSMIC operator. In 2012, MAE between the COSMIC and the N_0 derived soil water content at Wuestebach, Rollesbroich, Merzenhausen and Wildenrath were 0.015 cm^3 cm^{-3}, 0.012 cm^3 cm^{-3}, 0.024 cm^3 cm^{-3} and 0.024 cm^3 cm^{-3}, respectively.

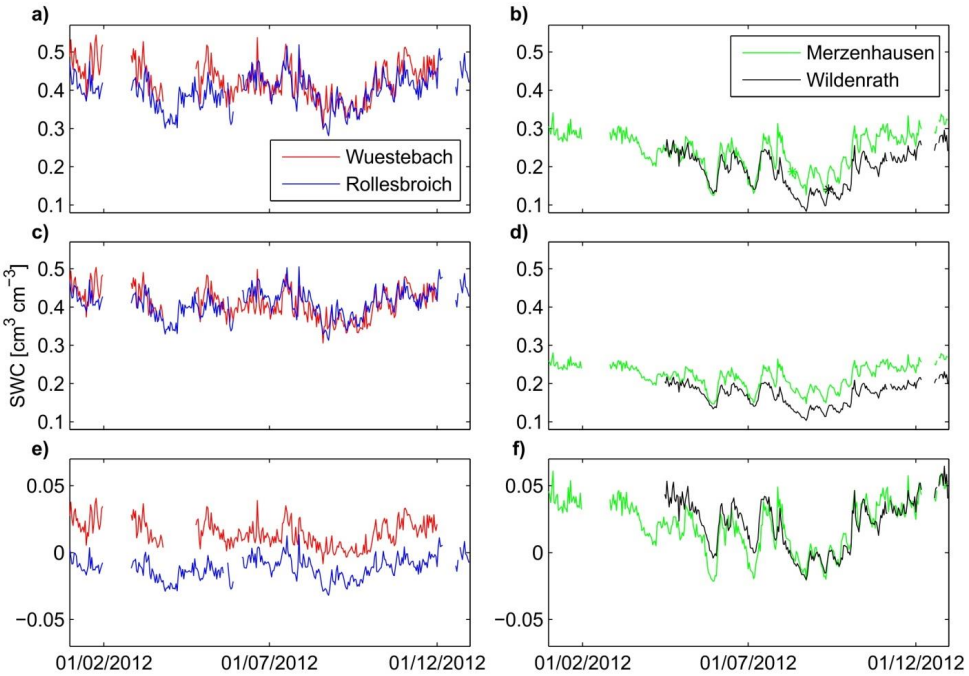

Figure 8: Daily average soil water content [cm^3 cm^{-3}] measured by four CRPs derived using the N_0-method (a and b) and derived with the COSMIC operator (c and d). Figure 8e and f show the difference of N_0-derived soil moisture and COSMIC derived soil moisture.

2.3.4 Results of repeated calibration campaigns

Calibration results for repeated calibration campaigns in November 2012 and July 2013 are shown in Table 3. Table 4 provides a comparison between two calibration campaigns for each location. The calibration parameters N_X differed considerably in magnitude amongst the

methods (being highest for N_0 and lowest for N_{COSMIC}). Therefore, the first part of Table 4 shows the relative difference between the site-specific calibration parameter N_X obtained from the first and second calibration campaign. The relative differences were lowest for the N_0-method, and higher for N_S and N_{COSMIC}.

Table 4: Summary results of the comparison between the first calibration campaigns (Table 3, calibrations 1 to 10) and the repeated calibration campaigns (Table 3, calibrations 11 to 16). Absolute difference soil water content is the difference between soil water content predicted (using calibrated parameters from first calibration campaign) and soil water content measured (at repeated campaign). The calibrations compared are identified by calibration ID in Table 3.

Location	Calibration	Percentage difference calibration parameter			Absolute difference soil water content		
	IDs	%			$cm^3\ cm^{-3}$		
		N_0	N_S	N_{COSMIC}	N_0	N_S	N_{COSMIC}
Merzenhausen	4 & 11	0.8	5.2	4.8	0.016	0.022	0.021
RurAue	8 & 12	0.0	2.1	1.9	0.016	0.014	0.010
Wildenrath	9 & 13	2.6	1.7	1.6	0.034	0.002	0.001
Merzenhausen	4 & 14	0.8	4.4	4.7	0.002	0.022	0.022
Gevenich	5 & 15	2.9	9.2	8.9	0.009	0.039	0.038
Aachen	10 & 16	0.4	2.4	2.0	0.023	0.009	0.005
MAE		1.3	4.2	4.0	0.017	0.018	0.016

The calibration curves from the first campaign were used to predict soil water content at the time of the second calibration campaign for all three methods. Table 4 shows the absolute differences between estimated soil water content with the CRP and in-situ measured vertically averaged soil water content. Again, the differences between the calibration methods were small with a slightly larger *MAE* for the *hmf*-method (0.018 $cm^3\ cm^{-3}$) than for the N_0-method (0.017 $cm^3\ cm^{-3}$) and the COSMIC operator (0.016 $cm^3\ cm^{-3}$).

2.3.5 Comparison with two sensor networks

Daily average soil water content at three depths (from SoilNet) and daily precipitation are shown in Figure 9 for the Rollesbroich and Wuestebach test sites. Both sites showed similar soil water content dynamics, which were highly responsive to precipitation. In both sites highest soil water content was observed at 5 cm depth. Two periods with long drying events can be

observed in April and late summer, especially in the Wuestebach site. Only in summer, soil water content in the top layer was lower than at 20 cm and 50 cm depth (Figure 9). Days with rainfall > 5 mm or consecutive days of rainfall were necessary to cause a soil water content increase at 20 cm and 50 cm depth. Vertically weighted mean soil water content was derived from the SoilNet measurements for comparison with the CRP measurements. For Rollesbroich, the average weight for the SoilNet measurements at 5 cm depth was 0.852, whereas the average weights for 20 cm and 50 cm depth were 0.146 and 0.002, respectively. The high weight for the sensor at 5 cm depth is related to the high average soil water content (0.42 cm^3 cm^{-3}) and the high fraction of lattice water (0.068 cm^3 cm^{-3}). For the Wuestebach test site similar weights were found: 0.832, 0.153 and 0.015 for 5 cm, 20 cm and 50 cm depth, respectively. As a consequence, the weighted average soil water content used in the evaluation of the CRP measurements is very similar to soil water content at 5 cm depth.

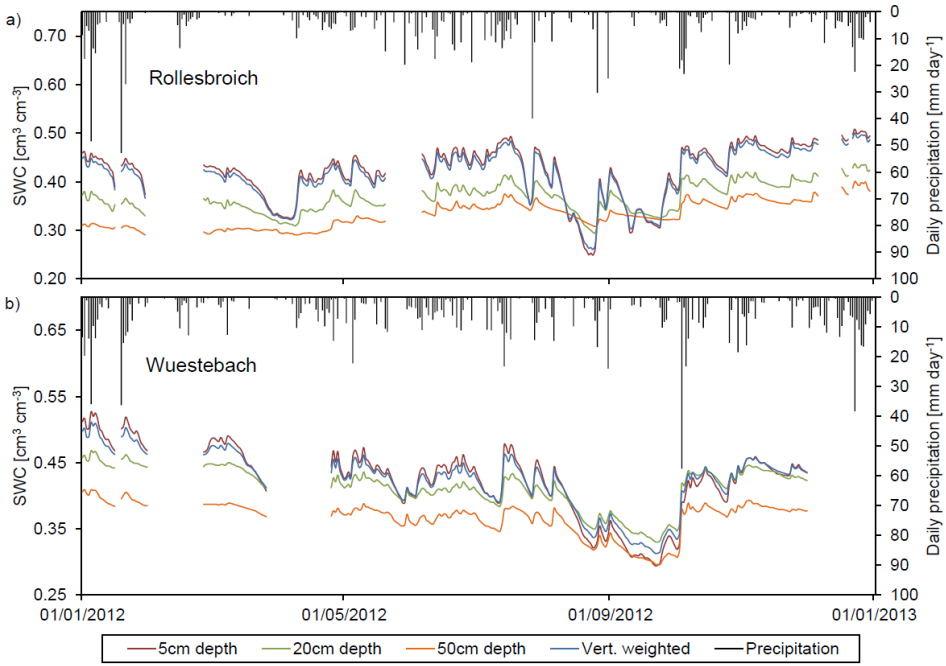

Figure 9: Precipitation and average, depth dependent, soil moisture of the sensor networks at the Rollesbroich and Wuestebach test site. Vertical weighting was performed using the weighting scheme of Bogena et al. (2013).

Cosmic-ray derived soil water content from all three calibration functions fitted well to the weighted soil water content of the SoilNet (Figure 10). Rain events, particularly strong rain events, are well captured by the cosmic-ray signal. Cosmic-ray derived soil water content is consistently larger than SoilNet derived soil water content after strong rain events due to the high sensitivity of the neutron flux to near-surface water. This can be seen particularly well in July and December 2012. Figure 10 also shows that the N_0-method captures the dry phases in April and August 2012 better than the COSMIC operator. The soil water content derived with the *hmf*-method is not shown in this figure, because it matches the COSMIC derived soil water content with a difference in RMSE of only 0.003 cm^3 cm^{-3}. Table 5 summarizes the results of the four methods to estimate soil water content at Rollesbroich during 2012. The RMSE between the parameterization methods and the sensor network was somewhat higher for the N_0-method (RMSE = 0.032 cm^3 cm^{-3}) as compared with the *hmf*-method and the COSMIC operator (RMSE =

0.030 cm^3 cm^{-3}). Similarly, the average soil water content determined with the *hmf*-method and the COSMIC operator were slightly closer to the average soil water content obtained from SoilNet than the one of the N_0-method.

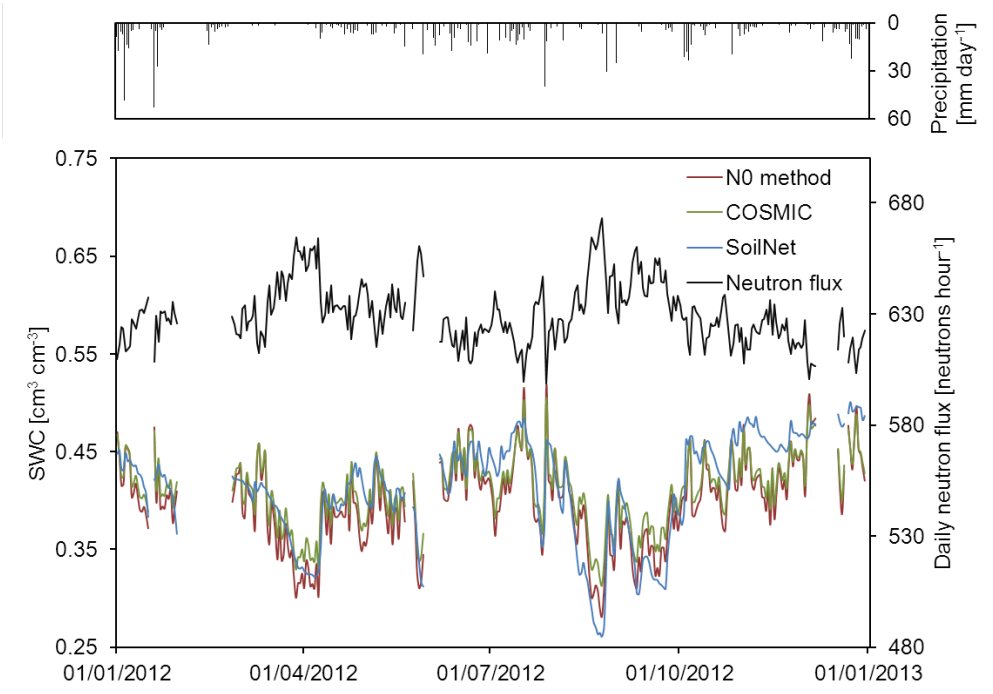

Figure 10: Soil water content at Rollesbroich measured by the sensor network (blue), measured daily averaged neutron flux (black) and cosmic-ray derived soil water content using two different methods: The N_0-method (red) and the COSMIC operator (green). Gaps in the data are due to snow cover, lack in power supply or soil temperatures below 1°C.

Table 5: Summary results at Rollesbroich and Wuestebach for daily averaged soil water content measurements in 2012. The upper part of the table provides RMSE of estimated soil water content. The second part of the table gives minima, maxima, range (maximum minus minimum) and mean soil water content.

	Rollesbroich (units in $cm^3\ cm^{-3}$)				Wuestebach (units in $cm^3\ cm^{-3}$)			
	SoilNet	N_0	hmf	COSMIC	SoilNet	N_0	hmf	COSMIC
SoilNet	0	0.032	0.030	0.030	0	0.033	0.032	0.032
N_0	0.032	0	0.022	0.019	0.033	0	0.018	0.018
hmf	0.030	0.017	0	0.003	0.032	0.018	0	0.001
COSMIC	0.030	0.014	0.003	0	0.032	0.018	0.001	0
Min	0.26	0.28	0.32	0.31	0.31	0.30	0.31	0.31
Max	0.50	0.52	0.50	0.51	0.51	0.54	0.50	0.50
Range	0.240	0.238	0.183	0.192	0.198	0.247	0.197	0.198
Mean	0.413	0.398	0.412	0.410	0.422	0.424	0.409	0.410

Estimated soil water content using the calibrated cosmic-ray measurements and the sensor network data for the Wuestebach test site are shown in Figure 11. The cosmic-ray signal shows stronger fluctuations in Wuestebach than in Rollesbroich. This might be the result of the low neutron count rates at the Wuestebach site (Bogena et al. 2013). Because neutron count rates are very low due to high additional hydrogen pools besides soil water content, the signal to noise ratio is smaller in Wuestebach than in Rollesbroich and the CRP signal is more sensitive to the dynamics of other hydrogen sources besides soil water (e.g. litter layer). This is also indicated by the fact that the standard deviation of daily soil water content values derived with e.g. the COSMIC operator at Wuestebach is slightly higher (0.039 $cm^3\ cm^{-3}$) than at Rollesbroich (0.036 $cm^3\ cm^{-3}$) although the standard deviation of daily averaged neutron flux at Wuestebach is much smaller (9.1 cph) than at Rollesbroich (13.8 cph).

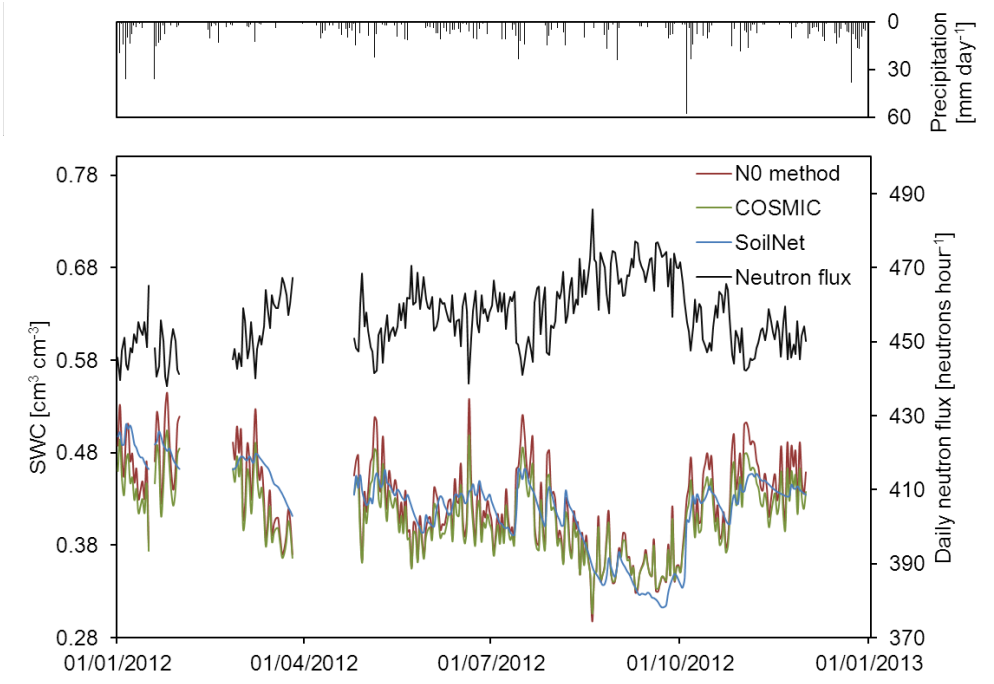

Figure 11: Soil water content at Wuestebach measured by the sensor network (blue), measured daily averaged neutron flux (black) and cosmic-ray derived soil water content using two different methods: The N_0-method (red) and the COSMIC operator (green). Gaps in the data are due to snow cover, lack in power supply or soil temperatures below 1°C.

Like in Rollesbroich, the RMSE of the N_0-method (0.033 cm^3 cm^{-3}) was slightly larger than the RMSE for the *hmf*-method (0.032 cm^3 cm^{-3}) and the COSMIC operator (0.032 cm^3 cm^{-3}) (see Table 5). However, the mean soil water content (0.424 cm^3 cm^{-3}) obtained by the N_0-method was closest to the weighted mean soil water content of the sensor network (0.422 cm^3 cm^{-3}) at the Wuestebach site.

2.4 Discussion

The N_0-method was the first method proposed to determine soil water content directly from neutron flux (Desilets et al. 2010) and is based on synthetic MCNPx simulations. Since this methods is straightforward to implement computationally, it is the most commonly used method (Bogena et al. 2013; Desilets and Zreda 2013; Franz et al. 2012b; Villarreyes et al. 2011).

The straightforward applicability of this method goes along with a possibly too simplified representation of the interaction between secondary cosmic-rays and hydrogen present in the soil. However, the results of the present study have shown that the N_0-method performs well for the given humid climatic conditions and the range of observed soil water content.

Results of the *hmf*-method have shown that consideration of the aboveground biomass has a minor effect on the shape of the calibration curve under various environmental and soil conditions (Figure 7). However, the calibration parameter N_S (Eq. 24) differed considerably for all test sites and the expected catchment wide constant N_S value was not found. A fixed value of N_S for all test sites did not provide accurate soil water content estimates (results not shown). This clearly limits the applicability of the *hmf*-method as a universal calibration method and local soil sampling campaigns and calibration of the N_S parameter are still necessary for the *hmf*-method to produce accurate soil water content measurements using our network of CRP.

The goal of the COSMIC operator is to represent the processes of the MCNPx model in a simplified manner and to allow the consideration of vertically heterogeneous soil water content (Shuttleworth et al. 2013). In this study, the COSMIC operator was used in an inverse mode to determine soil water content at the ten locations from observed neutron fluxes. The complexity of the calculations and the required time to run the COSMIC operator are significantly higher than for the *hmf*-method and the N_0-method. In this study, the COSMIC operator was not calibrated with the MCNPx model, but was still able to obtain soil water content close to the one measured by the two sensor networks. This result clearly indicates that the COSMIC operator can be used for data assimilation applications for the ten locations in the Rur catchment.

Wet aboveground biomass was estimated with a 15 m resolution land use map. Biomass at the forest sites Wuestebach and Wildenrath was higher than wet aboveground biomass reported by Franz et al. (2013a), but corresponded well with values found in other German and European forests (Ciais et al. 2008; Dieter and Elsasser 2002). The resulting hydrogen molar fractions were above the theoretical threshold value for the case of pure water beneath the sensor (*hmf* =

0.23), which was also the case for some COSMOS sites (Franz et al. 2013a). Uncertainty in the estimation of aboveground biomass propagates into the calibration of the CRP. This is particularly true when biomass changes with time (e.g. at agricultural sites). In this study, aboveground biomass was assumed to be constant in time due to the lack of information on crop development. This may have introduced an error in the calibration of the agricultural sites Merzenhausen, Gevenich and Aachen, where seasonal changes in aboveground biomass are expected to be larger due to crop growth and harvest compared to grassland and forest sites. Therefore, the calibration parameters N_0 and N_{COSMIC} are not expected to remain constant in time at the agricultural sites Merzenhausen, Gevenich and Aachen. This is reflected well for the three sites in the N_{COSMIC} parameter, while N_0 exhibits smaller changes (Table 4). In this light, the single-point calibration and evaluation results of RurAue (grassland) and Wildenrath (forest) shown in Table 3 and Table 4 are potentially more reliable than the single-point calibration and evaluation results at Merzenhausen, Gevenich and Aachen. Clearly, the validation of cosmic-ray derived soil water content using continuous measurements of soil water content should be preferred when significant changes in biomass with time are expected.

The calibration parameters N_{COSMIC} and N_0 were expected to indirectly include effects of biomass (Franz et al. 2013c). A comparison of N_0 and N_{COSMIC} across all sites indicates that the lowest values were found at the Wuestebach and Wildenrath sites where aboveground biomass was highest (Table 3). Additionally, a good linear correlation between N_{COSMIC} and N_0 was observed. Assuming that N_X values of one method should be the same under reference conditions, one more method to compare model performance is the normalized standard deviation of N_X. Calculation of the normalized standard deviation ($\sigma_n = \sigma/\mu$) using the N_X values in Table 3 yields the lowest σ_n for N_0 (0.086), a larger σ_n for N_{COSMIC} (0.095) and the largest σ_n for N_S (0.131). Exclusion of sites with high wet aboveground vegetation (> 5 kg m^{-2}), thus reducing the impact of vegetation, yields normalized standard deviations of 0.041, 0.051 and 0.054 for N_0, N_S and N_{COSMIC}, respectively. This indicates that for sites with substantial aboveground biomass (e.g. forests) the calibration parameters of all three methods will be significantly influenced by vegetation.

2.5 Conclusions

Ten cosmic-ray probes in the Rur catchment in western Germany were calibrated using three parameterization methods to estimate soil water content from fast neutron flux (i.e. N_0-method, *hmf*-method and COSMIC operator). The probes were calibrated using arithmetically averaged bulk density, lattice water and total soil carbon, vertically weighted soil water content and estimated aboveground biomass. The soil water content estimates resulting from the three methods were compared individually to independent measurements of two distributed soil water content sensor networks (SoilNet) and repeated gravimetric in-situ sampling.

We conclude that all three methods gave soil water content estimates with an acceptable error not much larger than the expected measurement uncertainty. CRP measurements represented soil water content dynamics well at all ten test sites (RMSEs ≤ 0.033 cm^3 cm^{-3}), although the sites had different characteristics (e.g., land use, aboveground biomass, meteorological conditions, soil properties). Calibration curves of the *hmf*-method and the COSMIC operator were very similar, but the calibration curves obtained for the N_0-method differed more strongly from the other two. Using the N_0-method for soil water content estimates led to a larger range in soil water content values than using the *hmf*-method or the COSMIC operator, with particularly strong deviations for low soil water content. This discrepancy was not reflected in our validation results because soil water content remained relatively high throughout our study period because of the humid climatic conditions. The capability of the COSMIC operator to directly include vertical gradients in soil water content and soil properties, together with the good performance in validation experiments, may make the COSMIC operator a favorable method for soil water content determination from neutron flux.

A direct relation of neutron flux to above ground biomass was already observed by Franz et al. (2013c), and is confirmed by the linear correlation of N_0 and N_{COSMIC} with the amount of above-ground biomass found in this study. This may give rise to an empirical vegetation correction for the calibration parameters N_0 and N_{COSMIC} in future research. Systematic deviations amongst the three parameterization methods (Figure 7), neutron flux uncertainty and correction for sensor efficiency need to be accounted for when empirical neutron flux correction factors are derived

for aboveground biomass. The results at Wildenrath and Wuestebach (see also Bogena et al. 2013) have shown that possible changes in the calibration function due to high above ground biomass (which shows limited temporal variability) are limited and present no obstacle to soil water content determination with CRPs.

The area-average soil water content determined using the CRP network is valuable for a broad community of environmental modelers for model verification, model calibration and data assimilation experiments. Future work should focus on (i) quantification of aboveground biomass effects on neutron flux and (ii) the effect of vertical gradients in bulk density on soil water content determination with CRP measurements. This will enable scientists to consider seasonal changes of aboveground biomass in neutron flux signal interpretation, particularly at agricultural sites, and to produce spatially distributed soil water content maps with mobile cosmic-ray probes (i.e. the cosmic-ray rover (Chrisman and Zreda 2013)) considering spatially heterogeneous soil properties and aboveground biomass.

3 Development of an empirical vegetation correction for cosmic-ray probe measurements*

3.1 Introduction

Hydrologic processes at the land surface are strongly influenced by surface soil water content because it controls water availability for transpiration, evaporation and groundwater recharge (Brutsaert 2005). Soil water content measurements are therefore a valuable source of information for hydrologic (Brocca et al. 2012), land surface (Jung et al. 2010) and atmospheric circulation models (Koster et al. 2004). The wealth of available soil water content measurement techniques at various temporal and spatial scales has extensively been reviewed (e.g. Robinson et al. 2008a; Vereecken et al. 2008; Vereecken et al. 2014). Amongst these techniques, cosmic-ray probes (CRPs) are an emerging technology to determine soil water content from passive neutron counting (Zreda et al. 2008). This new technique addresses the need for continuous soil water content measurements at the horizontal scale of several tens of ha. The method utilizes the fact that hydrogen moderates secondary cosmic-ray neutrons much more effectively than other atoms present in the soil. There are two main reasons for this. First, hydrogen nuclei have a similar mass as fast neutrons and thus fewer fast neutron-hydrogen nuclei collisions are needed to slow down a fast neutron to the thermal level. Second, hydrogen has the highest elastic scattering cross-section of the most abundant elements in the soil (Zreda et al. 2012). This results in an inverse relationship between the abundance of hydrogen atoms near the soil surface and secondary cosmic-ray intensity or neutron intensity (Hendrick and Edge 1966). Spatially averaged soil water content determined using in-situ calibrated CRPs was found to be in good agreement with independently determined areal average soil water content at sites where biomass showed little variation over the year (Baatz et al. 2014; Bogena et al. 2013; Desilets et al. 2010; Franz et al. 2012a; Zreda et al. 2008). However, it was also shown that aboveground biomass within the CRP footprint reduced measured fast neutron intensity due to the moderating power of hydrogen contained in vegetation water and plant tissue (Coopersmith et al. 2014; McJannet et al. 2014). Hence, dynamic changes in aboveground

*adapted from: Baatz, R., Bogena, H.R., Hendricks Franssen, H.-J., Huisman, J.A., Montzka, C., and Vereecken, H. (2015). An empirical vegetation correction for soil water content quantification using cosmic-ray probes. Water Resour. Res., 51,2030–2046, doi:10.1002/2014WR016443.

biomass were shown to affect the CRP counting rate, and thus the accuracy of the soil water content measurements (Franz et al. 2013c; Villarreyes et al. 2011).

At present, three methods of different complexity exist to convert measured neutron intensity into soil water content: the N_0-method (Desilets et al. 2010), the hydrogen molar fraction method (hmf-method) (Franz et al. 2013a), and the COSMIC operator (Shuttleworth et al. 2013). These methods were recently compared and evaluated by Baatz et al. (2014). Of these methods, only the hmf-method explicitly accounts for additional hydrogen contained in aboveground biomass. However, it is limited by a maximum hydrogen molar fraction of 0.23 moles moles^{-1} that corresponds with liquid water. Several studies have shown that this maximum hydrogen molar fraction can be exceeded in the case of high aboveground biomass (Baatz et al. 2014; Franz et al. 2013a). Moreover, numerical experiments with a neutron interaction model demonstrated that hydrogen contained in forest trees cannot simply be conceptualized as an additional layer of water on top of the soil (Franz et al. 2013c). Instead, these simulations indicated that the impact of aboveground biomass on neutron moderation depends on forest structure and tree geometry (e.g. tree spacing, tree trunk diameter etc.).

In principle, neutron interaction models (e.g. Pelowitz 2005) are viable tools to develop correction functions to account for biomass effects on soil water content estimates derived from CRPs. However, the accuracy of such physically-based modeling of neutron interactions with biomass is limited by the complexity of accurately representing and parameterizing total above- and belowground biomass, which depends on plant species and generally is strongly heterogeneous (Franz et al. 2013c). In addition, such simulations are computationally intensive, and thus unfavorable for practical applications of the CRP method.

Here, we aim to develop a simple empirical framework to account for aboveground biomass effects on fast neutron moderation. Such a correction method for biomass would enhance the functionality of the N_0-method and the COSMIC operator by eliminating the need for in-situ calibration when dry aboveground biomass is known or can be estimated with reasonable accuracy. In addition, such a correction for biomass would enable CRP applications in locations

with strong changes in aboveground biomass and the use of mobile CRP surveys (e.g. Chrisman and Zreda 2013) in areas with strong spatial variation in aboveground biomass. To develop the empirical framework, we quantified the moderating effect of aboveground biomass at a range of sites with different environmental conditions by calibrating ten permanent CRPs using soil sampling campaigns. Measured fast neutron intensity was corrected for air pressure, incoming cosmic-ray intensity, atmospheric humidity, and sensor-specific counting efficiency. We evaluated the efficiency of the correction method for aboveground biomass using several different datasets acquired on sites with different amounts of aboveground biomass.

3.2 Materials and methods

3.2.1 Site description and instrumentation

All measurements were made in the Rur catchment that covers an area of 2354 km^2 and is located at the western border of Germany (Figure 1). It is part of the Terrestrial Environmental Observatories (TERENO) infrastructure (Bogena et al. 2012; Zacharias et al. 2011). Elevation ranges between 15 m in the lowland region in the north and 690 m in the low-mountainous Eifel region in the south. Mean annual precipitation increases from less than 600 mm in the north to 1400 mm in the south (Montzka et al. 2008). The lower northern part of the catchment is dominated by crop land, while the low-mountainous part is dominated by grassland and forest.

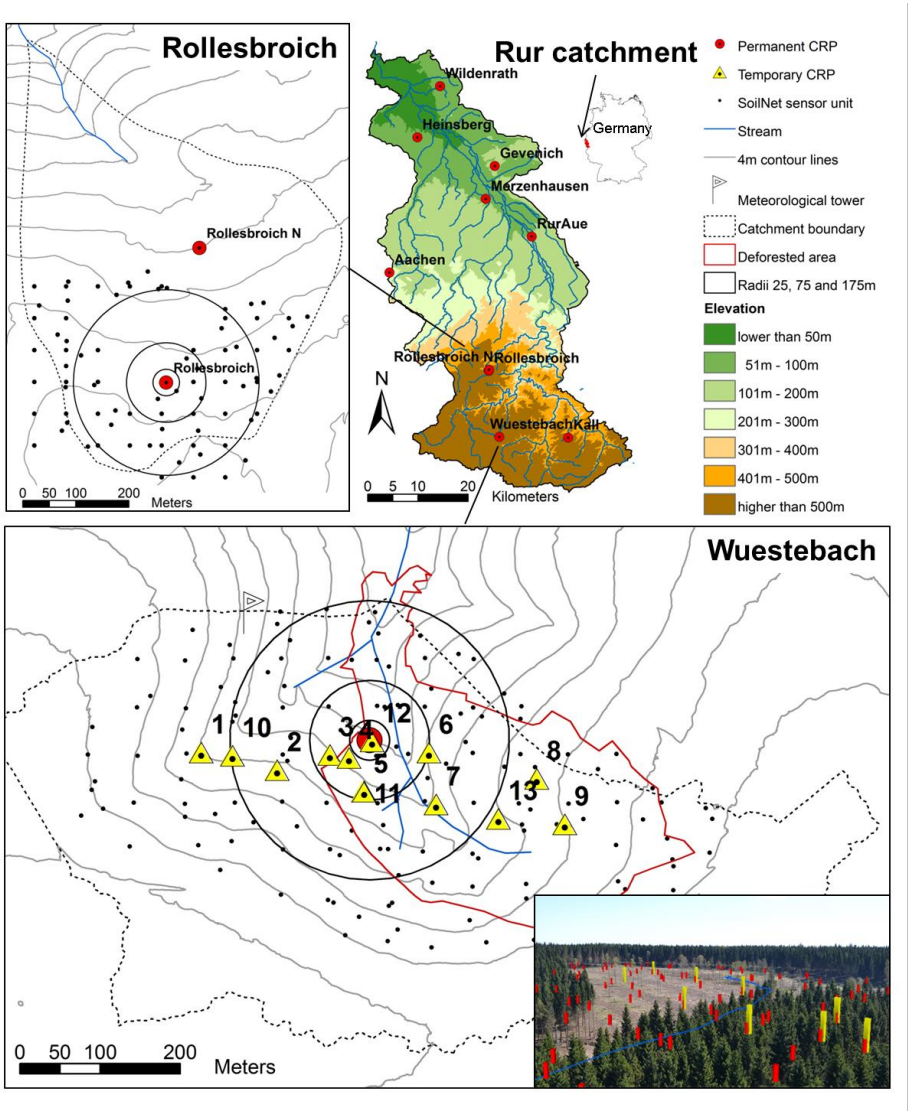

Figure 12: Locations of the ten permanently installed CRPs in the Rur catchment (top right), the Rollesbroich test site equipped with an in-situ soil water content sensor network (top left) and the Wuestebach test site with the temporary CRPs, the deforested area and radii used for calibration at 25, 75 and 175 meter (lower panel), and a photograph taken from the meteorological tower in 2014 with locations of in-situ SoilNet nodes (red), 9 of 13 temporary CRPs (yellow), and the Wuestebach stream (lower right).

We installed ten permanent cosmic-ray probes (CRPs) at a height of 1.5 m (CRS1000, HydroInnova LLC, 2009) in the Rur catchment (Figure 12). All ten probes contain a moderated neutron counter that consists of a metal tube (3 cm in diameter, 30 cm in length) filled with high pressure ^{3}He gas mantled with polyethylene. Five of the CRPs contain a second bare neutron counter without polyethylene mantle. A high voltage is applied to both ends of the tubes, which triggers an ionization process that produces a charged cloud that is registered as a single count by the pulse module when a neutron passes through the ^{3}He-tube. The network of CRPs has been operational since May 2012 and the CRP stations cover the main land use types of the Rur catchment: grassland (Rollesbroich, RollesbroichN, Kall, Rur Aue), crop land (Aachen, Gevenich, Heinsberg, Merzenhausen) and forest (Wildenrath, Wuestebach). Detailed information on altitude, mean annual precipitation and temperature, and land use fractions are presented in Table 6 for all sites.

Table 6: Site characteristics of the ten permanent CRPs in the Rur catchment (annual temperature, annual precipitation, land use fractions excluding surface water bodies (<1%)).

	Latitude	Longitude	Start of	Altitude	T(av)	P	Landuse [%]			
			measurement	m asl	°C	mm	Grasses	Crops	Forest	Urban
Aachen	50.798550 N	6.024716 E	13.01.2012	232	9.94	952	19	72	0	9
Gevenich	50.989220 N	6.323550 E	07.07.2011	108	10.16	884	0	85	0	15
Heinsberg	51.041104 N	6.104238 E	09.09.2011	57	10.25	814	35	39	2	24
Kall	50.501332 N	6.526450 E	15.09.2011	504	7.71	935	72	11	0	17
Merzenhausen	50.930325 N	6.297468 E	19.05.2011	94	10.22	825	1	82	0	16
Rollesbroich	50.621911 N	6.304241 E	19.05.2011	515	7.88	1307	92	0	0	8
RollesbroichN	50.624190 N	6.305142 E	22.05.2012	506	7.91	1309	87	0	0	12
RurAue	50.862329 N	6.427335 E	08.11.2011	102	10.13	743	58	25	11	6
Wildenrath	51.132744 N	6.169175 E	07.05.2012	76	10.28	856	3	7	88	2
Wuestebach	50.503487 N	6.333017 E	01.02.2011	605	7.47	1401	7	0	93	0

Two sites with CRPs (Rollesbroich and Wuestebach) were additionally equipped with a wireless soil water content sensor network (SoilNet, Forschungszentrum Jülich GmbH) described by Bogena et al. (2010). Soil water content sensors were installed in 5, 20 and 50 cm depth and provide soil water content estimates at 15 minute intervals. Calibration and data analysis of the SoilNet installed in the Wuestebach catchment is described by Bogena et al. (2010) and Rosenbaum et al. (2012), whereas Qu et al. (2013) provide this information for the Rollesbroich test site. The use of SoilNet data for calibration and evaluation of soil water content derived from neutron intensity measurements is described in more detail by Bogena et al. (2013) and Baatz et al. (2014).

As part of a deforestation experiment (Bogena et al. 2014), 9 ha of Norway Spruce trees were removed in August 2013 within a part of the Wuestebach catchment (Figure 12). The permanently installed CRP at Wuestebach was removed during the deforestation activities, and afterwards reinstalled at the original location. Additionally, neutron flux measurements for short periods (between 24 and 405 hours) were taken at 13 locations at the Wuestebach test site from January to May 2014 (Figure 12). These locations were selected in such a way that the CRP footprint contained distinctly different amounts of aboveground biomass.

3.2.2 Derivation of soil water content from CRP measurements

3.2.2.1 Required fast neutron flux corrections

The use of CRP measurements to determine soil water content requires a range of corrections of the measured neutron flux. Large-scale networks of CRPs need to consider corrections associated with varying cutoff rigidity (e.g. Zreda et al. 2012) but this is not required for the relatively small Rur catchment. In this study, we corrected measured fast neutron flux to standard air pressure (1013 hPa), a reference level of incoming cosmic ray intensity, and zero air humidity using the procedures described by Baatz et al. (2014). The corrected neutron flux is denoted as N_{pih}:

$$N_{pih} = N_{raw} \times \left\{ exp\left(\beta \times \left(P - P_{ref}\right)\right)\right\} \times \left\{I_{ref}/I\right\} \times \left\{1 + 0.0054 \times \left(\rho_{wv} - \rho_{ref}\right)\right\} \quad (29)$$

where the term $\left\{exp\left(\beta \times \left(P - P_{ref}\right)\right)\right\}$ describes the correction of air pressure P [hPa] at the time of measurement to a reference pressure P_{ref} = 1013 hPa using the barometric pressure coefficient β = 0.0076 hPa^{-1} (Desilets and Zreda 2003), $\left\{I_{ref}/I\right\}$ describes the correction of incoming cosmic ray intensity I [counts per second] to a reference incoming cosmic ray intensity I_{ref} [counts per second] (Zreda et al. 2012) obtained from the Neutron Monitor Database (NMDB), and $\left\{1 + 0.0054 \times \left(\rho_{wv} - \rho_{ref}\right)\right\}$ describes the correction for atmospheric water content at 2 meter height [g m^{-3}] to a reference atmospheric water content of ρ_{ref} = 0 g m^{-3} (Rosolem et al. 2013).

This study also considers corrections for sensor-specific counting efficiency as introduced by McJannet et al. (2014). Counting efficiency of a CRP may vary due to differences in the polyethylene shielding thickness or in the pressure of the Helium gas and should be considered to improve comparability between CRPs within a network. For this correction, a reference CRP with two moderated counters was placed next to each permanent CRP station for a period of at least 10 hours. An efficiency scaling factor η_{ref} was determined for each CRP from these reference CRP measurements using:

$$\eta_{ref} = N_{ref}/N_i \quad (30)$$

where N_{ref} [cph] is the mean raw neutron flux of the reference CRP over the measurement interval and N_i [cph] is the corresponding mean neutron flux of the CRP that requires correction for counting efficiency. The final corrected neutron flux that also considers counting efficiency, N_{epih}, was then obtained using:

$$N_{epih} = N_{pih} \times \eta_{ref} \quad (31)$$

3.2.2.2 Support volume of CRPs

The support volume of CRP measurements is often defined as the volume from which 86% of the fast neutrons originate (Zreda et al. 2008). According to Desilets and Zreda (2013), the horizontal CRP footprint is approximately 300 meter in radius at sea level, depending on air density, elevation, and air humidity. If soil water content within the CRP footprint follows a Gaussian random field model, the spatial variability of soil water content has a negligible impact

on fast neutron flux. In this case, the weighted horizontal average soil water content is measured by the CRP (Franz et al. 2013b). The decrease in sensitivity with distance from the CRP needs to be considered when environmental factors that affect CRP measurements, such as soil water content and biomass, are heterogeneously distributed within the footprint. This can be achieved with the COSMOS calibration scheme (Zreda et al. 2012), which divides the horizontal footprint into three radii at 25, 75 and 175 meters, and proposes to take calibration measurements every 60 degrees (i.e. 6 points). This results in a set of 18 calibration samples that can be arithmetically averaged to obtain the mean properties within the footprint because of the appropriately chosen radii (Zreda et al. 2012). A second approach for horizontal weighting was suggested by Bogena et al. (2013). They used the cumulative fraction of counts in the horizontal footprint (Zreda et al. 2008) to calculate appropriate weighting factors for horizontal segments with increasing radii up to 300 meters (Franz et al. 2013b).

The depth of the CRP support volume was investigated by Franz et al. (2012b) and ranges from 10 cm for moist soils up to 70 cm for dry silicate soils. We adopted the vertical weighting scheme developed by Bogena et al. (2013) to assign weights to vertical layers of soil water content. Similar to the exponential weighting used in the COSMIC operator (Shuttleworth et al. 2013), this scheme considers non-linear weighting for the vertically heterogeneous soil water content distributions that are typically encountered in real-world conditions.

3.2.2.3 Conversion of fast neutron flux to soil water content

We used three methods to convert neutron flux to soil water content: (i) the N_0-method, (ii) the COSMIC operator and (iii) the *hmf*-method. The N_0-method allows direct conversion of measured fast neutron flux (N_{epih}) to soil water content (Desilets et al. 2010) using:

$$\theta_{grav} = \theta_{vol} \times \rho_{h2o}/\rho_{bd} = a_0 \times \left(N_{epih}/N_0 - a_1\right)^{-1} - a_2 \quad (32)$$

where a_0 = 0.0808, a_1 = 0.372, and a_2 = 0.115 are semi-empirical parameters that are constant for all sites, N_0 is a site-dependent time-constant calibration parameter, θ_{grav} is the total gravimetric soil water content (soil water content plus lattice water in g g^{-1}) (Zreda et al. 2012), θ_{vol} is the total volumetric soil water content [cm^3 cm^{-3}], ρ_{h2o} is the density of water [g cm^{-3}],

and ρ_{bd} is the dry soil bulk density [g cm^{-3}]. N_0 is determined using weighted mean total gravimetric soil water content and measured corrected neutron flux over a short time interval.

The COSMIC operator was developed to use CRP measurements in data assimilation (Shuttleworth et al. 2013). The conversion of the neutron signal into soil water content profiles by the COSMIC operator was analyzed in detail by Rosolem et al. (2014). A recent evaluation by Baatz et al. (2014) showed that COSMIC can also be used to obtain accurate soil water content estimates from fast neutron flux measurements. In this study, the COSMIC operator was parameterized with a site-specific mean bulk density (0-30 cm), high-energy neutron-soil interaction constants L_1 = 162.0 g cm^{-2} and L_2 = 129.1 g cm^{-2}, fast neutron-soil interaction constants $L_3 = -31.65 + 99.29 \times \rho_{bd}$ and L_4 = 3.16 g cm^{-2}, and an efficiency factor $\alpha = 0.404 - 0.101 \times \rho_{bd}$ for the relative efficiency to create fast neutrons. Like for the N_0-method, lattice water and soil water content make up the total soil water content. A site-specific calibration parameter N_{COSMIC} was determined using measured corrected neutron flux and weighted mean total soil water content at the time of calibration.

The universal calibration function or hydrogen molar fraction method (*hmf*-method) was developed to enable calibration of CRPs at locations where it is difficult to undertake in-situ calibration measurements (Franz et al. 2013a). The hydrogen molar fraction (*hmf*) is calculated with:

$$hmf = \sum H / \sum E_{all} \quad (33)$$

where $\sum H$ in mol is the sum of all moles of hydrogen within the CRP footprint and $\sum E_{all}$ in mol is the sum of all moles of all elements which include for simplicity air (NO), dry soil (SiO_2), soil carbon (C), and vegetation besides the sources of water and hydrogen (H_2O). In this simplified approach, vegetation consists of water and cellulose ($C_6H_{12}O_5$) only, and it was initially assumed that vegetation was present as a layer on top of the soil. Using the MCNPx code, Franz et al. (2013a) found a monotonic decreasing exponential relationship between neutron flux and *hmf*:

$$N_{epih}/N_s = a \times \exp(b \times hmf) + c \times \exp(d \times hmf) \quad (34)$$

where N_S is a universal calibration parameter and a = 4.486, b = -48.1, c = 4.195 and d = -6.181 are constants. McJannet et al. (2014) updated the parameters of Eq. 34 to a = 3.007, b = -

48.391, c = 3.499 and d = 5.396 based on their calibration data and additional MCNPx simulations which assumed that CRPs measure an additional 30% of slow neutrons. We consider both parameterizations in the remainder of this study. Additional simulations and explicit modeling of tree trunks with the MCNPx code revealed that tree biomass cannot be simplified as a layer upon the soil as assumed in the derivation of *hmf* in Eq. 33 (Franz et al. 2013c). Therefore, Franz et al. (2013c) proposed an additional correction factor (CBWE) which has to be multiplied with corrected neutron flux to relate the moderation efficiency of water located in discrete objects (i.e. tree trunks) to an equivalent layer of water. One method to determine CBWE is to model trunk size, distribution and volume of trees in the CRP footprint using a neutron interaction model. Alternatively, N_S can be treated as a calibration parameter that includes the effect of all hydrogen pools and an appropriate value of N_S can be estimated from measured corrected neutron flux at the time of calibration.

3.2.3 Quantification of surface and sub-surface parameters

3.2.3.1 CRP calibration with in-situ soil sampling

Soil samples for calibration of the permanent CRPs were taken with a HUMAX soil corer (Martin Burch AG, Rothenburg, Switzerland; dimensions: 300 mm in length, 50 mm in diameter), following the COSMOS sampling scheme described earlier. Each soil core was split into six segments of 5 cm length and subsequently dried in the oven at 105°C for 48 hours. This resulted in 108 samples for which the gravimetric soil water content, dry soil bulk density, and volumetric soil water content were determined from the wet and dry weight and the known sample volume. Lattice water was determined through combustion of 15 mg aliquots of dried, grinded, and 2 mm sieved soil at 1000°C using a heat conductivity detector. Lattice water in the present study includes hydrogen from organic and inorganic compounds. Root biomass was not considered in this study because measurements of root biomass are difficult to make and subject to large uncertainty. In addition, hydrogen of root biomass contributes only to a small degree to the total hydrogen pools within a CRP footprint Bogena et al. (2013). Neutron flux was averaged over a 12 hour time window at the time of calibration to determine N_0, N_{COSMIC} and N_S from the sampling results (see Table 7).

Table 7: Results of the sixteen calibration campaigns at the permanent CRPs (dry soil bulk density (ρ_{bd}), lattice water (lw), volumetric water content (θ_{vol}), total gravimetric soil water content (θ_{grav}), CRP efficiency factor (η_{ref}), biomass water equivalent (BWE), dry aboveground biomass (AGB_{dry}), corrected fast neutron flux (N_{epih}), and calibration parameters N_0, $N_{S,a}$ *(after Franz et al. 2013a)* and $N_{S,b}$ *(after McJannet et al. 2014)*, and efficiency of a temporary CRP used in the Wuestebach experiment.

Location	ρ_{bd}	lw	θ_{vol}	θ_{grav}	η_{ref}	BWE	AGB_{dry}	N_{epih}	N_0	$N_{S,a}$	$N_{S,b}$
	g cm^{-3}	cm^3 cm^{-3}	cm^3 cm^{-3}	g g^{-1}		kg m^{-2}	kg m^{-2}	cph	cph	cph	cph
Aachen	1.12	0.058	0.38	0.39	1.01	3.3	1.2	631	1188	485	501
Aachen	1.20	0.063	0.27	0.28	1.01	3.3	1.2	691	1194	474	497
Gevenich	1.31	0.034	0.26	0.22	0.97	3.7	1.4	744	1216	475	503
Gevenich	1.42	0.037	0.15	0.13	0.97	3.7	1.4	829	1181	431	469
Heinsberg	1.27	0.039	0.34	0.30	0.97	2.7	1.2	683	1203	477	499
Kall	1.31	0.086	0.33	0.32	1.00	1.0	0.4	710	1277	500	523
Merzenhausen	1.39	0.039	0.19	0.16	0.98	3.6	1.3	808	1217	458	492
Merzenhausen	1.27	0.035	0.27	0.24	0.98	3.6	1.3	719	1198	470	496
Merzenhausen	1.34	0.037	0.12	0.12	0.98	3.6	1.3	865	1197	426	466
Rollesbroich	1.09	0.068	0.46	0.48	1.00	0.6	0.2	618	1218	483	498
RollesbroichN	1.09	0.072	0.56	0.58	1.01	0.7	0.3	535	1100	442	453
RurAue	1.11	0.046	0.28	0.29	1.04	4.9	2.5	673	1166	470	491
RurAue	1.12	0.047	0.35	0.35	1.04	4.9	2.5	634	1165	479	496
Wildenrath	1.21	0.027	0.14	0.14	1.07	29.1	16.3	735	1066	543	564
Wildenrath	1.15	0.026	0.19	0.19	1.07	29.1	16.3	661	1038	553	565
Wuestebach	0.83	0.067	0.35	0.50	0.90	53.2	30.0	428	848	633	602
Temp. CRP	-	-	-	-	1.19	-	-	-	-	-	-

3.2.3.2 CRP calibration with SoilNet data

Temporary CRP measurements were made at several locations in the deforested area of the Wüstebach catchment (see Figure 12). These temporary CRP measurements were calibrated using the mean soil water content determined from SoilNet for each time period and measurement location , the mean dry bulk density of the A and B horizon determined from soil samples at each SoilNet location (Bogena et al. 2014), and the mean lattice water content determined by Bogena et al. (2013) for this catchment (see Table 8). For this, SoilNet data were averaged to obtain hourly values. Periods with snow and soil temperatures below 0°C were not considered and soil water content measurements with unrealistic values (< 0 cm^3 cm^{-3} or > 1 cm^3 cm^{-3}) were excluded from the analysis. After adding lattice water to the volumetric soil water content measured by SoilNet, the mean vertically weighted total soil water content was calculated for each SoilNet node using the method described in Bogena et al. (2013). For each individual calibration for a particular time period and CRP measurement location, a variogram was estimated based on temporally averaged vertically weighted total soil water content at each SoilNet node. This variogram served to interpolate soil water content on a grid with 1 m resolution using ordinary kriging. The mean total soil water content for the CRP footprint was then obtained by averaging 360 interpolated total soil water content values at the three radii from the COSMOS sampling scheme (25, 75 and 175 m).

Table 8: Measurement and calibration results of the thirteen temporary CRP locations (measurement hours (nr), dry soil bulk density (ρ_{bd}), total gravimetric soil water content (θ_{grav}), biomass water equivalent (BWE), dry aboveground biomass (AGB_{dry}), neutron flux (N_{epih}), vegetation corrected neutron flux (N_{epihv}), the N_0 calibration parameter, N_{COSMIC} for not vegetation and vegetation corrected neutron flux, and calibration parameters $N_{S,a}$ *(after Franz et al. 2013a)* and $N_{S,b}$ *(after McJannet et al. 2014)*).

id	nr	ρ_{bd}	θ_{grav}	BWE	AGB_{dry}	N_{epih}	N_{epihv}	N_0	$N_{COSMIC,1}$	$N_{COSMIC,2}$	$N_{S,a}$	$N_{S,a}$
	hours	g g^{-1}	g g^{-1}	kg m^{-2}	kg m^{-2}	cph	cph	cph	cph	cph	cph	cph
1	72	0.90	0.56	51.5	29.1	420	574	854	152	207	633	600
2	191	0.85	0.63	47.4	26.7	419	556	872	156	207	624	593
3	98	0.83	0.65	36.9	20.8	447	553	936	168	208	603	580
4	94	0.83	0.69	28.5	16.1	491	577	1039	186	219	610	593
5	27	0.83	0.76	22.8	12.9	516	585	1111	200	227	611	598
6	24	0.80	0.69	16.0	9.0	517	564	1094	197	215	548	543
7	47	0.79	0.83	14.8	8.3	469	508	1025	185	201	509	503
8	405	0.82	0.71	15.5	8.7	531	578	1129	203	221	563	558
9	129	0.81	0.76	15.8	8.9	493	537	1060	191	208	532	526
10	112	0.88	0.45	50.3	28.4	434	588	840	148	200	609	583
11	190	0.83	0.65	22.6	12.8	490	556	1027	184	209	559	550
12	190	0.82	0.64	23.3	13.1	478	544	998	179	203	547	538
13	190	0.81	0.71	13.8	7.8	501	540	1065	192	206	518	515

3.2.3.3 Quantification of aboveground biomass

Aboveground biomass was estimated from biomass samples and land use maps at the permanent CRP locations. On the 18th and 19th of July 2013, 18 aboveground biomass samples were taken at the permanent CRP locations Aachen, Merzenhausen, and Gevenich with a clipper size of 20 by 20 cm. This resulted in samples of several different crop types (e.g. winter wheat, sugar beet, rape, maize and potato with 30, 9, 4, 3 and 1 sample each, respectively) and grassland (7 samples). These samples were weighted and dried individually at 105°C in a ventilated oven during 48 hours to determine dry aboveground biomass according to the ASTM E-1756 standard. The vegetation water content was estimated from the weight loss after drying. Total biomass water equivalent consists of vegetation water as well as hydrogen and oxygen present in other molecules within the dry aboveground biomass. Here, we assume that this water equivalent in dry aboveground biomass can be approximated by the amount of hydrogen and oxygen contained in cellulose ($C_6H_{10}O_5$), i.e. ~55.6 % by weight. The aboveground biomass samples taken in the cropland and grassland of these three sites are assumed to be representative for all grassland and cropland in the Rur catchment. In addition, dry aboveground biomass of forest in the Rur catchment was assumed to be 18.4 kg m^{-2} (Oehmichen et al. 2011) following average characteristics of coniferous and deciduous forests in Germany. We assumed that forest vegetation water content was 56 % (Nurmi 1999). Land use fractions within a 300 m radius around the CRP were determined using a 15 m resolution land use map obtained from remote sensing data (Waldhoff 2012). In a final step, the mean dry aboveground biomass and mean biomass water equivalent of each CRP footprint were determined from the biomass water equivalents and dry aboveground biomass for the respective land use fractions (Table 6).

At the Wuestebach test site, aboveground forest biomass was determined directly on site by Etmann (2009). Vegetation is primarily (97 % by weight) cultivated Norway Spruce (Picea abies L.) with an age of ~65 years. Median breast height diameter was 38.0 cm with an average density of 370 trees per ha. Extensive field sampling and application of allometric functions yielded a dry aboveground forest biomass of 30 kg m^{-2} (Etmann 2009), which is much higher

than the average aboveground biomass of German forests due to the high planting density of this Spruce stand. The vegetation water content at the Wuestebach site was found to be between 49 % and 67 % of total wet aboveground biomass (Etmann 2009), similar to what was found by Nurmi (1999).

For the deforested area at Wuestebach (Figure 12), we assumed that a small amount of aboveground biomass remained after deforestation as tree stumps, litter, and remaining or emerging vegetation (3 % or AGB_{dry} = 1 kg m^{-2}). The heterogeneous distribution of aboveground biomass within the footprints of the temporary CRPs located in the Wuestebach catchment (Figure 12) was considered using the radial segment-based weighting scheme described previously in Section 3.2.2.2.

3.2.4 Analysis of vegetation impacts on neutron flux

3.2.4.1 Regression of biomass and fast neutron flux

From the calibration data set of the permanent CRPs (Table 7), a regression equation between site-specific N_0 and dry aboveground biomass or biomass water equivalent was established:

$$N_0 = -r_1 \times AGB_{dry} + N_{0,AGB=0} \quad 35$$

$$N_0 = -r_2 \times BWE + N_{0,BWE=0} \quad 36$$

where r_1 in cph per kg dry aboveground biomass per m^2 and r_2 in cph per kg of biomass water equivalent per m^2 represent the change in N_0 with aboveground biomass AGB_{dry} [kg m^{-2}] or biomass water equivalent BWE [kg m^{-2}], and $N_{0,AGB=0}$ and $N_{0,BWE=0}$ [cph] is the reference N_0 for an aboveground biomass and biomass water equivalent of 0 kg m^{-2}.

3.2.4.2 The empirical vegetation correction for neutron flux

From the ratio $N_{epih} \,/\, N_0$ in Eq. 32 we derive the more general relationship $N_{epih}/N_0 = N_{epihv}/N_{0,AGB=0}$ where N_{epihv} is the fast neutron flux corrected for vegetation (v). In order to determine N_{epihv} directly, we substituted N_0 with Eqs. 35 and 36. The new vegetation-corrected neutron flux N_{epihv} is then determined with the vegetation correction factor f_{veg} using:

$$N_{epihv} = N_{epih} \times f_{veg} = N_{epih} \times \left(1 - r_1 / N_{0,AGB=0} \times AGB_{dry}\right)^{-1} \quad 37$$

$$N_{epihv} = N_{epih} \times f_{veg} = N_{epih} \times \left(1 - r_2 / N_{0,BWE=0} \times BWE\right)^{-1} \quad 38$$

The implementation of the vegetation correction into Eq. 32 yields the relationship between neutron flux and total gravimetric soil water content:

$$\theta_{grav} = a_0 \times \left(N_{epihv} / N_{0,AGB=0} - a_1\right)^{-1} - a_2 \quad 39$$

Eq. 39 represents a direct relationship between gravimetric soil water content, biomass, and fast neutron flux that should be valid across a wide range of soils. With knowledge on biomass variation in time and space, mean lattice water content, and the single vegetation independent calibration parameter $N_{0,AGB=0}$, it should be possible to determine soil water content directly from fast neutron flux. It is important to realize that the relationship between volumetric water content and fast neutron flux is more complicated because of the dependence on soil bulk density that varies considerably between sites (see Table 7). Therefore, CRP results that compare soil water content of more than one site are presented in terms of gravimetric water content in the remainder of this study. Results at a single site are presented in volumetric soil water content for ease of interpretation by the reader.

3.2.4.3 Evaluation of the proposed vegetation correction

We evaluated the proposed vegetation correction in four different ways. In the first test case, the predictions by Eqs. 35 and 36 were compared with results from the temporary CRP measurements at the Wuestebach test site (Figure 12). The measurements were made along a steep biomass gradient, which required horizontal weighting to obtain mean aboveground biomass in the CRP footprints as described in Section 3.2.3.3. Average soil water content was than determined as described in Section 3.2.3.2. Using mean neutron flux and total soil water content over the measurement period, N_0 was determined using Eq. 32 and compared to the predicted N_0 from the regression equations (Eqs. 35 and 36).

Secondly, we tested the vegetation correction (Eq. 35) for a case where an abrupt change in aboveground biomass occurred (i.e. a deforestation experiment). For this, the permanent Wuestebach CRP was calibrated using gravimetric sampling in 2012. The resulting soil water

content estimates were already compared to in-situ soil water content measurements from the SoilNet by Baatz et al. (2014). After the deforestation, both the measured neutron flux and the site-specific N_0 are expected to increase due to the removal of hydrogen contained in vegetation from the CRP footprint. Therefore, we used the relative change in dry aboveground biomass to determine a new site-specific N_0 from the previously in-situ determined N_0 using Eq. 35. From Apr. 3rd 2014 to May 27th 2014, daily soil water content estimates derived from CRP measurements using the N_0 of the 2012 calibration campaign and the vegetation-corrected N_0 were then compared to in-situ soil water content measurements from SoilNet.

In the third case, we compared in-situ SoilNet measurements of soil water content at locations with low, intermediate and high biomass with soil water content predictions obtained from CRP using efficiency and vegetation-corrected neutron flux measurements and a single $N_{0,\,AGB=0}$ (Eq. 39). The Rollesbroich test site is permanent grassland and represents the low biomass case. The Wuestebach test site before deforestation represents the high biomass case. For both sites, daily mean soil water content estimates derived from SoilNet and CRP were compared for 2012. These two sites were already used by Baatz et al. (2014) for evaluation of the CRP measurements. The difference in this study is that the neutron flux is corrected for counting efficiency and vegetation, and that a single $N_{0,AGB=0}$ is used to estimate soil water content (Eq. 39). For the intermediate biomass case, daily SoilNet data were compared with soil water content estimates derived from the permanent CRP measurements at the Wuestebach test site after the deforestation for the period from April to May 2014.

In the fourth and final test case, the COSMIC operator and the *hmf*-method were used. The COSMIC operator is much more complex in architecture than the N_0-method. The calibration parameter of the COSMIC operator N_{COSMIC} was determined for every CRP station in the Rur catchment using neutron flux data with and without a vegetation correction. The standard deviation of N_{COSMIC} was then used to test the efficiency of the vegetation correction in reducing variability of the site-specific N_{COSMIC} parameter. The same was done for the *hmf*-method, keeping in mind that vegetation is considered in the *hmf*-method (Eq. 33). The N_S calibration parameter was determined from measured corrected neutron flux with and without the

empirical vegetation correction. When calibrating N_S using vegetation-corrected neutron flux N_{epihv}, vegetation ($C_6H_{12}O_5$ and H_2O) was removed from the estimation of the hydrogen molar fraction (Eq. 33) because we assume that the vegetation correction also removes the vegetation signature in measured neutron flux.

3.3 Results

3.3.1 Calibration campaigns and vegetation estimates

Mean soil parameters for the different calibration campaigns are presented in Table 7. Bulk density was lowest at the Wuestebach test site (ρ_{bd} = 0.83 g cm^{-3}) and highest at the Gevenich test site (ρ_{bd} = 1.42 g cm^{-3}). Lattice water content ranged from 0.03 cm^3 cm^{-3} to 0.09 cm^3 cm^{-3}, volumetric water content from 0.12 cm^3 cm^{-3} to 0.56 cm^3 cm^{-3}, and gravimetric soil water content ranged from 0.12 g g^{-1} to 0.58 g g^{-1}.

Mean dry aboveground biomass of cropland and grassland were 1.61 kg m^{-2} and 0.27 kg m^{-2}, respectively, whereas the associated mean biomass water equivalent was 4.46 kg m^{-2} and 0.64 kg m^{-2}. These mean values compare well with other measurements in the Rur catchment during the same time of the year (Korres et al. 2013). After consideration of the land use fractions, the mean dry aboveground biomass within the footprint of the 10 CRP stations ranged from 0.2 kg m^{-2} to 30 kg m^{-2}, or between 0.6 kg m^{-2} and 53.2 kg m^{-2} in terms of total biomass water equivalent (Table 7).

3.3.2 Sensor-specific efficiency correction

Sensor-specific counting efficiencies for all ten CRPs ranged from 0.90 to 1.19 (Table 7). This large variation in counting efficiency indicates a significant sensor-to-sensor variability for the CRP probe type used in this study. To test our efficiency correction approach, we compared fast neutron flux measurements of the permanent Wuestebach station (lowest counting efficiency) with data from a nearby temporary measurement location (<5 m) with a CRP that showed the highest counting efficiency. The uncorrected neutron flux measurements of both CRPs show considerable differences in magnitude (Figure 13). After application of the efficiency correction,

this offset has been removed, which demonstrates the effectiveness of this simple correction approach (Figure 13).

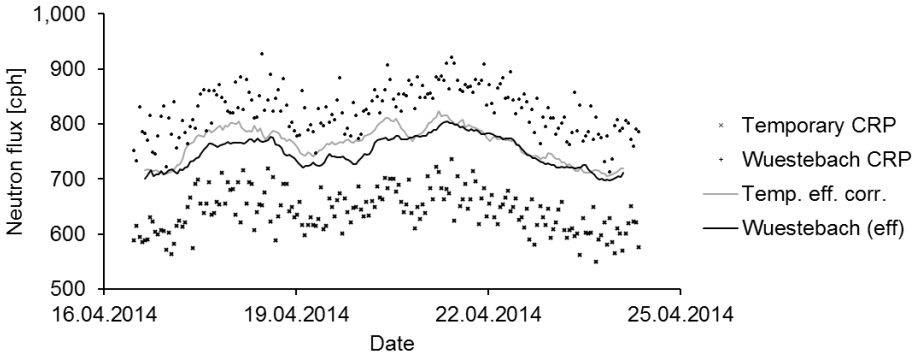

Figure 13: Parallel neutron flux measurements of the permanent Wuestebach CRP (η_{ref} = 0.90) and a temporary CRP (η_{ref} = 1.19) placed next to the Wuestebach CRP for testing the efficiency correction. Hourly raw neutron flux measurements are shown as points. Ten hour running mean efficiency corrected neutron flux for both CRPs are shown as lines.

3.3.3 Vegetation correction

We used data from the sixteen in-situ soil sampling campaigns (Table 7) to determine site-specific N_0-values according to the approach of Baatz et al. (2014). The lowest N_0 value was found for the permanent CRP at the Wuestebach site (forest, N_0 = 848 cph), and the largest value was found for the CRP at the Kall site (grassland, N_0 = 1277 cph). These N_0 values show a strong correlation to dry aboveground biomass (R^2 = 0.87, Figure 14) and biomass water equivalent (R^2 = 0.86). Therefore, we used a linear regression to estimate N_0 as function of dry aboveground biomass (Eq. 35). We found r_1 = 11.2 cph per kg of dry aboveground biomass per m^2 (i.e. a decrease of N_0) and the intersection with the y-axis at $N_{0,AGB=0} = 1210$ cph (i.e. for 0 kg m^{-2} aboveground biomass). For BWE, we found r_2 = 6.4 cph per kg of BWE per m^2 and $N_{0,BWE=0} = 1215$ cph. For the more generalized form of the vegetation correction or reference conditions different than ours (efficiency, pressure, incoming cosmic ray intensity, air humidity and cutoff rigidity), we found a neutron flux reduction by $r_1/N_{0,AGB=0} = 0.9\,\%$ per kg of dry

aboveground biomass or $r_2/N_{0,AGB=0} = 0.5\ \%$ per kg of biomass water equivalent (Eqs. 37 and 38).

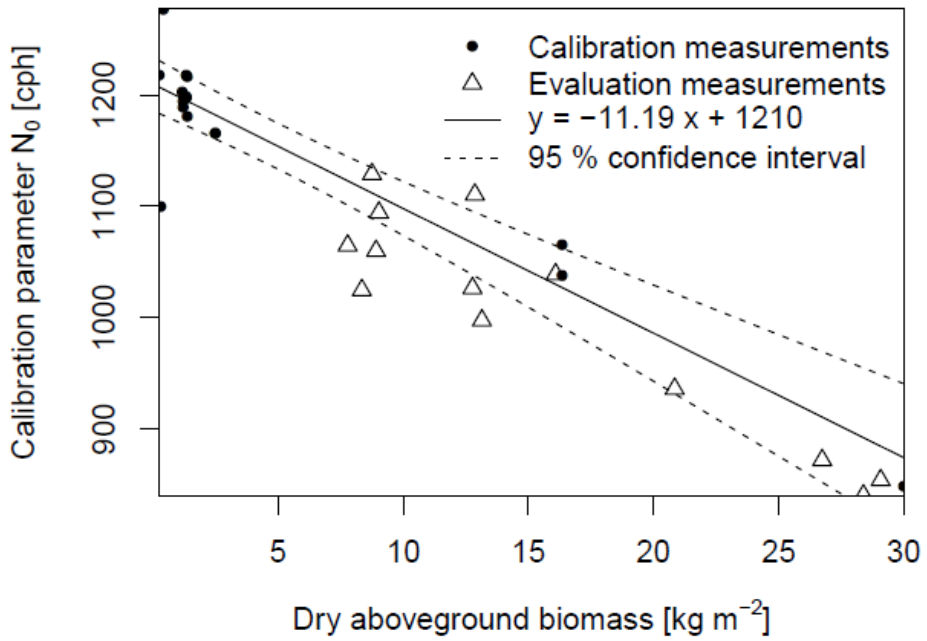

Figure 14: Calibration parameter N_0 in relation to aboveground biomass for the 16 field calibrations from Baatz et al. (2014) with sensor-specific efficiency correction included (dots), the regression of N_0 to dry aboveground biomass (black line) and 95 % confidence interval, and the Wuestebach calibration parameters (triangles). Intercept and slope are 1210 cph and 11.18 cph per kg of dry aboveground biomass per m^2, respectively, R^2 = 0.866 and p = 1.702e-07.

3.3.4 Evaluation of biomass correction at the Wuestebach test site

The temporary CRP measurement locations at the Wuestebach test site (Figure 12) were selected to cover a wide range of dry aboveground biomass. The aboveground biomass for every 5 meter segments for each of the thirteen temporary CRP locations is shown in Figure 15. It can be seen that CRPs located in the center of the deforested area showed low aboveground biomass at small distances to the CRP station, but biomass progressively increased with increasing distance. Even CRP stations located in the center of the deforested area were only

200 m away from the large amount of aboveground biomass in the nearby forest. CRP stations located in the forest show a decreasing aboveground biomass with increasing radius to the CRP. Weighted biomass of those stations is relatively high with $AGB_{dry} \geq 20.8$ kg m^{-2}. After applying the horizontal weighting function (also see Figure 15) to these biomass distributions, we obtained weighted mean dry aboveground biomass ranging from 7.7 kg m^{-2} to 29.1 kg m^{-2} for the temporary CRP stations.

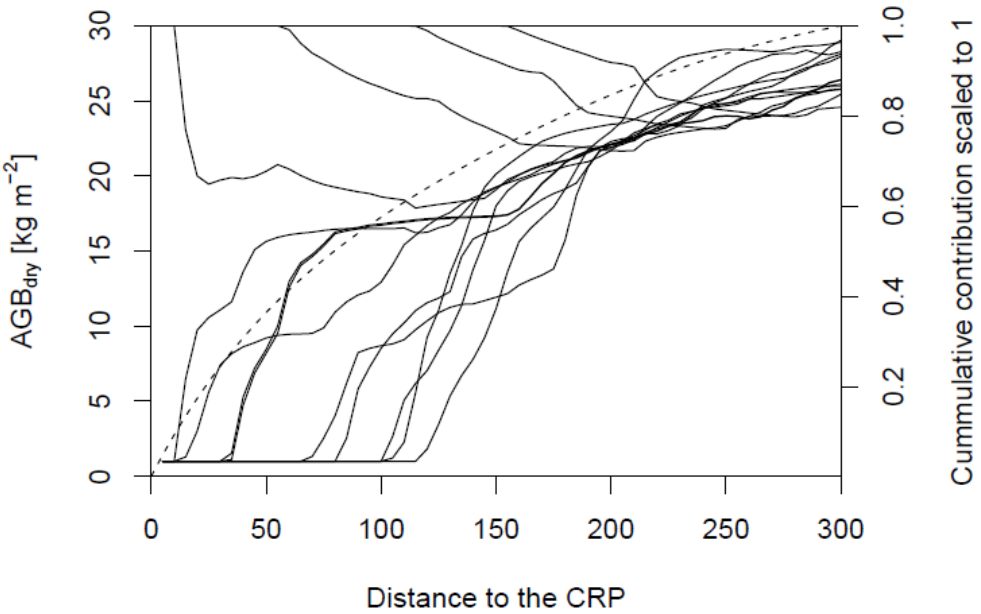

Figure 15: Aboveground biomass estimates for radial segments of the temporary CRPs at Wuestebach using the horizontal weighting scheme of Bogena et al. (2013) with 5 meter steps. The dashed line shows the cumulative contribution of the segments to a total of 1.

As expected, measured neutron flux (N_{epih}) was lowest in the forested part of the Wuestebach catchment (367 cph), and highest in the deforested area (464 cph) during the calibration period of the temporary CRP measurements. Mean total volumetric soil water content for calibration of the temporary CRPs ranged from 0.39 to 0.65 cm^3 cm^{-3}, and total gravimetric soil water content ranged between 0.44 and 0.82 g g^{-1}. The derived N_0 for the temporary CRP measurements decreased from 1129 cph for the deforested area to 840 cph for the forested

area (Figure 12). The evaluation data confirm the clear trend of a reduction in N_0 with increasing aboveground biomass and were close to the regression line derived from the soil sampling calibration data set (Root Mean Squared Error (RMSE) = 47 cph). Overall, these measurements strongly support the relationship between N_0 and dry aboveground biomass that was presented earlier.

3.3.5 Evaluation of vegetation correction in case of an abrupt change in biomass

The second evaluation of the vegetation correction uses data from the Wuestebach test site under forested (in 2012) and deforested (in 2014) conditions. The Wuestebach CRP was calibrated in 2012 with in-situ soil samples (Table 7) and we found N_0 = 848 cph and an RMSE of 0.03 cm^3 cm^{-3} between soil water content estimates from CRP and SoilNet. After the deforestation, the corrected neutron flux (N_{epih}) showed a strong increase (Figure 16), as expected from the decrease in biomass. Soil water content estimates with the previously obtained N_0 resulted in an underestimation of soil water content in 2014 and a high offset (RMSE = 0.29 cm^3 cm^{-3}). Using the previously derived vegetation correction, we found a new N_0 = 1037 cph for a vegetation reduction from 30 to 13.1 kg m^{-2}. The accuracy of the soil water content estimates using the corrected N_0 was close to the accuracy achieved in 2012 before deforestation (RMSE = 0.03 cm^3 cm^{-3}).

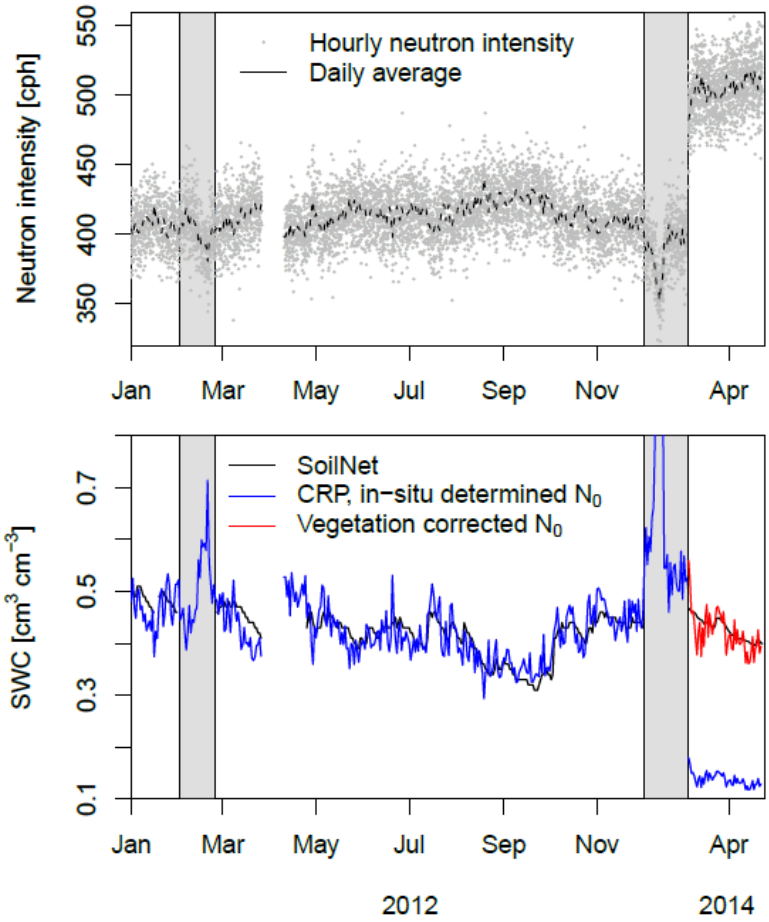

Figure 16: Measured corrected neutron flux (N_{epih}) from the Wuestebach CRP, hourly (gray dots) and daily averaged (dashed). The lower panel shows daily volumetric soil water content estimated with the calibrated site-specific N_0 (blue) and with the N_0 estimated from the vegetation correction function (red) under deforested conditions. The black line represents horizontally and vertically weighted soil water content measured with SoilNet. Gray shaded areas indicate periods with snow.

3.3.6 Evaluation of vegetation-corrected neutron flux N_{epihv} at multiple sites

The third evaluation of the vegetation correction compares soil water content derived with efficiency and vegetation-corrected neutron flux (N_{epihv}) and a single $N_{0,AGB=0} = 1210$ cph for three sites with different aboveground biomass to independent SoilNet measurements. The

estimated dry aboveground biomass at Rollesbroich was AGB_{dry} = 0.25 kg m^{-2}. At Wuestebach, dry aboveground biomass was estimated to be 30 kg m^{-2} before deforestation and 13.1 kg m^{-2} after deforestation. Hence, the vegetation correction (Eq. 37) was highest for the CRP station located in the forest of the Wuestebach catchment (f_{veg} = 1.38), intermediate for the CRP station located in the deforested area (f_{veg} = 1.14) and lowest for the grassland test site Rollesbroich (f_{veg} = 1.002). Figure 17 summarizes the three independent daily averaged time series of total gravimetric soil water content generated from horizontally and vertically weighted SoilNet measurements and fast neutron flux measurements from the permanent CRPs with (N_{epihv}) and without correction (N_{epih}). The gray markers indicate neutron flux measurements without vegetation correction. The vegetation correction shifted the count rates observed at all sites towards the previously derived calibration curve for $N_{0,AGB=0}$ = 1210 cph by the factor f_{veg}. Ideally, all measurements should fall together on the single calibration curve. Indeed, the fully corrected neutron flux data are closely grouped and coincide with the neutron flux – soil water content conversion derived earlier for the Rur catchment (Eq. 39, $N_{0,AGB=0} = 1210$ cph). Overall, the RMSE between gravimetric soil water content determined from CRP measurements and the reference gravimetric soil water content derived using SoilNet was 0.076 g g^{-1}. In terms of volumetric soil water content, the RMSE was 0.066 cm^3 cm^{-3}.

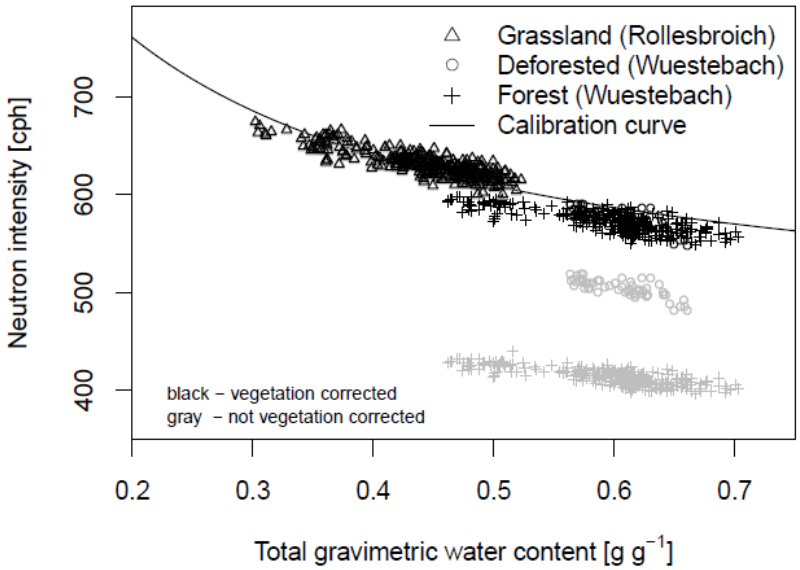

Figure 17: Daily average measured total gravimetric water content by SoilNet, not vegetation corrected (gray, N_{epih}) and vegetation corrected neutron flux (black, N_{epihv}) at the permanent CRP locations Rollesbroich and Wuestebach in 2012 and 2014. The black line represents the calibration curve with $N_{0,AGB=0}$ = 1210 cph to estimate soil water content from vegetation corrected neutron flux.

3.3.7 Indirect evaluation of the vegetation correction

In a fourth indirect evaluation of our method, we compared the standard deviation of the COSMIC calibration parameter N_{COSMIC} for calibrations with and without vegetation-corrected neutron flux. The standard deviation of N_{COSMIC} for the case without vegetation correction was 20 cph with a mean N_{COSMIC} of 187 cph. For this case, N_{COSMIC} showed a strong correlation with dry aboveground biomass and biomass water equivalent (R^2 = 0.80, Figure 18). If vegetation-corrected neutron flux N_{epihv} was used for COSMIC calibration, the resulting N_{COSMIC} calibration parameters had a reduced standard deviation of 9 cph and a mean N_{COSMIC} = 206 cph. Furthermore, correlation of N_{COSMIC} with aboveground biomass was strongly reduced (R^2 = 0.01). Our findings agree with Shuttleworth et al. (2013), who suggested that a large part of the N_{COSMIC} variability amongst different sites may be explained by variation in aboveground biomass amongst calibration sites.

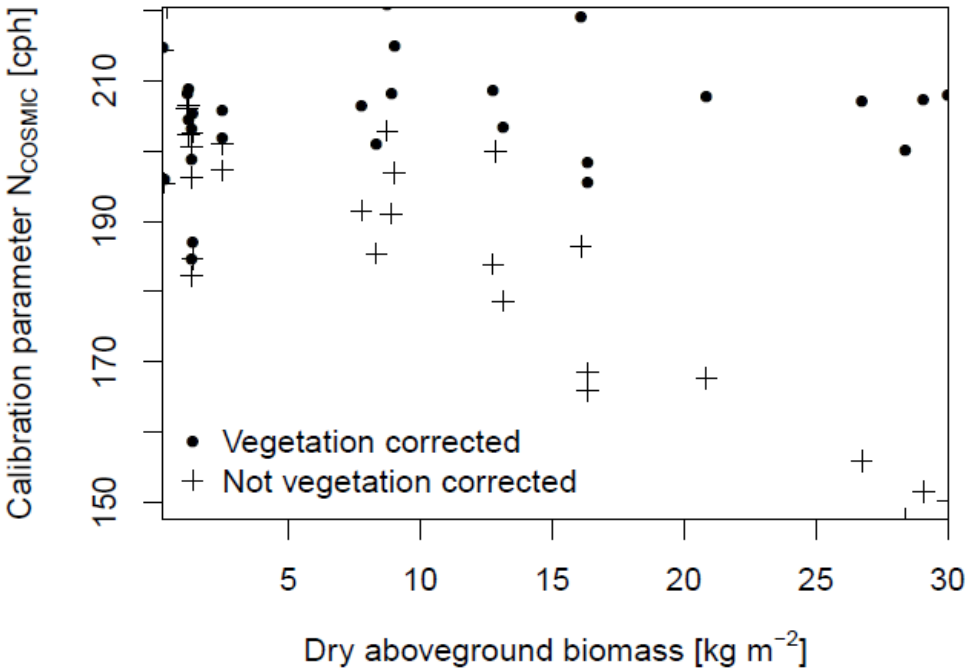

Figure 18: The COSMIC calibration parameter N_{COSMIC} without (N_{epih}, σ = 20 cph) and with vegetation corrected neutron flux (N_{epihv}, σ = 9 cph).

We also tested the hydrogen molar fraction method (*hmf*-method) (Franz et al. 2013a) with the complete calibration data set. After correction for sensor specific counting efficiency, the calibration parameter N_S was determined with N_{epih} (Table 7 and Table 8) for the parameters in Eq. 34 introduced by *Franz et al.* [2013b] and *McJannet et al.* [2014]. As in an earlier study made in the Rur catchment (Baatz et al. 2014), we found that the calibration parameter N_S correlated with aboveground biomass with R^2 = 0.92 and R^2 = 0.89 for the parameterizations of Franz et al. (2013a) and McJannet et al. (2014), respectively. The standard deviation of N_S was 64 cph and 44 cph, respectively. This strong correlation confirms that an additional *hmf*-specific correction factor (CBWE) is required by the *hmf*-method (Franz et al. 2013c). After application of the vegetation correction (Eq. 39) to neutron flux, the standard deviation of N_S decreased to 21 cph

and 17 cph for both parameterizations, respectively. The newly calculated hydrogen molar fraction without vegetation was then able to explain the variation of fast neutron flux at each location for both parameterizations to a satisfactory degree with R^2 = 0.91 and R^2 = 0.86, respectively. These results indicate that the empirical vegetation correction method is also able to enhance the *hmf*-method.

3.3.8 Sensitivity of fast neutron flux to aboveground biomass

Using the relationship between soil water content and vegetation-corrected neutron flux (Eq. 39), a sensitivity analysis was conducted to determine how soil water content predictions (Eq. 32) are affected by aboveground biomass. Figure 19 presents the calibration functions for four different amounts of dry aboveground biomass (0 kg m^{-2}, 1.5 kg m^{-2}, 15 kg m^{-2}, and 30 kg m^{-2}). The curves deviate from the reference calibration curve $N_{0,AGB=0} = 1210$ cph due to enhanced neutron moderation by additional hydrogen contained in the vegetation (Eq. 39). Soil water content estimates from CRP measurements are more affected by vegetation if soil water content is high, as illustrated by the triangles in Figure 19. For example, suppose that a CRP was calibrated at point A with $\theta_{grav} = 0.14$ g g^{-1} and neutron flux equaled 833 cph. We assume an increase in dry aboveground biomass from 0 to 15 kg m^{-2} (surely an extreme case). If the next neutron flux measured would be 718 cph, neglecting the change in aboveground biomass would result in a wrong soil water content estimate of θ_{grav} = 0.25 g g^{-1}, at point C. Instead the true soil water content is much lower θ_{grav} = 0.14 g g^{-1}. Repeating this experiment for higher soil water content would increase this offset. In many agricultural sites, much smaller changes in aboveground biomass are expected (e.g. up to 1.5 kg m^{-2}) due to growing crops. Using the calibration functions of AGB_{dry} = 0 kg m^{-2} and AGB_{dry} = 1.5 kg m^{-2} in Figure 19, it is possible to estimate the error introduced by neglecting this change in agricultural biomass. For low gravimetric soil water content of 0.1 g g^{-1}, the error is small with 0.006 g g^{-1}. For higher soil water content, the error increases to e.g. 0.025 g g^{-1} for a soil water content of 0.4 g g^{-1}.

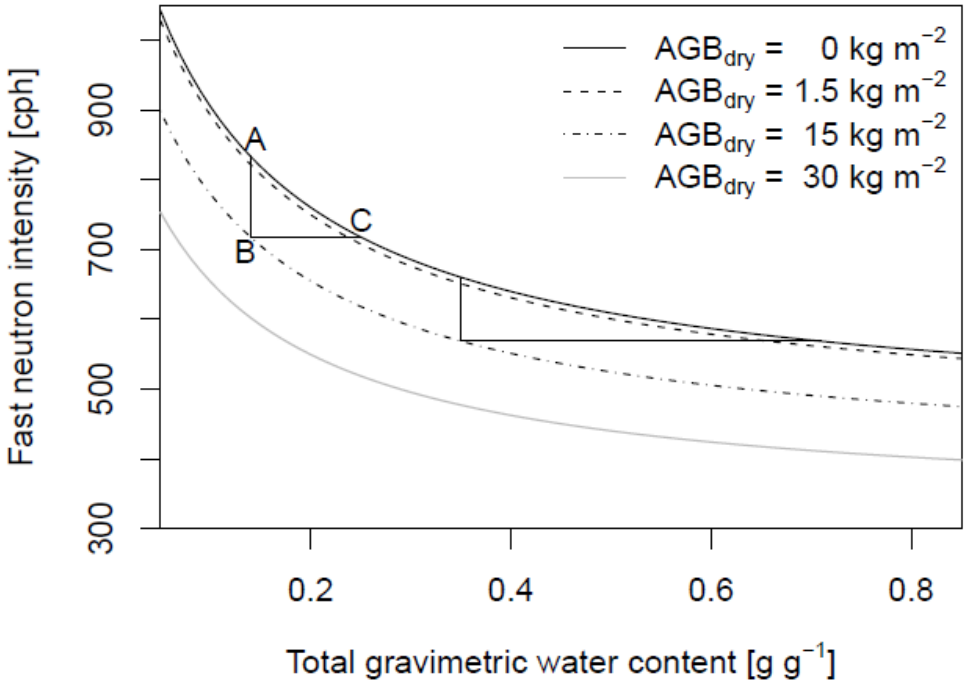

Figure 19: Sensitivity analysis of neutron flux soil water content calibration function (Eq. 29) for four cases of aboveground biomass. The four cases were calculated assuming $N_{0,AGB=0}$ = 1210 cph and the proposed neutron flux correction (Eq. 37). Applying the vegetation correction on measured fast neutron flux shifts the dashed and dotted to the solid line. As a result, the single extended N_0-method (Eq. 39) could be used for soil water content estimation. If transient vegetation is not considered, the triangles illustrate how this will increasingly impact soil water content estimates from neutron flux with increasing soil water content.

3.4 Discussion

The major advance in this study is the representation of neutron flux variability by a single relationship between soil water content and vegetation-corrected neutron flux. In particular, our measurements are well described by a single $N_{0,AGB=0}$ calibration function that explains 95 % of the observed vegetation-corrected neutron flux variability by soil water content variation for all sites analyzed in the Rur catchment (Figure 20). The remaining 5 % unexplained variability may be related to inter-annual changes in biomass, vegetation water content, the uncertainty of the empirical parameters in the vegetation correction, as well as uncertainties in the soil water

content and biomass estimation. In addition, strong spatial clustering of biomass in the CRP footprint might affect the relationship between CRP measurements and biomass (Franz et al. 2013c). Finally, root zone biomass has not been considered in our study. In forest systems this hydrogen pool is temporally stable and of less significance (Bogena et al. 2013). For agricultural sites, root biomass is temporally dynamic, which might lead to additional uncertainties associated with the transferability of the vegetation correction from one site to another. If neutron flux is not corrected for aboveground biomass, only 76 % of the fast neutron flux variability can be explained by variations in gravimetric soil water content (Figure 21).

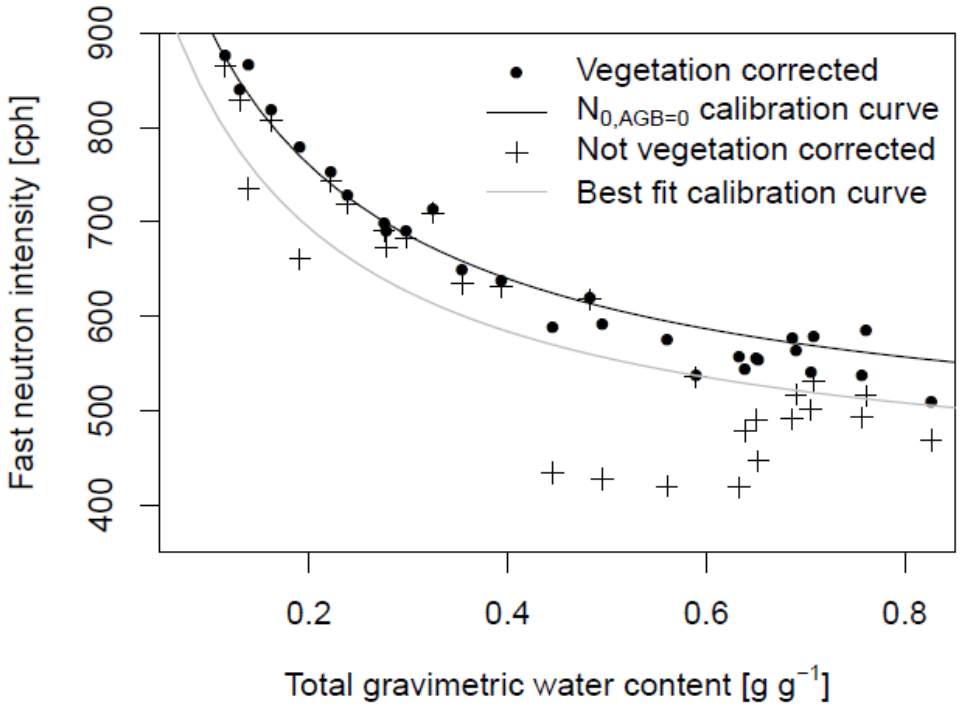

Figure 20: Neutron flux without vegetation correction (N_{epih}, R^2 = 0.75) and a fitted calibration function (gray), and neutron flux with vegetation correction (N_{epihv}, R^2 = 0.95) together with the extended calibration function $N_{0,AGB=0}$ = 1210 cph plotted jointly for the 16 calibration measurements in the Rur catchment and the 13 evaluation measurements at the Wuestebach test site.

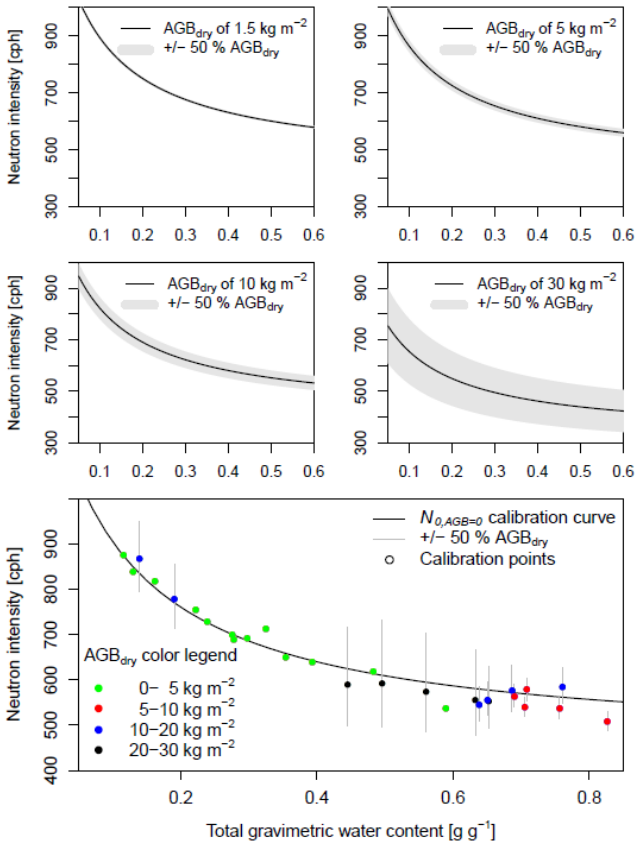

Figure 21: Uncertainty in neutron flux assuming an uncertainty of ± 50 % AGB_{dry} and $N_{0,AGB=0}$ = 1210 cph. The upper two panels, show resulting measured fast neutron flux N_{epih} for different biomass values, the lower panel shows the uncertainty of vegetation corrected neutron flux at the times of calibration based on biomass uncertainty.

In order to assess how uncertainty in the biomass estimates affects soil water content predictions, we assumed that the accuracy of the dry aboveground biomass estimate is 50 % (Figure 21). This is a realistic value for low biomass and a rather high value for high biomass. The resulting uncertainty in uncorrected neutron flux is shown for four cases of aboveground biomass in Figure 21 (top panel). For low biomass, the uncertainty is minor, but for large biomass the uncertainty is up to ± 50 neutron counts (10 kg m^{-2}) and ± 100 neutron counts (30 kg m^{-2}). We propagated this uncertainty using the vegetation correction on neutron flux into our

sets of calibration data (as in Table 7 and Table 8). The resulting uncertainty is shown as error bars in Figure 21. Particularly for conditions with high amounts of biomass, the error bars are large. This illustrates that a substantial part of the deviation from the $N_{0,AGB=0}$ calibration curve is possibly explained by the uncertainty in the biomass estimates.

It should be noted that hydrogen is the most important neutron moderator contained in vegetation. This highlights the relevance of vegetation water content for fast neutron moderation. Especially plants with high or variable vegetation water content (e.g. maize) require consideration of total hydrogen content. In such cases, vegetation correction should be based on BWE instead of AGB_{dry}.

The obtained results in the evaluation of the proposed correction confirm that reasonable soil water content estimates can be obtained using the empirically derived vegetation correction. Because of the additional uncertainty involved in the estimation of lattice water and bulk density, we found that site-specific calibration approaches provide more accurate volumetric soil water content estimates than e.g. regional and global calibration functions (see also Franz et al. 2013a). As shown in other studies (e.g. Franz et al. 2013c), a combined approach of site-specific calibration and a vegetation correction for changing biomass appears to be the optimal approach for soil water content retrieval using CRPs. In future work, remote sensing of vegetation (e.g. Butterfield and Malmstrom 2009; Jackson et al. 2004) could be a viable tool to account for transient vegetation states and to complement soil water content retrieval with CRPs (e.g. Coopersmith et al. 2014).

Another approach to correct fast neutron intensity for aboveground biomass was presented by Hawdon et al. (2014). In contrast to the findings in this study, Hawdon et al. (2014) suggested a non-linear relationship with an asymptotic behaviour towards intermediate wet aboveground biomass. However, our data set shows no asymptotic behaviour for high amounts of biomass. Indeed, the relationship between fast neutron flux and dry aboveground biomass could be weakly non-linear, particularly for small amounts of biomass. Given the current data set, we nevertheless believe that the assumption of linearity is the most conservative one. In addition,

the linear model provided a satisfactory fit to the evaluation data and required only few fitting parameters. Similar to the linear correction for absolute water vapor in air developed by Rosolem et al. (2013), our data set does not indicate a remarkable change in the shape of the N_0-calibration function even for high amounts of aboveground biomass.

The correction of neutron flux for aboveground biomass derived in this study relies heavily on data from forest ecosystems in humid climatic conditions. Future work should investigate whether the derived relationship is also valid for other forest types (e.g. with significant undergrowth). This may not be the case because of the known effects of the geometrical distribution of biomass on measured neutron flux (Franz et al. 2013c). It seems tempting to also consider the empirical vegetation correction for correcting soil water content measurements at agricultural fields with fast changing biomass during the crop growth season. However, the derived vegetation correction has not been evaluated yet for its ability to correct for dynamical changes in agricultural biomass. Since the expected range of dynamical change in agricultural biomass is much lower than the range of biomass used to derive the vegetation correction, it has to be used with caution in this case. Furthermore, given the apparent discrepancies between our data and those of Hawdon et al. (2014), and with respect to the effect of small amounts of biomass (< 5 kg m^{-2} AGB_{dry}) on measured neutron flux, more research is required to address uncertainties associated with soil water content monitoring with CRP in agricultural fields. Finally, the obtained empirical relationship between the amount of aboveground biomass and N_0 should be tested for other regions of the world. This was not possible in the context of this study because cut-off rigidities and sensor-specific counting efficiencies for installed CRPs at other locations (e.g., within the COSMOS network in North America) were not available.

3.5 Conclusions

We presented a new correction method that extends the capabilities of the N_0-method, the COSMIC operator and the *hmf*-method to estimate soil water content from fast neutron flux to sites and areas with strong spatial variation in aboveground biomass. In addition, we present a simple approach to account for sensor-specific counting efficiencies amongst multiple CRPs. The vegetation correction was developed using an extensive data set from a network of ten CRPs

located in the Rur catchment, Germany. An evaluation was performed using additional CRP measurements, the COSMIC operator, and the *hmf*-method. The vegetation correction is applicable for either biomass water equivalent (BWE) or dry aboveground biomass (AGB_{dry}).

Overall, there are four main conclusions that could be drawn from this study. First, the variation in sensor-specific counting efficiency was higher than 10% amongst our 11 CRPs which is the same order of magnitude as the water vapor correction in humid climates (Rosolem et al. 2013). Without correction of this variable counting efficiency, the subsequent analysis of the effect of aboveground biomass on the fast neutron flux measurements would not have provided meaningful results. Second, a linear correlation was found between the calibration parameter N_0 and dry aboveground biomass or biomass water equivalent, which was successfully used to develop a vegetation correction for fast neutron flux measurements. Third, the reduction in fast neutron flux was quantified to be 0.9 % per kg dry aboveground biomass per m^2 or 0.5 % per kg of biomass water equivalent per m^2 independent of the chosen reference conditions. Finally, our results indicate that the N_0-method, the COSMIC operator and the *hmf*-method work similarly well for the Rur catchment with the empirical vegetation correction. It is desirable to extend the results of this study to other CRP networks (e.g. COSMOS) but this would require an accurate assessment of counting efficiency of each CRP.

4 Assimilation of cosmic-ray soil moisture measurements into a land surface model*

4.1 Introduction

Soil water content (SWC) is a key variable of land surface hydrology and has a strong control on the partitioning of net radiation between latent and sensible heat flux. Knowledge of SWC is relevant for the assessment of plant water stress and agricultural production, as well as runoff generation as a response to precipitation events (Robinson et al. 2008a; Vereecken et al. 2008). In atmospheric circulation models, SWC is important as a lower boundary condition and is calculated as a state variable in land surface models. Coupling of atmospheric circulation models and land surface models allows quantifying the role of soil moisture on atmospheric processes such as soil moisture-precipitation feedbacks (Eltahir 1998; Koster et al. 2004) and summer climate variability and drought (Bell et al. 2015; Oglesby and Erickson 1989; Seneviratne et al. 2006; Sheffield and Wood 2008). It is therefore important to improve the modelling and prediction of SWC, but this is hampered by model deficiencies and lack of high quality data (Vereecken et al. 2016). Soil moisture measured by space-born remote sensing technologies provides information over large areas (e.g. Temimi et al. 2014). However, space-born remote sensing supplies only information on the upper few centimeters, and data are not reliable for areas with dense vegetation. Therefore, in this paper an alternative source for soil moisture information is explored. Cosmic-ray probes (CRPs) measure fast neutron intensity which allows estimating SWC at an intermediate scale (Cosh et al. 2016; Desilets et al. 2010; Lv et al. 2014; Zreda et al. 2008) which is closer to the desired application scale of land surface models (Ajami et al. 2014; Chen et al. 2007; Shrestha et al. 2014). Fast neutrons originate from moderation of secondary cosmic particles from outer space by terrestrial atoms. These particles are mainly fast neutrons, which are moderated most effectively by hydrogen because of the similar atomic mass. Therefore, the corresponding neutron intensity measured by CRPs strongly depends on the amount of hydrogen within the CRP footprint, allowing for a continuous non-invasive soil moisture estimate over an area of ~15 ha (Kohli et al. 2015). The spatial extend of this measurement is desirable as it matches with the desired grid cell size of a

*adapted from: Baatz, R., Hendricks Franssen, H.-J., Han, X., Hoar, T., Bogena, H. and Vereecken, H. (2016). Evaluating the value of a network of cosmic-ray probes for improving land surface modeling. Hydrol. Earth Syst. Sci. Discuss., doi:10.5194/hess-2016-432.

land surface model (Crow et al. 2012) and small scale heterogeneities are averaged over a larger area (Desilets and Zreda 2013; Franz et al. 2013b). Vertical measurement depth ranges from a maximum of ~70 cm under completely dry conditions and decreases to roughly ~12 cm under wet conditions (e.g. 40 vol. % soil moisture) (Bogena et al. 2013). Worldwide several CRP networks exist, like the North American COSMOS network (Zreda et al. 2012), the German CRP network (Baatz et al. 2014) installed in the context of the TERENO infrastructure measure (Zacharias et al. 2011) and the Australian COSMoZ network (Hawdon et al. 2014).

Soil moisture data assimilation provides a way to improve imperfect land surface model predictions with measured soil moisture data by merging model predictions and data, and can consider the uncertainty of initial conditions, model parameters and model forcings. Ensemble Kalman Filtering (EnKF) is one of the most commonly applied data assimilation methods (Burgers et al. 1998; Evensen 1994). Soil moisture data assimilation has been the subject of intensive study for more than a decade now. An early contribution was provided by Houser et al. (1998) who assimilated remotely sensed soil moisture observations from a microwave radiometer into a land atmosphere transfer scheme using four-dimensional variational data assimilation. Rhodin et al. (1999) assimilated soil moisture data for a four-day period in order to obtain an improved characterization of the lower boundary condition for an atmospheric circulation model. They also used a variational data assimilation approach. More recently, the Ensemble Kalman Filter (Crow 2003; Dunne and Entekhabi 2005; Reichle et al. 2002a), the Extended Kalman Filter (Draper et al. 2009; Reichle et al. 2002b), four-dimensional variational methods (Hurkmans et al. 2006) and the Local Ensemble Transform Kalman Filter (Han et al. 2015; Han et al. 2013) were applied for updating soil moisture states in land surface models. Reichle et al. (2002a) performed a synthetic experiment using L-band microwave observations of the Southern Great Plains Hydrology Experiment (Jackson et al. 1999) to analyze the effect of ensemble size and prediction error. Dunne and Entekhabi (2005) showed that an Ensemble Kalman Smoother approach, where data from multiple time steps was assimilated to update current and past states, can yield a reduced prediction error compared to a pure filtering approach.

More recent work addressed joint state-parameter estimation in hydrologic land surface models with data assimilation methods. Joint state-parameter estimation with EnKF is possible by an augmented state vector approach (Chen and Zhang 2006), a dual approach (Moradkhani et al. 2005b) or an approach with an additional external optimization loop (Vrugt et al. 2005). Pauwels et al. (2009) optimized soil hydraulic parameters of a land surface model with synthetic aperture radar data. Lee (2014) used Synthetic Aperture Radar soil moisture data to estimate soil hydraulic properties at the Tibetan plateau using the EnKF and a Soil Vegetation Atmosphere Transfer model. Bateni and Entekhabi (2012) assimilated land surface temperature with an Ensemble Kalman Smoother and achieved a better estimate of the partitioning of energy between sensible and latent heat fluxes. (Han et al. 2014) updated soil hydraulic parameters of the Community Land Model (CLM) by assimilation of synthetic brightness temperature data with the Local Ensemble Transform Kalman Filter (LETKF) (Hunt et al. 2007). Shi et al. (2014) used the Ensemble Kalman Filter for a synthetic multivariate data assimilation problem with a land surface model and then applied it to real data (Shi et al. 2015). The cases illustrated a way to use real world data for estimating several parameters in hydrologic land models. (Kurtz et al. 2016) developed a particular CPU-efficient data assimilation framework for the coupled land surface-subsurface model TerrSysMP (Shrestha et al. 2014). They successfully updated 2×10^7 states and parameters in a synthetic experiment. Whereas these studies were made with land surface models, also in soil hydrological applications recently data assimilation was used to estimate soil hydraulic parameters. Early work was by Wu and Margulis (2011, 2013) in the context of real-time control of waste water reuse in irrigation. Erdal et al. (2014) investigated the role of bias in the conceptual soil model and explored bias aware EnKF as a way to deal with it. Erdal et al. (2015) focused on handling of strong non-Gaussianity of the state variable in EnKF under very dry conditions. Montzka et al. (2011; 2013) explored the role of the particle filter for handling non-Gaussianity in soil hydrology data assimilation. They showed that the ability of a data assimilation system to correct the soil moisture state and estimate hydraulic parameters strongly depends on the nonlinear character of the soil moisture retention characteristic. Song et al. (2014) worked on a modified iterative filter to handle the non-linearity and non-Gaussianity of data assimilation for the vadose zone. For a further literature review on

data assimilation in the context of hydrological and land surface models we refer to Reichle (2008) and Montzka et al. (2012).

Shuttleworth et al. (2013) developed the Cosmic Ray Soil Moisture Interaction Code (COSMIC), which is a forward operator to be applied for assimilating neutron intensity observations from CRPs. The COSMIC code was evaluated for several sites (Baatz et al. 2014; Rosolem et al. 2014). Its capability to propagate surface soil moisture information into the deeper soil column was analyzed by Rosolem et al. (2014). The COSMIC operator was successfully implemented in the Data Assimilation Research Testbed (Rosolem et al. 2014) to allow for state updating by the Ensemble Adjustment Kalman Filter (Anderson 2001). The COSMIC operator was implemented in a python interface that couples the land surface model CLM and the LETKF for joint state parameter updating (Han et al. 2015). Neutron counts measured by CRP have been used in data assimilation studies to update model states (Han et al. 2015; Rosolem et al. 2014). Soil hydraulic parameters were also updated by assimilation of neutron counts (Han et al. 2016), but only for a synthetic study which showed its feasibility. CRPs were also used for inverse estimation of soil hydraulic parameters of the Hydrus-1D model (Villarreyes et al. 2014).

This work further explores the value of measured neutron intensity by CRPs to improve modelling of terrestrial systems at the catchment scale (Simmer et al. 2015) using a land surface model. Compared to existing work the main novelties are:
(i) Data from a network of nine CRPs were assimilated in the Community Land Model version 4.5 (CLM) with an evaluation of the information gain by this assimilation at the larger catchment scale. Until now evaluations with CRPs were made for a single location, but not for a complete network of CRPs. It is a very important question whether CRPs can also improve the soil moisture characterization at the larger catchment scale and how dense the CRP network should be. The high variability of soil moisture at a short distance could potentially limit the CRP measurement value and make updating of soil moisture contents further away from the sensor meaningless. On the other hand, soil maps and atmospheric forcings show spatial correlations over larger distances which suggests that CRP measurements potentially carry important information to update soil moisture contents for larger regions. If it is found that CRP networks

with a density like in this study (10 stations per 2354 km^2) can improve soil moisture content characterization at the larger catchment scale, this is of high relevance and importance for agricultural applications, flood prediction and protection, and regional weather prediction (Koster et al. 2004; Seneviratne et al. 2010; Whan et al. 2015). The main research question addressed in this paper is therefore whether a CRP network of the density in this study can improve large scale soil moisture characterization by state and parameter updates.

(ii) Soil hydraulic parameters were updated together with the soil moisture states in a real-world case study at the larger catchment scale. The study in this paper also allows some evaluation of the feasibility of the updated large scale soil hydraulic parameters.

In the following paragraphs are presented the model site and the measurements (4.2.1), the Community land Model and its parameterization (4.2.2), the COMIC forward model (4.2.3) and the data assimilation procedure (4.2.4).

4.2 Materials and methods

4.2.1 Site description and measurements

The model domain, the Rur catchment (2354 km^2), is situated in western Germany and illustrated in Figure 3. Most prominent vegetation types are agricultural land use (mainly in the North), grassland, and coniferous and deciduous forest. The altitude varies between 15 m a.s.l. in the flat northern part and 690 m a.s.l. in the hilly southern part. Precipitation, evapotranspiration and land use follow the topography. Annual precipitation ranges between less than 600 mm in the North to 1200 mm in the hilly South (Montzka et al. 2008). Annual potential evapotranspiration varies between 500 mm in the South and 700 mm in the North (Bogena et al. 2005). The Rur catchment CRP network comprises nine CRPs (CRS1000, HydroInnova LLC, 2009) which were installed in 2011 and 2012 (Baatz et al. 2014). Climate and soil texture of the CRP sites can be found in Table 9. The CRPs were calibrated in the field using gravimetric soil samples. At each site, 18 soil samples were taken along three circles with distances of 25, 75 and 175 meters from the CRP, six samples evenly distributed along each circle. Each sample was extracted with a 50.8 x 300 mm round HUMAX soil corer (Martin Burch AG, Switzerland). The samples were split into 6 sub-samples with 5 cm length each and oven

dried at 105 °C for 48 hours to measure dry soil bulk density and soil moisture. Lattice water was determined for each site using a heat conductivity detector. Soil bulk density, soil moisture, lattice water and 12 hour averaged measured neutron intensity were used to determine calibration parameters specific for each CRP and the COSMIC operator.

Table 9: Site information on elevation (m.a.s.l.), average annual precipitation (mm/year), CLM plant functional type, sand content (%), clay content (%), and the date of the first SWC retrieval assimilated.

Name	m.a.s.l.	Precip.	Plant functional type	Sand	Clay	Date of first assimilation
Aachen	232	952	Crops	22	23	13.01.2012
Gevenich	108	884	Crops	22	20	07.07.2011
Heinsberg	57	814	Crops	18	19	09.09.2011
Kall	504	935	C3 non arctic grass	20	22	15.09.2011
Merzenhausen	94	825	Crops	21	22	19.05.2011
Rollesbroich	515	1307	C3 non arctic grass	22	23	19.05.2011
RurAue	102	743	C3 non arctic grass	19	26	08.11.2011
Wildenrath	76	856	Broadleaf deciduous temperate tree	65	12	07.05.2012
Wuestebach	605	1401	Needleleaf evergreen temperate tree	19	23	20.03.2011

4.2.2 Community land model and parameterization

The Community Land Model version 4.5 (CLM) was the land surface model of choice for simulating water and energy exchange between the land surface and the atmosphere (Oleson et al. 2013). Some of the key processes which are solved by CLM are radiative transfer in the canopy space, interception of precipitation by the vegetation and evaporation from intercepted water, water uptake by vegetation and transpiration, soil evaporation, photosynthesis, as well as water and energy flow in the subsurface. SWC in CLM is influenced by precipitation, infiltration into the soil, water uptake by vegetation, surface evaporation and surface and subsurface runoff. Oleson et al. (2013) provide further details on CLM4.5. To limit the scope and complexity of this study, CLM was run using satellite phenology, e.g. prescribed leaf area index data and the biogeochemical module turned off.

The spatial domain is discretized by rectangular grid cells by CLM. Each grid cell may have several types of land cover: Lake, urban, vegetated, wetland, and glacier. The vegetated part of the grid cell can be covered by several plant functional types which are all linked to a single soil column. The soil column is vertically discretized by ten soil layers and five bedrock layers. Layer thickness increases exponentially from 0.007 m at the surface to 2.86 m for layer 10. Vertical water flow in soils is modelled by the 1D Richards equation. Soil hydraulic parameters are determined from sand and clay content using pedotransfer functions for the mineral soil fraction (Clapp and Hornberger 1978; Cosby et al. 1984), and organic matter content for the organic soil fraction (Lawrence and Slater 2008).

The following equations describe how soil texture and organic matter define the soil hydraulic properties in CLM such as porosity, hydraulic conductivity, the empirical exponent *B* and soil matric potential. Hydraulic conductivity ($k[z]$ in mm/s) at the depth z between two layers (*i* and *i*+1) is a function of soil moisture (θ in m^3/m^3 in layers *i* and *i+1*), saturated hydraulic conductivity (k_{sat} in mm/s at *z*), saturated soil moisture (θ_{sat} in m^3/m^3) and the empirical exponent *B*:

$$k[z] = \begin{cases} \phi_{ice} k_{sat,z} \left[\frac{0.5(\theta_i + \theta_{i+1})}{0.5(\theta_{sat,i} + \theta_{sat,i+1})} \right]^{2B_i+3} & 1 \le i \le N_{levsoi} - 1 \\ \phi_{ice} k_{sat,z} \left(\frac{\theta_i}{\theta_{sat,i}} \right)^{2B_i+3} & i = N_{levsoi} \end{cases} \quad (40)$$

where ϕ_{ice} is the ice impedance factor. The ice impedance factor was implemented to simplify an increased tortuosity of water flow in a partly frozen pore space. It is calculated with $\phi_{ice} = 10^{-\Omega F_{ice}}$ using the resistance factor $\Omega = 6$ and the frozen fraction of soil porosity $F_{ice} = \theta_{ice}/\theta_{sat,i}$. Soil hydraulic properties are calculated separately for the mineral (*min*) and organic matter (*om*) soil components. Total porosity $\theta_{sat,i}$ is calculated using the fraction of organic matter ($f_{om,i}$) with:

$$\theta_{sat,i} = (1 - f_{om,i})\theta_{sat,min,i} + f_{om,i}\theta_{sat,om} \quad (41)$$

where the organic matter porosity is $\theta_{sat,om} = 0.9$ and sand content in % determines the mineral soil porosity $\theta_{sat,min}$ as:

$$\theta_{sat,min} = 0.489 - 0.00126 \times \%sand \quad (42)$$

Analogous, the exponent *B* is calculated with

$$B_i = (1 - f_{om,i})B_{min,i} + f_{om,i}B_{om} \quad (43)$$

Where $B_{om} = 2.7$ is the organic exponent and the mineral exponent $B_{min,i}$ is determined by clay content in % with:

$$B_{min,i} = 2.91 + 0.159 \times \%clay \quad (44)$$

Saturated hydraulic conductivity is calculated for a connected and an unconnected fraction of the grid cell with:

$$k_{sat}[z_i] = (1 - f_{perc})k_{sat,uncon}[z_i] + f_{perc,i}k_{sat,om}[z_i] \quad (45)$$

where $f_{perc,i}$ is the fraction of a grid cell where water flows with saturated hydraulic conductivity of the organic matter ($k_{sat,om}[z_i]$ in mm/s) through the organic material only, the so called connected flow pathway, whereas the saturated hydraulic conductivity of the unconnected part ($k_{sat,uncon}[z_i]$ in mm/s) depends on organic and mineral saturated soil hydraulic conductivity:

$$k_{sat,uncon} = (1 - f_{perc})\left(\frac{1 - f_{om}}{k_{sat,min}} + \frac{f_{om} - f_{perc}}{k_{sat,om}}\right)^{-1} \quad (46)$$

where saturated hydraulic conductivity for mineral soil is calculated from the grid cell sand content as:

$$\mathrm{k}_{sat,min}[z_i] = 0.0070556 \times 10^{-0.884 + 0.0153 \times \%sand} \quad (47)$$

The fraction f_{perc} is calculated with:

$$f_{perc} = 0.908 \times (f_{om} - 0.5)^{0.139} \qquad f_{om} \geq 0.5 \quad (48)$$

$$f_{perc} = 0 \qquad f_{om} < 0.5 \quad (49)$$

Soil matric potential (mm) is defined as function of saturated soil matric potential (mm) with:

$$\psi_i = \psi_{sat,i}\left(\frac{\theta_i}{\theta_{sat,i}}\right)^{-B_i} = \left[(1 - f_{om,i})\psi_{sat,min,i} + f_{om,i}\psi_{sat,om}\right]\left(\frac{\theta_i}{\theta_{sat,i}}\right)^{-B_i} \quad (50)$$

where saturated organic matter matric potential is $\psi_{sat,om} = -10.3\ mm$ and saturated mineral soil matric potential is calculated from sand content as:

$$\psi_{sat,min,i} = -10.0 \times 10^{1.88 - 0.0131 \times \%sand} \quad (51)$$

4.2.3 Cosmic-ray forward model

SWC retrievals were calculated from neutron intensity observations with the Cosmic-ray Soil Moisture Interaction Code COSMIC (Shuttleworth et al. 2013) following calibration results and

the procedure of Baatz et al. (2014). COSMIC parameterizes interactions between neutrons and atoms in the subsurface, relevant for soil moisture estimation. COSMIC was calibrated against the more complex Monte Carlo Neutron Particle model MCNPx (Pelowitz 2005) and needs considerably less CPU-time than the MCNPx model. The reduced CPU-time need and the physically based parameterization make COSMIC a suitable data assimilation operator. The code was tested at multiple sites for soil moisture determination (Baatz et al. 2014; Rosolem et al. 2014) and analyzed in detail by Rosolem et al. (2014).

COSMIC assumes that a number of high energy neutrons enter the soil. In the soil, high energy neutrons are reduced by interaction with the soil leading to isotropic generation of fast neutrons with less energy in each soil layer. Before resurfacing, fast neutrons are reduced again by soil interaction (Shuttleworth et al. 2013). The number of neutrons N_{CRP} that reaches the CRP can be summarized in a single integral as

$$N_{CRP} = N_{COSMIC} \int_0^{\infty} \left\{ A(z)[\alpha\rho_S(z) + \rho_w(z)] exp\left(-\left[\frac{m_s(z)}{L_1} + \frac{m_w(z)}{L_2} \right] \right) \right\} \cdot dz \qquad 52$$

where N_{COSMIC} is an empirical coefficient that is CRP specific and needs to be estimated by calibration, $A(z)$ is the integrated average attenuation of fast neutrons, $\alpha = 0.404 - 0.101 \times \rho_S$ is the site specific empirical coefficient for the creation of fast neutrons by soil, ρ_S is the dry soil bulk density in g/cm^3, ρ_w is the total soil water density in g/cm^3, m_s and m_w are the mass of soil and water, respectively, per area in g/cm^2. $L_1 = 162.0$ g cm^{-2} and $L_2 = 129.1$ g cm^{-2} are empirical coefficients that were estimated using the MCNPx code (Shuttleworth et al. 2013). The integrated average attenuation of fast neutrons $A(z)$ can be found numerically by solving

$$A(z) = \left(\frac{2}{\pi}\right) \int_0^{\pi/2} exp\left(\frac{-1}{cos(\theta)} \left[\frac{m_s(z)}{L_3} + \frac{m_w(z)}{L_4} \right] \right) \cdot d\theta \qquad 53$$

where θ is the angle along a vertical line below the CRP detector to the element that contributes to the attenuation of fast neutrons, $L_3 = -31.65 + 99.29 \times \rho_S$ is determined from soil bulk density and L_4 = 3.16 g cm^{-2} is another empirical coefficient estimated using the MCNPx code (Shuttleworth et al. 2013). The COSMIC operator is discretized into 300 vertical layers of one cm thickness up to a depth of three meters. For each CLM grid cell in the model

domain, simulated SWC is used to generate a SWC retrieval using the COSMIC code. Simulated SWC is handed from the CLM simulation history files to the COSMIC operator. Given the vertical SWC distribution of the individual CLM soil column, COSMIC internally calculates the contribution of each layer to the simulated neutron intensity signal at the COSMIC soil surface. In this study, the contribution of each layer was used to calculate the weighted CLM SWC retrieval corresponding to the vertical distribution of simulated SWC in each grid cell. Measured neutron intensity of CRPs was used to inversely determine a CRP SWC retrieval as by Baatz et al. (2014) assuming a homogeneous vertical SWC distribution. Then, the weighted CLM SWC retrieval is used in the data assimilation scheme to relate the CRP SWC retrieval to the model state.

4.2.4 Data assimilation

This study uses the local ensemble transform Kalman filter (LETKF) (Hunt et al. 2007) to assimilate SWC retrievals by CRPs into the land surface model CLM. Besides other Ensemble Kalman Filter variants, the LETKF is applied in atmospheric sciences (Liu et al. 2012; Miyoshi and Kunii 2012), ocean science (Penny et al. 2013) and also in land surface hydrology (Han et al. 2014; Han et al. 2015). Updates were calculated either for states or jointly for states and parameters. For state updates only, the LETKF was used as proposed by Hunt et al. (2007). Calculations were made for an ensemble of model simulations which differed related to variations in model forcings and input parameters. The states of the different ensemble members are indicated by $\mathbf{x}_i^f$ where *i*=1, …., *N* and *N* is the number of ensemble members. The individual state vectors $\mathbf{x}_i^f$ contain the CLM-simulated SWC of the ten soil layers and the vertically weighted SWC retrieval obtained with the COSMIC operator. For each grid cell, a vector $\mathbf{X}^f$ can be constructed which contains the deviations of the simulated states with respect to the ensemble mean $\bar{\mathbf{x}}^f$:

$$\mathbf{X}^f = \left[\mathbf{x}_1^f - \bar{\mathbf{x}}^f, \dots, \mathbf{x}_N^f - \bar{\mathbf{x}}^f\right] \quad 54$$

In case of joint state-parameter updates, a state augmentation approach was followed (Han et al. 2014; Hendricks Franssen and Kinzelbach 2008). In this case, the augmented model state vector $\mathbf{X}^f$ is constructed from the weighted SWC, and the grid cell's sand, clay and organic matter content.

In order to relate the measured neutron intensity with the simulated SWC of CLM, the observation operator **H** (COSMIC) is applied on the measured neutron intensity in order to obtain the expected weighted SWC retrieval for each of the stochastic realizations:

$$\mathbf{y}_i^f = \mathbf{H}(\mathbf{x}_i^f) \quad 55$$

The ensemble realizations of the modelled SWC retrieval $\boldsymbol{y}_1^f$ to $\boldsymbol{y}_N^f$ with respect to the ensemble mean $\bar{\boldsymbol{y}}^f$ are stored in the vector $\mathbf{Y}^f$:

$$\mathbf{Y}^f = \left[\mathbf{y}_1^f - \bar{\mathbf{y}}^f, \ldots, \mathbf{y}_N^f - \bar{\mathbf{y}}^f\right] \quad 56$$

The observation error correlation was reduced in space by the factor f_{red} using the spherical model:

$$f_{red} = 1 - (1.5 \times d/d_{max}) + (0.5 \times [d/d_{max}]^3) \quad 57$$

where *d* is the distance to the observation and $d_{max} = 40km$ is the maximum observation correlation length, about half the size of the catchment. Only SWC retrievals within the maximum observation correlation length were used for assimilation. This leads to a 'localized' size of $\mathbf{Y}^f$ and the observation error covariance matrix **R**. The intermediate covariance matrix $\mathbf{P}^a$ (also called analysis error covariance matrix) is calculated according to:

$$\mathbf{P}^a = [(\mathrm{N}-1)\mathbf{I} + \mathbf{Y}^{fT}\mathbf{R}^{-1}\mathbf{Y}^f] \quad 58$$

In addition, the mean weight vector $\bar{\mathbf{w}}^a$ is obtained as follows:

$$\bar{\mathbf{w}}^a = \mathbf{P}^a\mathbf{Y}^{fT}\mathbf{R}^{-1}(\mathbf{y}^0 - \bar{\mathbf{y}}^f) \quad 59$$

where $\mathbf{y}^0$ is CRP SWC retrieval. In the ensemble space, a perturbation matrix $\mathbf{W}^a$ is calculated from the symmetric square root of $\mathbf{P}^a$:

$$\mathbf{W}^a = [(N-1)\mathbf{P}^a]^{1/2} \quad 60$$

The final analysis $\mathbf{X}^a$ is obtained from:

$$\mathbf{X}^a = \bar{\mathbf{x}}^f + \mathbf{X}^f[\bar{\mathbf{w}}^a + \mathbf{W}^a] \quad 61$$

A more detailed description of the LETKF can be found in (Hunt et al. 2007) and details on the implementation of the LETKF in combination with CLM are given by (Han et al. 2015).

4.3 Model and experiment setup

4.3.1 Model setup

In this study, discretization and parameterization of the hydrological catchment was done on the basis of high resolution data. The Rur catchment domain is spatially discretized by rectangular grid cells of 0.008 degree size (~750 m, Figure 3: Locations of the ten CRPs installed in the Rur catchment (left), setup of the Rollesbroich test site (upper right) and the Wuestebach test site (lower right panel) with the SoilNet sensor units.Figure 3). The model time step was set to hourly. Land cover was assumed to consist of vegetated land units only, and a single plant functional type (PFT) for each grid cell was defined. The plant functional types were derived from a remotely sensed land use map using RapidEye and ASTER data with 15 m resolution (Waldhoff 2012). Sand content, clay content and organic matter content were derived from the high resolution regional soil map BK50 (Geologischer Dienst Nordrhein-Westfalen 2009). The BK50 soil map provides the high resolution soil texture for the catchment and is the most detailed soil map available for the defined region. As an alternative, simulations were also performed for a biased soil texture distribution with a fixed sand content of 80 % and clay content of 10 % (S80 soil map). This represents a large error with respect to the expected true soil properties. It allows evaluating the joint state-parameter estimation approach because given the expected bias, we can evaluate whether and to what extend the soil properties are modified by the data assimilation to be closer to the available high resolution soil map. In addition, in many regions across the Earth a high resolution soil map is not available and land surface models which are applied for those regions, for example in the context of global simulations, might be strongly affected by the error in soil properties. It was tested how this impacted the simulation results. Maximum saturated fraction, a surface parameter which is used for runoff generation, was calculated from a 10 meter digital elevation model (scilands GmbH 2010). Leaf area index data were derived from monthly averaged Moderate Resolution Imaging Spectrometer data (MODIS). CLM was supplied with hourly atmospheric forcing data from a reanalysis data set for the years 2010 to 2013 from the German Weather Service (DWD). The data was downscaled from a resolution of 2.8 km^2 to the CLM resolution using linear interpolation based on Delaunay triangulation. Forcing data include precipitation in mm/s,

incident solar and longwave radiation in W/m^2, air temperature in K, air pressure in hPa, wind speed in m/s and relative humidity in kg/kg at the lowest atmospheric level.

4.3.2 Model ensemble

Uncertainty was introduced into the regional CLM model by perturbed soil parameters and forcings. Contents of sand, clay and organic matter were perturbed with spatially correlated noise from a uniform sampling distribution with mean zero and standard deviation 10 % or 30 % (Han et al. 2015). By perturbing texture, soil parameters are also perturbed through the pedotransfer functions used in CLM as specified in Section 4.2.2. Precipitation (σ = 0.5 or 1.0; lognormal distribution) and shortwave radiation (σ = 0.3; lognormal distribution) were perturbed with multiplicative noise with mean equal to one. Longwave radiation (σ = 20 W m^{-2}) and air temperature (σ = 1K) were perturbed with additive noise. The forcing perturbations were imposed with correlations in space (5 km) using a fast Fourier transform. Correlation in time was introduced with an AR(1)-model with autoregressive parameter=0.33. These correlations and standard deviations were chosen based on previous data assimilation experiments (De Lannoy et al. 2012; Han et al. 2015; Kumar et al. 2012; Reichle et al. 2010). In this work, only results for precipitation perturbation with σ = 0.5 will be shown as results for σ = 1.0 were very similar. An ensemble size of 95 realizations was used in the simulations. Based on previous work (Baatz et al. 2015), the SWC retrieval uncertainty for CRPs was estimated to be 0.03 cm^3/cm^3.

4.3.3 Experiment set-up

All simulation experiments in this study used initial conditions from a single five year spin-up run. For the five year spin-up run, a single forcing data set of the year 2010 was repeatedly used as atmospheric input. The soil moisture regime became stable after five years spin-up period, and additional spin-up simulations would not affect soil moisture in the consecutive years. After this five year spin-up, soil parameters and forcing data of the consecutive years were perturbed. From 1st Jan. 2011 onwards, CLM was propagated forward with an ensemble of 95 realizations. On 20th Mar. 2011, the first SWC retrieval was assimilated and assimilation of SWC retrievals continued until 31st Dec. 2012. From 1st January 2013 to 31st December 2013 the model was

propagated forward without data assimilation but with an ensemble of 95 realizations. The year 2013 was used exclusively as evaluation period for data assimilation experiments.

In total, 26 simulation experiments were carried out using different setups (Table 10). Two open loop simulations were run for the BK50 soil map (OL-BK50) and the S80 soil map (OL-S80), respectively, without data assimilation and soil parameter perturbation of 30 %. These simulations are referred to as reference runs for the respective soil map. Simulation results of data assimilation runs were compared to the reference runs for quantification of data assimilation benefits. Simulations were done with joint state-parameter estimation (PAR-), two for the S80 soil map (PAR-S80-) and two for the BK50 soil map (PAR-BK50-), for which soil texture was perturbed by 10 % and 30 %. Two simulations were done with state updates only for the BK50 soil map (Stt-BK50) and the S80 soil map (Stt-BK50), where soil texture was perturbed by 30 %. These eight simulations form the basic set of experiments.

Table 10: Overview of simulation scenarios: Open loop (OL-*) with variation in the soil map BK50 or S80, data assimilation run with state update (Stt) or joint state- and parameter update (PAR) with variation in the soil map perturbation (-10 or -30), and jackknife evaluation runs (jk-S80-1 to 9, and jk-BK50-1 to 9).

Simulation Code	Soil Perturbation		Sand Content		Update	
	10	30	BK50	80 % fix	State	Parameter
OL-BK50		+	+			
OL-S80		+		+		
Stt-BK50		+	+		+	
Stt-S80		+		+	+	
PAR-BK50-30		+	+		+	+
PAR-BK50-10	+		+		+	+
PAR-S80-30		+		+	+	+
PAR-S80-10	+			+	+	+
jk-BK50-1 to 9		+	+		+	+
jk-S80-1 to 9		+		+	+	+

Besides the data assimilation experiments also a larger number of jackknifing simulations was run to evaluate the data assimilation performance. These simulations allow evaluating the impact of the CRP network to improve SWC characterization at other locations, without CRP. In a jackknife experiment, data from eight CRP locations were assimilated and one CRP was excluded from the assimilation for evaluation purpose. At the evaluation location, simulated SWC (which is affected by the assimilation of the other eight probes) was compared to CRP SWC retrievals. For jackknife simulations, the perturbation of soil texture was set to 30 % and precipitation perturbation was done with σ= 0.5. States and parameters at these sites were jointly updated, and simulations were made using the BK50 and the S80 soil maps as input. Therefore, a total of 18 jackknife simulations (jk-S80-* and jk-BK50-*) was performed (two soil maps times nine different simulations leaving away one CRP at a time).

Simulation results were evaluated with the root mean square error (RMSE):

$$RMSE = \sqrt{\frac{\sum_{t=1}^{n}\left(SWC_{t,CLM} - SWC_{t,CRP}\right)^2}{n}} \quad 62$$

where *n* is the total number of time steps, $SWC_{t,CLM}$ is the CLM SWC retrieval at time step *t* and $SWC_{t,CRP}$ is the CRP SWC retrieval at time step *t*. In case SWC was assimilated at the corresponding time step, $SWC_{t,CLM}$ is SWC prior to assimilation. In the case the RMSE is estimated at a single point in time over all CRPs available, the number of time steps *n* can be replaced by the number of CRPs available. The second evaluation measurement in this study is the bias:

$$bias = \frac{\sum_{t=1}^{n}\left(SWC_{t,CLM} - SWC_{t,CRP}\right)}{n} \quad 63$$

4.4 Results

4.4.1 General results

Table 11 summarizes the performance statistics in terms of RMSE for the assimilation period (2011 and 2012). Presented are results for the open loop scenario and six data assimilation scenarios. Errors of open loop simulations are higher for the S80-simulation than for the BK50-simulation at all sites but Merzenhausen. At Merzenhausen RMSE was 0.054 cm^3/cm^3 for the

S80 soil map and 0.067 cm^3/cm^3 for the BK50 soil map. Open loop simulations with the S80 soil map resulted in RMSE-values above 0.10 cm^3/cm^3 at five of nine sites. At all sites data assimilation results with the S80 soil map improved SWC compared to the open loop simulations. This was also the case for the BK50 soil map simulations at all sites but Aachen where RMSE was larger than for the open loop run. In general, data assimilation improved simulations more for the S80 soil map (RMSE reduced by 0.079 cm^3/cm^3) than for the BK50 soil map (RMSE reduced by 0.01 cm^3/cm^3). Room for improvement with the BK50 soil map runs was more limited because of the smaller open loop errors. Nevertheless, after state updating alone the BK50 soil map still gave smaller errors than the S80 soil map. However, joint state-parameter estimation further improved simulation results by reducing RMSE-values and the parameter updating resulted in similar RMSE-values for the BK50 (0.028 cm^3/cm^3) and S80 soil map (0.03 cm^3/cm^3). The E_{RMS} for simulations with 10 % and 30 % perturbation of soil texture values did not show very different results.

Table 11: RMSE (cm^3/cm^3) at CRP sites for open loop runs and different data assimilation scenarios, for the assimilation period (2011 and 2012).

2011 & 2012	Rolles-broich	Merzen-hausen	Geve-nich	Heins-berg	Kall	RurAue	Wueste-bach	Aachen	Wilden-rath	Average RMSE
OL-BK50	0.054	0.067	0.039	0.035	0.042	0.027	0.041	0.032	0.017	0.039
Stt-BK50	0.033	0.041	0.021	0.022	0.030	0.024	0.038	0.023	0.017	0.028
PAR-BK50-10	0.036	0.036	0.019	0.021	0.033	0.025	0.035	0.045	0.015	0.029
PAR-BK50-30	0.031	0.034	0.018	0.019	0.027	0.023	0.040	0.044	0.016	0.028
jk-BK50-*	0.070	0.058	0.073	0.035	0.048	0.050	0.053	0.050	0.091	0.059
OL-S80	0.170	0.053	0.081	0.117	0.149	0.158	0.065	0.169	0.020	0.109
Stt-S80	0.104	0.020	0.037	0.051	0.083	0.056	0.060	0.086	0.018	0.057
PAR-S80-10	0.032	0.038	0.024	0.023	0.033	0.023	0.036	0.048	0.015	0.030
PAR-S80-30	0.029	0.035	0.018	0.019	0.027	0.023	0.039	0.068	0.016	0.030
jk-S80-*	0.082	0.038	0.063	0.026	0.062	0.034	0.038	0.073	0.095	0.057

The temporal course of soil moisture in 2011 at the two sites Gevenich and Merzenhausen is shown in Figure 22. The figures illustrates that SWC at both sites was lower with the S80 soil

map than with the BK50 soil map. In Gevenich and Merzenhausen, mean open loop SWC in 2011 was 0.17 cm^3/cm^3 for the S80 soil map at both sites and 0.27 cm^3/cm^3 for the BK50 soil map at both sites. CRP measurements at Merzenhausen started in May 2011. In the data assimilation runs SWC was immediately affected at the Merzenhausen and Gevenich sites as soon as Merzenhausen CRP SWC retrievals were assimilated. The simulated SWC for the PAR-S80-30 data assimilation run increased as compared to the S80 open loop simulation. The first observation at Gevenich was recorded on July 7th, 2011. By that date, the simulated CLM SWC retrieval was already close to the CRP SWC retrieval at the Gevenich site (Figure 22) due to SWC updates which showed to have a beneficial impact. Figure 22 also shows that the BK50 open loop run was close to the observed SWC at both sites, even without data assimilation.

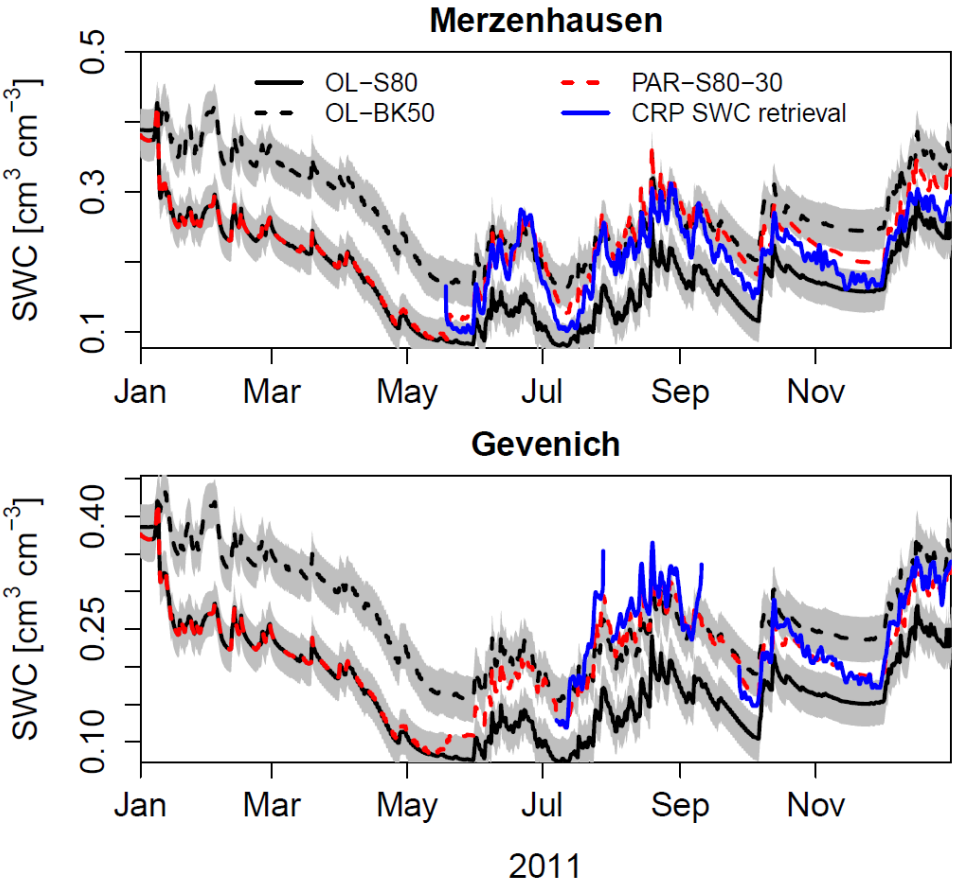

Figure 22: Temporal evolution of simulated SWC, calculated with open loop (OL-*) simulations and data assimilation including parameter updating (PAR-S80-30), together with the CRP soil water content retrieval (SWC) during the first year of simulation at the sites Merzenhausen and Gevenich. Simulated SWC was vertically weighted using the COSMIC operator to obtain the appropriate SWC corresponding to the CRP SWC retrieval.

Figure 23 shows the temporal course of SWC from January 2011 to December 2013 at Heinsberg and Wildenrath. Assimilation and evaluation results are shown for the case of joint state-parameter updates (PAR-S80-30), only state updates (Stt-S80), open loop (OL-S80) and CRP SWC retrievals. At Heinsberg, results show that assimilated SWC was closer to the CRP SWC retrieval

when both states and parameters were updated (PAR-S80-30) than if only states were updated (Stt-S80). This is the case in the assimilation period and in the evaluation period. At the beginning of the evaluation period, the Stt-S80 simulation shows an increase in bias between modeled CLM SWC retrievals and CRP SWC retrieval within the first few days of 2013. The bias of Stt-S80 remained throughout the evaluation period. In contrast, modeled SWC during the evaluation period was close to the CRP SWC retrieval if parameters were previously updated (PAR-S80-30).

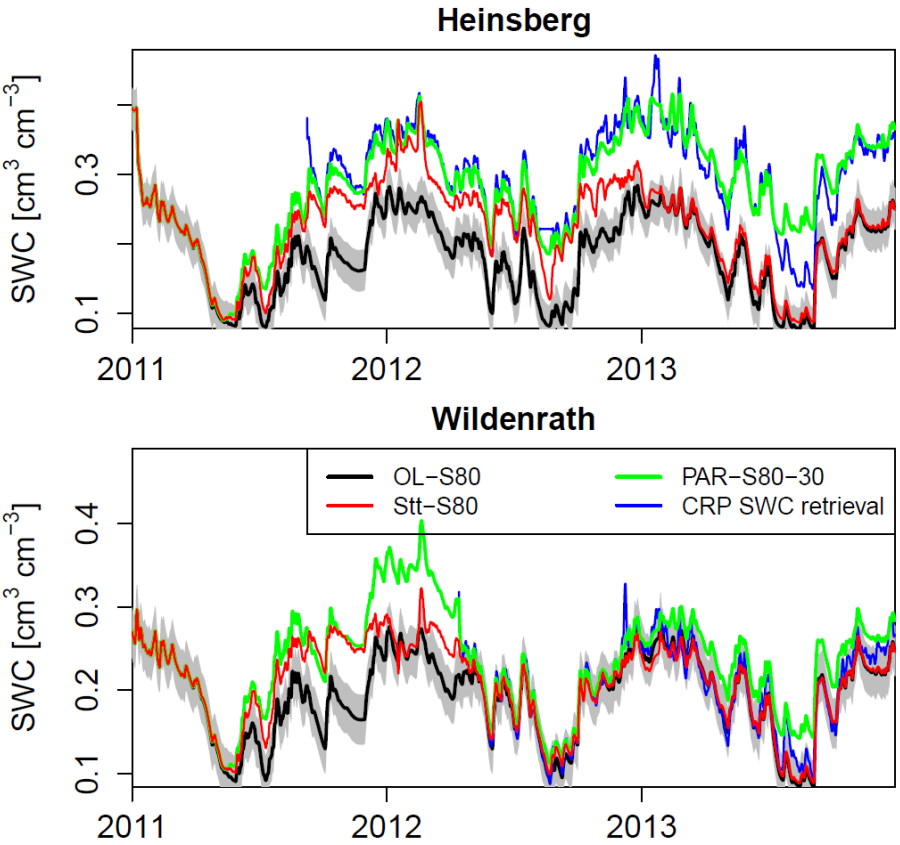

Figure 23: Temporal evolution of simulated SWC retrievals, calculated with open loop (OL-S80), data assimilation with state update only (Stt-BK50), and data assimilation including parameter updating (PAR-S80-30), together with the CRP soil water content (SWC) retrieval at the sites Heinsberg and Wildenrath for the data assimilation period 2011 and 2012, and the evaluation period 2013. Simulated SWC was vertically weighted to obtain the appropriate SWC corresponding to the CRP SWC retrieval.

The CRP at Wildenrath started operating on May 7th, 2012. SWC retrievals at other CRPs were assimilated already from May 2011 onwards and affected SWC at Wildenrath (Figure 23). Until May 2012, Figure 23 shows assimilated SWC (Stt-S80 and PAR-S80-30) was higher than open loop SWC. However, no SWC retrievals were available at the Wildenrath site for comparison

during this period. When SWC retrievals from the CRP at Wildenrath became available and were assimilated into the model, assimilated (Stt-S80 and PAR-S80-30) and open loop (OL-S80) SWC were close to CRP SWC retrievals. This was the case throughout the remaining assimilation and evaluation period. These results suggest that the high sand content of the biased soil map is not far from the optimal sand content at Wildenrath. Therefore, at Wildenrath, the high sand content of both soil maps (60 % and 80 %) resulted in good modeling results already for the open loop runs. This suggests that before May 2012, simulated SWC of the open loop runs with either soil map represented more realistic SWC than assimilated SWC during this period. This will be discussed further in the discussion section.

4.4.2 Verification period

The year 2013 was the verification year without data assimilation. RMSE values for the evaluation period 2013 are reported in Table 12. On the one hand, BK50 data assimilation runs with joint state-parameter estimation resulted in improved SWC at three out of the nine sites compared to open loop BK50-runs. For the other six sites results worsened compared to the corresponding BK50 open loop run. RMSE values increased from an average of 0.041 cm^3/cm^3 (OL-BK50) over all sites to 0.047 cm^3/cm^3 (PAR-BK50-30). On the other hand, for the S80 soil map, all sites except Wildenrath had significantly reduced RMSE values for the case of data assimilation including parameter updating compared to the S80 open loop run. For the S80 simulations, average RMSE over all sites for 2013 was on average 0.12 cm^3/cm^3 for the open loop run and 0.04 cm^3/cm^3 for the run including data assimilation. In case only states were updated (Stt-S80 and Stt-BK50), RMSE was also slightly reduced (compared to open loop runs) for the majority of sites during the evaluation period in 2013. On average, this reduction was 0.016 cm^3/cm^3 for the S80 soil map (Stt-S80) and 0.002 cm^3/cm^3 for the BK50 soil map (Stt-BK50). At sites, where RMSE was larger for data assimilation runs with state updating (compared to open loop runs), the increase was only 0.001 cm^3/cm^3.

Table 12: RMSE (cm^3/cm^3) at CRP-sites for open loop, data assimilation and jackknife simulations on the basis of a comparison with CRP SWC retrievals during the verification period (2013). For each jackknife simulation only one RMSE is reported: The RMSE of the location that is meant for evaluation.

Year 2013	Rolles-broich	Merzen-hausen	Geve-nich	Heins-berg	Kall	RurAue	Wueste-bach	Aachen	Wilden-rath	Average RMSE
OL-BK50	0.044	0.065	0.036	0.027	0.048	0.038	0.048	0.042	0.017	0.041
Stt-BK50	0.041	0.054	0.034	0.027	0.049	0.038	0.048	0.041	0.018	0.039
PAR-BK50-10	0.068	0.062	0.036	0.038	0.056	0.056	0.043	0.058	0.017	0.048
PAR-BK50-30	0.052	0.061	0.035	0.033	0.068	0.048	0.043	0.048	0.035	0.047
jk-BK50-*	0.036	0.047	0.028	0.025	0.042	0.031	0.040	0.054	0.106	0.045
OL-S80	0.157	0.062	0.106	0.115	0.160	0.154	0.099	0.167	0.019	0.115
Stt-S80	0.100	0.063	0.107	0.106	0.099	0.146	0.097	0.158	0.020	0.100
PAR-S80-10	0.060	0.039	0.043	0.040	0.064	0.043	0.052	0.060	0.019	0.047
PAR-S80-30	0.049	0.059	0.037	0.036	0.053	0.032	0.046	0.047	0.035	0.044
jk-S80-*	0.079	0.046	0.042	0.036	0.059	0.038	0.063	0.044	0.105	0.057

Bias calculated on the basis of a comparison of hourly SWC measured by CRP and simulated for 2013 is reported in Table 13. The average bias for the S80 open loop run is 0.11 cm^3/cm^3 while it is 0.02 cm^3/cm^3 for the BK50 open loop run. Bias of the BK50 open loop run was positive at Merzenhausen, Gevenich, Heinsberg, and Aachen, and it was negative at Rollesbroich, Kall, RurAue, and Wuestebach. Bias was zero at Wildenrath for the BK50 open loop run. Bias of the S80 open loop run was negative at all sites indicating that modeled SWC was higher than measured SWC. Joint state-parameter updates reduced the absolute bias on average to 0.03 cm^3/cm^3 (PAR-S80-30) and 0.02 cm^3/cm^3 (PAR-S80-10) for the S80 soil map. In case of the BK50 soil map, the bias in 2013 increased to 0.03 cm^3/cm^3 by joint state-parameter updates. State updates without parameter updates reduced the biases only marginally to 0.01 cm^3/cm^3 for the BK50 soil map and to 0.09 cm^3/cm^3 for the S80 soil map. This indicates that state updates also can slightly improve SWC-characterization in the verification period due to improved initial conditions.

Table 13: Bias (cm^3/cm^3) at CRP-sites for open loop, data assimilation and jackknife simulations compared to CRP SWC retrievals during the verification period (2013). For each jackknife simulation only one bias is reported: The bias of the location that is meant for evaluation.

Year 2013	Rolles-broich	Merzen-hausen	Geve-nich	Heins-berg	Kall	Rur-Aue	Wueste-bach	Aachen	Wilden-rath	Mean absolute bias
OL-BK50	-0.03	0.06	0.01	0.00	-0.02	0.00	-0.02	0.01	0.00	0.02
Stt-BK50	-0.01	0.04	0.00	0.00	-0.01	-0.01	-0.02	0.00	0.00	0.01
PAR-BK50-10	0.06	0.05	0.01	0.02	0.04	0.04	0.02	-0.04	0.00	0.03
PAR-BK50-30	0.03	0.05	0.00	0.02	0.04	0.03	-0.01	-0.03	0.03	0.03
jk-BK50-*	-0.02	0.04	0.01	-0.01	-0.03	-0.02	-0.03	-0.05	0.11	0.04
OL-S80	-0.17	-0.05	-0.08	-0.12	-0.15	-0.16	-0.09	-0.17	-0.01	0.11
Stt-S80	-0.09	-0.05	-0.10	-0.10	-0.08	-0.14	-0.09	-0.15	-0.01	0.09
PAR-S80-10	0.03	0.05	-0.01	0.02	0.03	0.01	-0.01	-0.03	0.03	0.02
PAR-S80-30	0.04	0.02	-0.03	0.02	0.05	0.03	0.03	-0.04	-0.01	0.03
jk-S80-*	-0.07	0.03	0.02	0.02	-0.04	-0.02	-0.04	-0.03	0.10	0.04

4.4.3 Temporal evolution of mean RMSE

Figure 24 shows the temporal evolution of the hourly RMSE calculated for all nine CRPs. RMSE was highest for the S80 open loop run and lowest for the PAR-S80-30 simulation. State updates did not improve modeled SWC as much as joint state-parameter updates improved modeled SWC. The RMSE in case of Stt-S80 also falls behind the RMSE of the BK50 open loop run through most of the time. Joint state-parameter updates for the S80 soil map improved the RMSE throughout most of the time compared to the open loop simulations based on the BK50 and S80 soil maps. During the assimilation period 2011-2012, the PAR-S80-30 simulation performed best out of the four simulations. During the evaluation period 2013, OL-BK50 and PAR-S80-30 performed equally well except in summer 2013 when the PAR-S80-30 simulation yielded much higher RMSE-values than the BK50 open loop run.

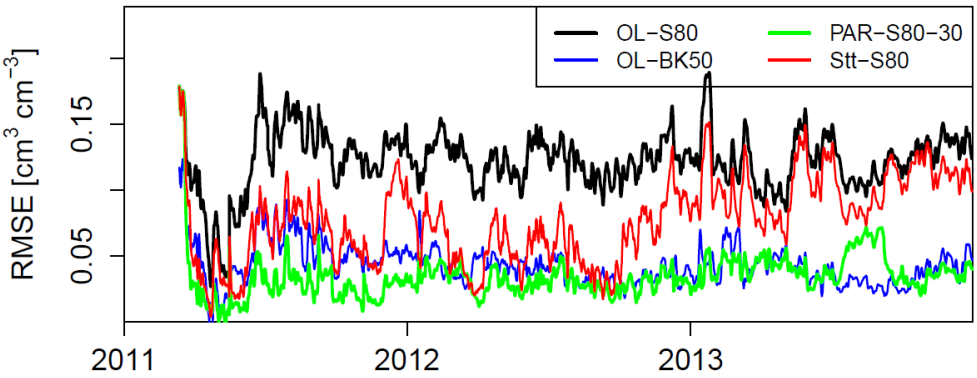

Figure 24: Temporal evolution of root mean square error (RMSE) for hourly SWC retrievals. RMSE is calculated hourly for nine CRP´s for open loop runs for soil maps S80 and BK50, joint state-parameter updates (PAR-S80-30) and state updates only (Stt-S80) during the assimilation period (2011 and 2012) and verification period (2013).

4.4.4 Jackknife simulations

The jackknife simulations investigated the impact of the network of CRPs for improving estimates of SWC at locations between the CRPs, outside the network. The errors shown in Table 12 refers to the two open loop simulations (for the S80 soil map and the BK50 soil map) and the 18 jackknife simulations. All simulations with the S80 soil map resulted in an improved RMSE in the jackknife simulations compared to the open loop simulation, except for Wildenrath. In all cases the RMSE was smaller than 0.10 m^3/m^3. Error reduction was smaller at sites where the open loop error was smaller. At sites with large open loop RMSE, the assimilation could reduce the RMSE by 50 % or more. In case of the BK50 soil map, the jackknife simulations resulted in RMSE-values below 0.10 m^3/m^3 at all sites. However, in this case only at Merzenhausen the RMSE was reduced during the data assimilation period. At Wildenrath, the RMSE was highest for jk-BK50 (0.091 m^3/m^3) and jk-S80 (0.095 m^3/m^3). The average absolute bias for the jackknife experiments was 0.04 cm^3/cm^3 for both soil maps, BK50 and S80, in the evaluation period 2013 (Table 13). Hence, bias in the jk-S80-* simulations improved compared to the open loop run but not in the jk-BK50-* simulations, where bias was already small.

4.4.5 Temporal evolution of parameters

The temporal evolution of the percentage sand content during the assimilation period for the nine CRP sites is shown in Figure 25 for PAR-S80-30, PAR-S80-10, PAR-BK50-30, PAR-BK50-10, jk-S80-30* and jk-BK50-30*. Time series start on March 20th, 2011, the date of the first assimilated CRP SWC retrieval at Wuestebach. Wuestebach and sites within the influence sphere of Wuestebach (Aachen, Kall and Rollesbroich) show also a change in sand content from this date onwards. All other sites show a change in sand content in May 2012 when Rollesbroich and Merzenhausen start operating and their data is assimilated. All sites show variability in sand content over time. Wuestebach, Kall, RurAue, Rollesbroich and Heinsberg show some peaks in the time series. Merzenhausen, Aachen, Gevenich, and Wildenrath show a smoother course compared to the other sites. Sand levels approach a constant site-specific value for the sites Merzenhausen (45 %), Kall (30 %), Gevenich (41 %), RurAue (30 %), Heinsberg (42 %) and Wildenrath (62 %) with a reasonable spread amongst the experiments. The spread in estimated sand content for the sites Wuestebach, Aachen and Rollesbroich is larger, and it seems not to have stabilized at the end of the assimilation. Sand content estimates of the jackknife simulations was close to the sand content of the other data assimilation experiments with joint state-parameter estimation at the sites Merzenhausen, Gevenich, RurAue and Heinsberg. Evolution of the sand content for the jackknife simulations showed larger deviations from the sand content estimated by other data assimilation experiments for the sites Wuestebach, Kall, Aachen, Rollesbroich and Wildenrath.

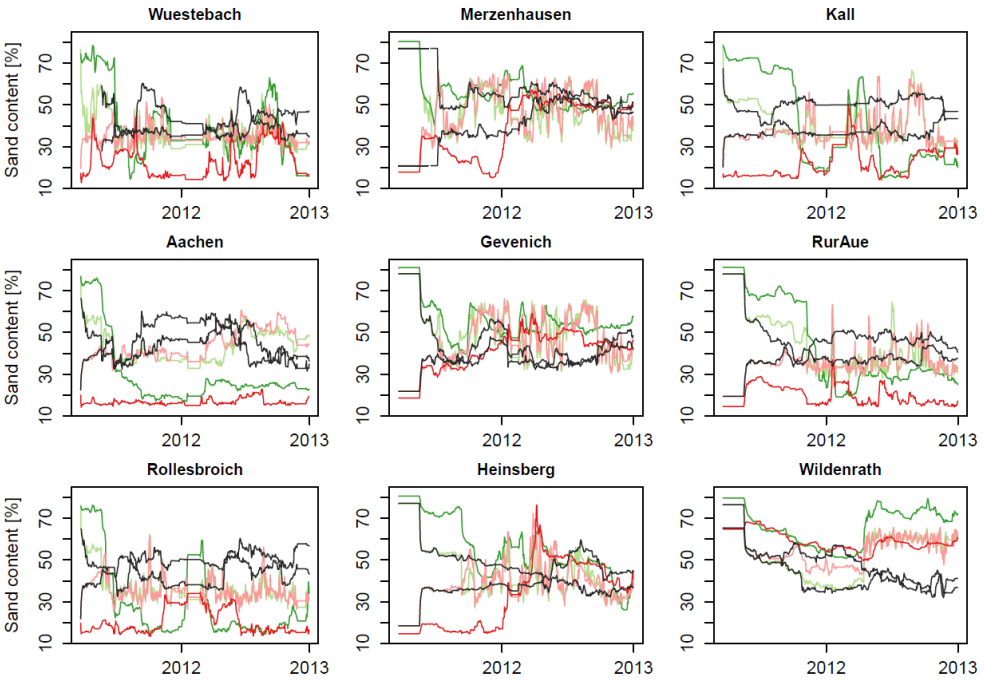

Figure 25: Temporal evolution of the percentage sand content for simulations with parameter update: PAR-S80-30 (green), PAR-S80-10 (light green), PAR-BK50-30 (red), PAR-BK50-10 (light red), jk-S80-30* (black) and jk-BK50-30* (black).

The soil hydraulic parameter B and saturated hydraulic conductivity are shown in Figure 26 and Figure 27 for PAR-S80-30, PAR-S80-10, PAR-BK50-30, PAR-BK50-10, jk-S80-30* and jk-BK50-30*. Updates of soil hydraulic parameters start in March and May 2011 with the assimilation of SWC retrievals depending on the location. The B parameter increases for all simulations. Throughout the whole assimilation period B varies considerably within short time intervals. The total range of the B parameter is between 2.7 and 14 at all sites. At the sites Merzenhausen, Kall, Aachen, Gevenich and Rollesbroich, it generally ranges between 6 and 10. At Wuestebach, Heinsberg and RurAue, B ranges most of the time between 8 and 12, and at Wildenrath, B is below 8. Initial saturated hydraulic conductivity is rather high (k_{sat}>0.015 mm/s) in case of high sand content i.e. for the S80 soil map, and rather low (k_{sat}<0.005 mm/s) in case of low sand content i.e. for the BK50 soil map. In case of the S80 soil map, at all sites except Wildenrath, high initial

saturated hydraulic conductivity decreases quickly by parameter updates to values below 0.01 mm/s. The initial spread in k_{sat} values amongst the simulation scenarios decreases at most sites. At Wuestebach, Merzenhausen, Aachen, Gevenich, RurAue and Heinsberg, the spread is rather small particularly at the end of the assimilation period, while at Wildenrath k_{sat} ranges from 0.005 to 0.015 for individual experiments at the end of the assimilation period. The discussion section will elaborate more on this.

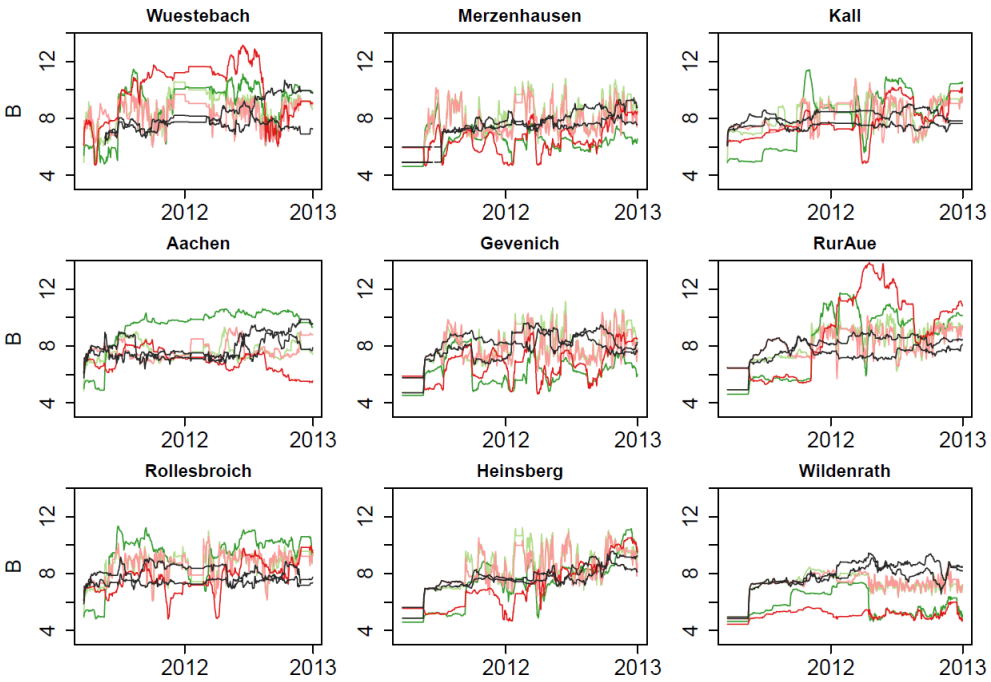

Figure 26: Temporal evolution of the B parameter (top 15cm) for simulations with parameter update: PAR-S80-30 (green), PAR-S80-10 (light green), PAR-BK50-30 (red), PAR-BK50-10 (light red), jk-S80-30* (black) and jk-BK50-30* (black).

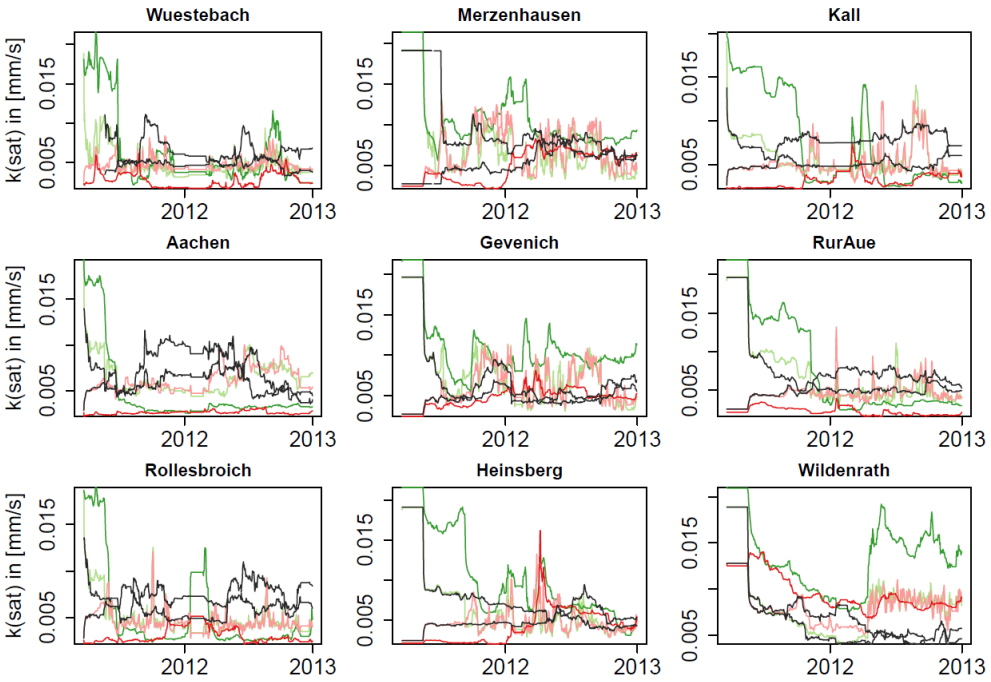

Figure 27: Temporal evolution of saturated hydraulic conductivity (top 15cm) for simulations with parameter update: PAR-S80-30 (green), PAR-S80-10 (light green), PAR-BK50-30 (red), PAR-BK50-10 (light red), jk-S80-30* (black) and jk-BK50-30* (black).

4.4.6 Latent heat and sensible heat

Latent heat flux or evapotranspiration (ET) is another important diagnostic variable of the CLM model and of importance for atmospheric models. Results of the data assimilation experiments showed that soil texture updates altered soil moisture states significantly. In Figure 28 it is shown that joint state-parameter estimation also altered ET. Figure 28 shows ET within the evaluation period 2013 across the whole catchment for four simulations. On the one hand, ET was similar for both open loop simulations in the South of the catchment. On the other hand, ET in the North was up to 80 mm per year lower for the S80 open loop run compared to the BK50 open loop run. Regarding open loop runs, the differences can be linked to the drier soil conditions in case OL-S80 compared OL-BK50 simulation results. For PAR-S80-10, ET increased by up to 40 mm per year in the Northern part of the catchment through data assimilation. The

differences between open loop ET and data assimilation ET were larger for the S80 soil map than for the BK50 soil map. This could be related to the larger update in SWC in case of the S80 scenario compared to the BK50 scenario.

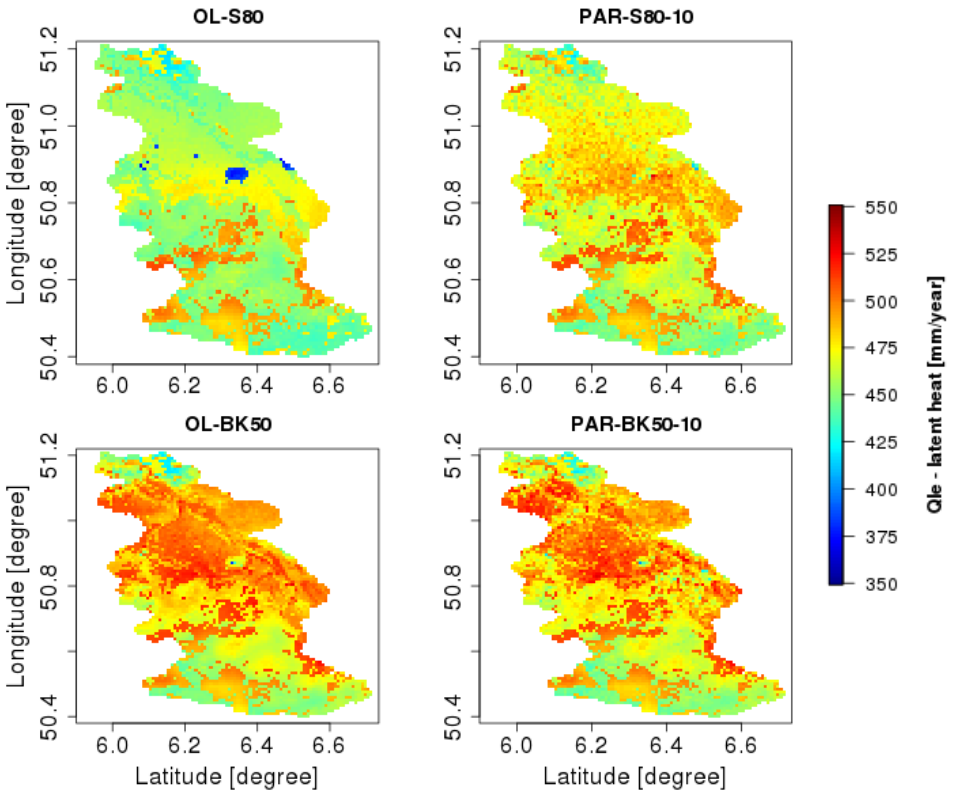

Figure 28: Annual evapotranspiration in the evaluation period (year 2013) for simulations OL-S80, OL-BK50, PAR-S80-10 and PAR-BK50-10.

4.5 Discussion

The applied data assimilation scheme improved soil moisture characterization in the majority of simulation experiments with the regional Community Land Model (CLM). During 2011 and 2012, the biased S80 soil map gave a RMSE up to 0.17 cm^3/cm^3 (at Rollesbroich) in the open loop simulation which left plenty of room for improvements. The soil map BK50 led to RMSE-values

in open loop simulations below 0.05 cm^3/cm^3 which left little room for error reduction considering the measurement error of 0.03 cm^3/cm^3. For the simulations starting with 80 % sand content, sand content was closer to the values of the BK50 soil map after joint state-parameter estimation. However, the temporal evolution of the updated soil texture and the soil hydraulic parameters was not stable. Temporal fluctuations imply that there may be multiple or seasonal optimal parameter values. This is also supported by the findings of the temporal behavior of RMSE during the evaluation period e.g. when in the dry summer 2013 the RMSE peaked in the PAR-S80-30 simulation. Many possible error sources were not subject to calibration in this study but they could be crucial for an even better soil moisture and more stable soil parameter estimation. In this study we only considered uncertainty of soil parameters, but also vegetation parameters are uncertain. Also a number of other CLM-specific hydrologic parameters (e.g. decay factor for subsurface runoff and maximum subsurface drainage) strongly influence state variables in CLM and hence show also potential for optimization. Considering this uncertainty could give a better uncertainty characterization. Precipitation is an important forcing for the model calculations and its estimate could be improved. For this study, precipitation data from the COSMO_DE re-analysis were used. A product which optimally combines gauge measurements and precipitation estimates from radar could give better precipitation estimates. This could improve the soil moisture characterization and also potentially lead to better parameter estimates. Also other error sources like the ones related to the model structure play a significant role. This should be subject of future investigation.

Evaluation simulations for 2013 led to partly improved and partly deteriorated RMSE values when the BK50 soil map was used as prior information on the soil hydraulic properties. The simulations with the S80 soil map on the contrary showed an improved soil moisture characterization in all simulation scenarios and the updated soil hydraulic parameter estimates for those simulations approached the values of the BK50 soil map. These results indicate that the soil hydraulic parameters derived from the BK50 soil map were already well suited for soil moisture predictions and updating soil texture and soil parameters could not improve further the results. RMSE values for simulations with state updates only (Stt-BK50 and Stt-BK50) in 2013

imply the beneficial role of state updates only. However, the improvements in the evaluation period by state updates (without parameter values) are small compared to the improvements obtained by joint state-parameter estimation. This illustrates the benefits of joint state-parameter updates compared to state updates only, and that soil moisture states are strongly determined by soil hydraulic parameters. It also illustrates that the improved characterization of soil moisture states in the assimilation period which results in improved initial states for the verification period loses its influence in the verification period fast over time.

The jackknife simulations illustrated that a network of CRPs can improve modeled SWC if the soil map information is not sufficient. Temporal evolution of subsurface parameters of the jackknife simulations (e.g. jk-S80-*) was close to the evolution of parameter estimates by other simulations (e.g. PAR-S80-10). Parameter estimates at jackknife test sites were inferred from multiple surrounding CRP sites, while updates at sites with CRP information were strongly inferred from single site information. A comparison of parameter estimates at the end of the assimilation period indicates that initial soil parameterization has a limited effect on the resulting parameter estimates. Parameter estimates of jk-BK50-30* and jk-S80-30* are close together at the end of the assimilation period. The CRP network led to improved results for the jackknife evaluation simulations in case of the biased soil map. This suggests that assimilation of CRP data is particularly useful for regions with little information on subsurface parameters. We expect a tradeoff between the initial uncertainty on soil moisture content (related to the quality of the soil map and meteorological data) and the density of a CRP network. In case of a large uncertainty, like in regions with limited information about soils and a low density of meteorological stations, a sparse network of probes can already be helpful for improving soil moisture characterization. On the other hand, in regions with a high density of meteorological stations and a high resolution soil map it can be expected that a high resolution CRP network is needed to further lower the error of soil moisture characterization. Further experiments in other regions with networks of CRPs are needed to get more quantitative information about this.

A question that remains to be answered is whether it is more beneficial to assimilate neutron counts measured by CRPs directly or to assimilate CRP SWC retrievals derived from the neutron counts, as done in this study. Fast neutron intensity measured by CRPs is also affected by vegetation. Neutron count rate decreases with increasing biomass because of the hydrogen content in vegetation (Baatz et al. 2015). Seasonal biomass changes at a single site have a rather small impact on neutron intensity compared to differences between grass land site and a forest site (Baatz et al. 2015). Therefore, using measured neutron flux directly in a data assimilation framework in a catchment with different vegetation types would require to account for the effects of vegetation types on neutron intensity. Hence, vegetation estimates for each grid cell would be necessary. At present, there are two methods that include biomass in the CRP calibration process (Baatz et al. 2015; Franz et al. 2013a) but both methods naturally require accurate biomass estimates, which are typically not available. Besides the uncertainty associated with CRP methods using biomass in the calibration process, biomass estimates also come along with high uncertainties. Therefore, in the case of a catchment with different vegetation types, it is desirable to circumvent the use of biomass estimates, and assimilate directly SWC retrievals obtained at the observation sites instead of assimilating neutron intensity. Therefore, this study uses CRP SWC retrievals in the data assimilation scheme assuming that seasonal changes of biomass can be neglected.

4.6 Conclusions and outlook

This study demonstrates the benefits of assimilating data from a network of nine cosmic-ray probes (CRP) in the land surface model CLM version 4.5. Although information on neutron flux intensity was only available at few locations in the catchment, the local ensemble transform Kalman filter (LETKF) allows updating of soil water content (SWC) at unmonitored locations in the catchment considering model and observation uncertainties. Joint state-parameter estimates improved soil moisture estimates during the assimilation and during the evaluation period. The RMSE and bias for the soil moisture characterization reduced strongly for simulations initialized with a biased soil map and approached values similar to the ones obtained when the regional soil map was used as input to the simulations. RMSE-values in simulations with a regional soil map were not improved, because open loop simulation results

were already close to the observations. The beneficial results of joint state-parameter updates were confirmed by additional jackknife experiments. This real-world case study on assimilating CRP SWC retrievals into a land surface model shows the potential of CRP networks to improve subsurface parameterization in regional land surface models, especially if prior information on soil properties is limited. In many areas of the world, less detailed soil maps are available than the high resolution regional soil map applied in this study. In these areas, more advanced sub-surface characterization is possible using CRP measurements and the data assimilation framework presented in this study.

For now, CRP neutron intensity observations were not assimilated directly. In future studies it would be desirable to use the COSMIC operator for assimilating neutron intensity observations directly. However, in this case the impact of biomass on the CRP measurement signal would have to be taken into account. Therefore, it is desirable to further develop the COSMIC operator to include the impact of biomass on neutron intensities. Using the biogeochemical module of CLM would then allow to characterize local vegetation states as input for the measurement operator. Remotely sensed vegetation states are another option to characterize vegetation states as input for the measurement operator. Both methods require additional field measurements for the verification of vegetation state estimates. The further extension of the data assimilation framework would also enable the estimation of additional sub-surface parameters. The impact of other sub-surface parameters such as subsurface drainage parameters and the surface drainage decay factor on SWC states and radiative surface fluxes has already been shown (Sun et al. 2013). Estimation of these parameters is desirable because of the inherent uncertainty of these globally tuned parameters. However, estimation of soil texture and organic matter content was demonstrated to be already beneficial for improved SWC modeling. Hence, this study represents a way forward towards the integration of CRP information in the calibration of large scale weather prediction models.

5 Synthesis and outlook

5.1 Synthesis

The cosmic-ray probe (CRP) method for soil water content (SWC) estimation was first developed and tested in a dry desert-like environment in Arizona (Zreda et al. 2008). In less than a decade since the first publication on the CRP method, CRPs became an established SWC observation tool. However, the highly diverse environmental conditions encountered on the Earth challenge the precision of SWC estimates using CRPs. This dissertation investigated the accuracy of three CRP parameterization methods to relate measured neutron counts to SWC under humid climate conditions. A vegetation correction method was developed to enhance SWC estimation using CRPs in densely vegetated areas, e.g. forests. In addition, a record of more than two years of CRP measurements obtained from 2011 to 2013 was used in a data assimilation framework to investigate the benefits of a CRP network for characterization of soil moisture content at the larger catchment scale and estimating soil hydraulic parameters of a land surface model (LSM).

In this study, it was shown that the CRP method works well in particularly challenging conditions, a temperate humid climate and the presence of high biomass. Ten CRPs were calibrated individually with gravimetric soil sampling campaigns. Six additional soil sampling campaigns confirmed that SWC is well estimated over a footprint of about 30 ha (average RMSE=0.017 cm^3/cm^3) for three parameterization methods (N_0-method, *hmf*-method and COSMIC operator) and different land use types: grass land, agricultural crop land, forest and mixed land use. Moreover, the evaluation measurements highlighted for the first time simultaneously the high accuracy of all three parameterization methods for SWC estimation. The CRP SWC estimates also compared well with weighted in-situ SWC sensor networks at the grassland test site Rollesbroich (RMSE=0.031 cm^3/cm^3) and the forest test site Wuestebach (RMSE=0.031 cm^3/cm^3). Particularly challenging was the horizontal and vertical weighting of the heterogeneous SWC distribution measured by the in-situ SWC sensor networks. Certainly, homogeneous spatial distributions of hydrogen pools are favorable conditions for setup and evaluation of CRPs. However, homogeneous footprints are rarely met in natural environments. This stresses the importance to further development of horizontal weighting methods for interpreting CRP measurements. Some part of the discrepancy between CRP and in-situ SWC

sensor networks can result from the mismatch between the measurement volumes of CRP and the in-situ SWC sensors. The CRP is most sensible to SWC of the top cm of the soil. However, in-situ sensors are typically installed at a certain depth, e.g. 5 cm, and thus are missing SWC information of the top four cm. By using appropriate LSMs that account for soil moisture dynamics (e.g. Community Land Model, HYDRUS1D) resolution of the vertical SWC distribution could be improved by supplying modeled SWC states of unobserved soil layers. In return, the LSM could be calibrated using in-situ SWC observations from sensor networks. The highly resolved vertical SWC profiles from calibrated LSMs could, for instance, be used for an improved CRP validation.

It was shown that aboveground biomass significantly impacted neutron flux measured by CRPs for SWC estimation. Thus, in this dissertation the impact of aboveground biomass on neutron flux was directly quantified by measurements based on which a vegetation correction method for neutron flux measurements was developed. It was found that an increase in one kg of dry aboveground biomass per m^2 or two kg of biomass water equivalent per m^2 resulted in a 0.9% reduction of the counted neutron fluxes per hour observed by a CRP. The vegetation correction was successfully applied to a calibrated CRP to account for a strong decline in aboveground biomass by deforestation. Without vegetation correction a second calibration would have been necessary after the deforestation. Hence, the vegetation correction has the potential to save high labor costs for labor intensive soil sampling campaigns and analysis. A similar experiment successfully validated the vegetation correction by imitating a roving CRP across a strong biomass gradient and using an in-situ SWC sensor network as reference. The vegetation correction is particularly valuable for large CRP networks or difficult on-site conditions. In this case, parameterization of the N_0-method, the *hmf*-method or the COSMIC operator could be done with soil and land use maps. In addition, the vegetation correction method opens the possibility for SWC measurements with roving CRP over large areas even with strong biomass gradients.

CRP measurements were found to be well suited for soil hydraulic parameter estimation in LSMs. It can be expected that CRPs measurements are useful for estimating subsurface

parameters in hydrologic models. However, LSMs describe land surface states, mass and energy fluxes on the regional scale, and CRPs are only capable of measuring at few locations within a region but continuous in time. Data assimilation techniques allow CRP measurements to be propagated into space while taking into account parameter-, state- and observation uncertainties at individual grid cells. In this study, CLM was successfully coupled to the local ensemble transform Kalman filter (LETKF) and several data assimilation experiments were run to test state updates (SWC) compared to state-parameter updates (SWC, soil texture and organic matter content), the role of soil hydraulic parameter uncertainty, and the importance of the quality of prior information on soil texture. The LETKF was able to improve a biased soil map by assimilating SWC retrievals by CRPs. It was found that joint state-parameter estimation should be preferred over only state updates. In case of state updates, parameters of the biased soil map remained constant during the assimilation period and did not allow convergence of assimilated SWC towards SWC retrievals by CRPs at all sites. Joint state-parameter estimates produced an overall high accuracy in reproducing observed SWC (RMSE=0.030 cm^3/cm^3) which was better than only state updates (RMSE=0.057 cm^3/cm^3) and better than the open loop run with the biased soil map (RMSE=0.109 cm^3/cm^3) during the assimilation period. Furthermore, parameter updates had a lasting positive effect on the evaluation period which succeeded the assimilation period. In the evaluation period, parameter updates reduced the RMSE from 0.115 cm^3/cm^3 (open loop) to 0.045 cm^3/cm^3. If prior information on the soil map was already good in terms of a regional soil map parameterization, data assimilation did not always improve modeled SWC with respect to SWC retrievals by CRPs. In this study, soil texture estimates showed still temporal variability during the assimilation period and did not converge stably towards one final value. The strong temporal soil texture variability at some sites indicated that a damping factor on parameter updates could add additional value to the assimilation scheme by reducing soil texture variability during the assimilation period.

To conclude, in the very first evaluation study of this dissertation, the true CRP measurement uncertainty was quantified under challenging land use and climate conditions and then used in the LETKF data assimilation framework. This data assimilation study successfully utilized the measurements obtained by the CRP network for improved land surface modeling. Results of the

data assimilation experiments highlight the suitability of the LETKF for joint state-parameter estimation in LSMs using measured SWC retrievals of a catchment wide CRP network. Future research has the potential to further improve the obtained results of these first data assimilation experiments and to further reduce the uncertainty in SWC retrievals by CRPs.

5.2 Outlook

Until now, few studies have examined the impact of vegetation on neutron flux and SWC estimation. The development of the empirical vegetation correction in this study enables the N_0-method, the *hmf*-method and the COSMIC operator to account for changes in aboveground biomass. In future, it would be desirable to test the empirical vegetation correction at other CRP networks. Further work should also investigate seasonal changes of biomass. Remote sensing observations may be a suitable tool to characterize key vegetation parameters for correcting the CRP SWC estimates for seasonal biomass changes. Not all relevant hydrogen pools (e.g. above and below ground vegetation, ponded and intercepted water, spatial 3D distribution of SWC) can be measured simultaneously and continuously in the field. Therefore, simultaneous measurements of more hydrogen pools within the CRP footprint than just SWC should be accompanied by modeling the most relevant hydrogen pools with appropriate models e.g. the Community Land Model. Modeling would enhance knowledge and continuous quantification of these additional hydrogen pools. This quantification would be beneficial for a better understanding of the CRP signal and to further develop CRP correction methods. Additionally, combining LSMs, CRP measurements and field measurements in a single framework would be optimal to evaluate neutron flux parameterization methods for vegetation and SWC. These neutron flux parameterization methods could be of empirical origin or from Monte Carlo Neutron Particle simulations. For evaluation, CRPs could also be co-located e.g. on a grass land and on a close-by agricultural crop field, or below canopy and above canopy. In addition, co-location in homogeneous land use and heterogeneous SWC patterns could be helpful to characterize and validate the horizontal footprint of CRPs. As shown in this work, in future studies it is advisable to account for the measurement efficiency of each individual CRP used.

These first data assimilation experiments with measurements obtained by a CRP network have shown the capability of CRPs to improve subsurface parameters in a land surface model. The work was done in a catchment which was characterized in advance with a detailed soil map. In many areas of the world, there is less detailed information on soil maps available. In these regions, the data assimilation framework enables the characterization of subsurface soil parameters with appropriate CRP measurements. As in many real and synthetic case studies, the device's observation (neutron flux) was not assimilated directly but soil water content retrievals from CRP observations were assimilated. Ideally, the CRP forward operator would be used to directly assimilate the neutron flux observation. However, neutron flux observations are strongly depending on aboveground biomass as illustrated in this study. Therefore, the assimilation of neutron flux observations at multiple sites should take into account the vegetation hydrogen content and the uncertainty in biomass estimates. In the present CLM, satellite phenology was used to characterize vegetation states. It is desirable to also use the biogeochemical module of CLM to characterize vegetation states depending on model forcings and states for enabling the measurement operator to appropriately reflect biomass changes in the neutron flux signal. This would enable the full functionality of the CLM. Verification of CLM vegetation states implies the need for further field measurements on the most important vegetation state variables (e.g. vegetation water content, dry aboveground biomass).

Further development of the data assimilation framework can enable the estimation of a larger set of surface and sub-surface parameters. In this study, parameter updates were constrained to soil texture and organic matter content associated to soil hydraulic parameters. CLM specific subsurface parameters which were assumed constant in this study are the surface drainage decay factor, maximum subsurface drainage, and subsurface drainage decay factor. Literature has shown a sensitivity of SWC states and radiative surface fluxes to these parameters. Future work should attempt to increase the number of estimated parameters in order to address the inherent uncertainty in globally calibrated subsurface parameters.

The presented results of this study on data assimilation represent a first step towards addressing parameter uncertainty in a land surface model by assimilation of CRP SWC retrievals.

The Rur catchment CRP network will not only be beneficial for future studies on parameter estimation, but also for validation of present and future Earth satellite observations on surface SWC. Furthermore, this study illustrated means and results that can be used as a basis for an improved characterization of terrestrial Earth surface processes by modeling and observations. Regarding the future challenges in water and food scarcity under growing population and more extreme climate, it is essential to further develop these tools which aim for a better understanding of terrestrial processes, a more efficient use of water resources and an increased agricultural production.

6 Bibliography

Abdu, H., D. A. Robinson, M. Seyfried, and S. B. Jones, 2008: Geophysical imaging of watershed subsurface patterns and prediction of soil texture and water holding capacity. *Water Resour Res*, **44**.

Ajami, H., M. F. McCabe, J. P. Evans, and S. Stisen, 2014: Assessing the impact of model spin-up on surface water-groundwater interactions using an integrated hydrologic model. *Water Resour Res*, **50,** 2636-2656.

Akbar, M. A., A. L. Kenimer, S. W. Searcy, and H. A. Torbert, 2005: Soil water estimation using electromagnetic induction. *T Asae*, **48,** 129-135.

Altese, E., O. Bolognani, M. Mancini, and P. A. Troch, 1996: Retrieving soil moisture over bare soil from ERS 1 synthetic aperture radar data: Sensitivity analysis based on a theoretical surface scattering model and field data. *Water Resour Res*, **32,** 653-661.

Anderson, J., T. Hoar, K. Raeder, H. Liu, N. Collins, R. Torn, and A. Avellano, 2009: THE DATA ASSIMILATION RESEARCH TESTBED A Community Facility. *B Am Meteorol Soc*, **90,** 1283-1296.

Anderson, J. L., 2001: An ensemble adjustment Kalman filter for data assimilation. *Mon Weather Rev*, **129,** 2884-2903.

Annan, J. D., and J. C. Hargreaves, 2004: Efficient parameter estimation for a highly chaotic system. *Tellus A*, **56,** 520-526.

Baatz, R., H. R. Bogena, H. J. Hendricks Franssen, J. A. Huisman, C. Montzka, and H. Vereecken, 2015: An empirical vegetation correction for soil water content quantification using cosmic ray probes. *Water Resour Res*, **51,** 2030-2046.

Baatz, R., H. R. Bogena, H. J. Hendricks Franssen, J. A. Huisman, W. Qu, C. Montzka, and H. Vereecken, 2014: Calibration of a catchment scale cosmic-ray probe network: A comparison of three parameterization methods. *J Hydrol*, **516,** 231-244.

Bateni, S. M., and D. Entekhabi, 2012: Surface heat flux estimation with the ensemble Kalman smoother: Joint estimation of state and parameters. *Water Resour Res*, **48**.

Bell, J. E., R. D. Leeper, M. A. Palecki, E. Coopersmith, T. Wilson, R. Bilotta, and S. Embler, 2015: Evaluation of the 2012 Drought with a Newly Established National Soil Monitoring Network. *Vadose Zone J*, **14**.

Best, M. J., and Coauthors, 2011: The Joint UK Land Environment Simulator (JULES), model description - Part 1: Energy and water fluxes. *Geosci Model Dev*, **4,** 677-699.

Blonquist, J. M., S. B. Jones, and D. A. Robinson, 2005: A time domain transmission sensor with TDR performance characteristics. *J Hydrol*, **314,** 235-245.

Bogena, H. R., J. A. Huisman, R. Baatz, H. J. Hendricks-Franssen, and H. Vereecken, 2013: Accuracy of the cosmic-ray soil water content probe in humid forest ecosystems: The worst case scenario. *Water Resour Res*, **49**.

Bogena, H. R., M. Herbst, J. A. Huisman, U. Rosenbaum, A. Weuthen, and H. Vereecken, 2010: Potential of Wireless Sensor Networks for Measuring Soil Water Content Variability. *Vadose Zone J*, **9,** 1002-1013.

Bogena, H. R., and Coauthors, 2005: MOSYRUR - Water balance analysis in the Rur basin. *Schriften des Forschungszentrums Jülich. Reihe Umwelt/Environment*.

Bogena, H. R., and Coauthors, 2012: TERENO - Ein langfristiges Beobachtungsnetzwerk für die terrestrische Umweltforschung. *Hydrol Wasserbewirts*, **3,** 138-143.

Bogena, H. R., and Coauthors, 2014: A terrestrial observatory approach to the integrated investigation of the effects of deforestation on water, energy, and matter fluxes. *Sci. China Earth Sci.***,** 1-15.

Brent, R. P., 1973: Some Efficient Algorithms for Solving Systems of Nonlinear Equations. *Siam J Numer Anal*, **10,** 327-344.

Brocca, L., T. Tullo, F. Melone, T. Moramarco, and R. Morbidelli, 2012: Catchment scale soil moisture spatial-temporal variability. *J Hydrol*, **422,** 63-75.

Brutsaert, W., 2005: *Hydrology : an introduction.* Cambridge University Press, xi, 605 p. pp.

Burgers, G., P. J. van Leeuwen, and G. Evensen, 1998: Analysis scheme in the ensemble Kalman filter. *Mon Weather Rev*, **126,** 1719-1724.

Butterfield, H. S., and C. M. Malmstrom, 2009: The effects of phenology on indirect measures of aboveground biomass in annual grasses. *Int J Remote Sens*, **30,** 3133-3146.

Chen, F., and Coauthors, 2007: Description and evaluation of the characteristics of the NCAR high-resolution land data assimilation system. *J Appl Meteorol Clim*, **46,** 694-713.

Chen, Y., and D. X. Zhang, 2006: Data assimilation for transient flow in geologic formations via ensemble Kalman filter. *Adv Water Resour*, **29,** 1107-1122.

Chrisman, B., and M. Zreda, 2013: Quantifying mesoscale soil moisture with the cosmic-ray rover. *Hydrol Earth Syst Sc*, **17,** 5097-5108.

Ciais, P., and Coauthors, 2008: Carbon accumulation in European forests. *Nat Geosci*, **1,** 425-429.

Clapp, R. B., and G. M. Hornberger, 1978: Empirical Equations for Some Soil Hydraulic-Properties. *Water Resour Res*, **14,** 601-604.

Clark, D. B., and Coauthors, 2011: The Joint UK Land Environment Simulator (JULES), model description - Part 2: Carbon fluxes and vegetation dynamics. *Geosci Model Dev*, **4,** 701-722.

Coopersmith, E. J., M. H. Cosh, and C. S. T. Daughtry, 2014: Field-scale moisture estimates using COSMOS sensors: A validation study with temporary networks and Leaf-Area-Indices. *J Hydrol*, **519, Part A,** 637-643.

Cosby, B. J., G. M. Hornberger, R. B. Clapp, and T. R. Ginn, 1984: A Statistical Exploration of the Relationships of Soil-Moisture Characteristics to the Physical-Properties of Soils. *Water Resour Res*, **20,** 682-690.

Cosh, M. H., and Coauthors, 2016: The Soil Moisture Active Passive Marena, Oklahoma, In Situ Sensor Testbed (SMAP-MOISST): Testbed Design and Evaluation of In Situ Sensors. *Vadose Zone J*, **15**.

Crow, W. T., 2003: Correcting land surface model predictions for the impact of temporally sparse rainfall rate measurements using an ensemble Kalman filter and surface brightness temperature observations. *J Hydrometeorol*, **4,** 960-973.

Crow, W. T., and Coauthors, 2012: Upscaling Sparse Ground-Based Soil Moisture Observations for the Validation of Coarse-Resolution Satellite Soil Moisture Products. *Rev Geophys*, **50**.

Dai, Y. J., and Coauthors, 2003: The Common Land Model. *B Am Meteorol Soc*, **84,** 1013-+.

De Lannoy, G. J. M., R. H. Reichle, K. R. Arsenault, P. R. Houser, S. Kumar, N. E. C. Verhoest, and V. R. N. Pauwels, 2012: Multiscale assimilation of Advanced Microwave Scanning Radiometer-EOS snow water equivalent and Moderate Resolution Imaging Spectroradiometer snow cover fraction observations in northern Colorado. *Water Resour Res*, **48**.

Denmead, O. T., and R. H. Shaw, 1962: Availability of Soil Water to Plants as Affected by Soil Moisture Content and Meteorological Conditions. *Agron J*, **54,** 385-&.

Desilets, D., and M. Zreda, 2001: On scaling cosmogenic nuclide production rates for altitude and latitude using cosmic-ray measurements. *Earth Planet Sc Lett*, **193,** 213-225.

——, 2003: Spatial and temporal distribution of secondary cosmic-ray nucleon intensities and applications to in situ cosmogenic dating. *Earth Planet Sc Lett*, **206,** 21-42.

——, 2013: Footprint diameter for a cosmic-ray soil moisture probe: Theory and Monte Carlo simulations. *Water Resour Res*, **49,** 3566-3575.

Desilets, D., M. Zreda, and T. Prabu, 2006: Extended scaling factors for in situ cosmogenic nuclides: New measurements at low latitude. *Earth Planet Sc Lett*, **246,** 265-276.

Desilets, D., M. Zreda, and T. P. A. Ferre, 2010: Nature's neutron probe: Land surface hydrology at an elusive scale with cosmic rays. *Water Resour Res*, **46**.

Dieter, M., and P. Elsasser, 2002: Carbon stocks and carbon stock changes in the tree biomass of Germany's forests. *Forstwiss Centralbl*, **121,** 195-210.

Dingman, S. L., 2008: Physical hydrology. Second edition. ed., Waveland Press Inc.

Dorigo, W. A., and Coauthors, 2011: The International Soil Moisture Network: a data hosting facility for global in situ soil moisture measurements. *Hydrol Earth Syst Sc*, **15,** 1675-1698.

Draper, C. S., J. F. Mahfouf, and J. P. Walker, 2009: An EKF assimilation of AMSR-E soil moisture into the ISBA land surface scheme. *J Geophys Res-Atmos*, **114**.

Duan, Q. Y., S. Sorooshian, and V. Gupta, 1992: Effective and Efficient Global Optimization for Conceptual Rainfall-Runoff Models. *Water Resour Res*, **28,** 1015-1031.

Dunne, S., and D. Entekhabi, 2005: An ensemble-based reanalysis approach to land data assimilation. *Water Resour Res*, **41**.

Eltahir, E. A. B., 1998: A soil moisture rainfall feedback mechanism 1. Theory and observations. *Water Resour Res*, **34,** 765-776.

Entekhabi, D., and Coauthors, 2010: The Soil Moisture Active Passive (SMAP) Mission. *P Ieee*, **98,** 704-716.

Eppstein, M. J., and D. E. Dougherty, 1998: Efficient three-dimensional data inversion: Soil characterization and moisture monitoring from cross-well ground-penetrating radar at a Vermont test site. *Water Resour Res*, **34,** 1889-1900.

Erdal, D., I. Neuweiler, and U. Wollschlager, 2014: Using a bias aware EnKF to account for unresolved structure in an unsaturated zone model. *Water Resour Res*, **50,** 132-147.

Erdal, D., M. A. Rahman, and I. Neuweiler, 2015: The importance of state transformations when using the ensemble Kalman filter for unsaturated flow modeling: Dealing with strong nonlinearities. *Adv Water Resour*, **86,** 354-365.

Etmann, M., 2009: Dendrologische Aufnahmen im Wassereinzugsgebiet Oberer Wüstebach anhand verschiedener Mess- und Schätzverfahren, Westfälische Wilhelms-Universität Münster, 91 pp.

Evensen, G., 1994: Sequential Data Assimilation with a Nonlinear Quasi-Geostrophic Model Using Monte-Carlo Methods to Forecast Error Statistics. *J Geophys Res-Oceans*, **99,** 10143-10162.

Franz, T. E., M. Zreda, R. Rosolem, and T. P. A. Ferre, 2012a: Field Validation of a Cosmic-Ray Neutron Sensor Using a Distributed Sensor Network. *Vadose Zone J*, **11**.

——, 2013a: A universal calibration function for determination of soil moisture with cosmic-ray neutrons. *Hydrol Earth Syst Sc*, **17,** 453-460.

Franz, T. E., M. Zreda, T. P. A. Ferre, and R. Rosolem, 2013b: An assessment of the effect of horizontal soil moisture heterogeneity on the area-average measurement of cosmic-ray neutrons. *Water Resour Res*, **49,** 6450-6458.

Franz, T. E., and Coauthors, 2012b: Measurement depth of the cosmic ray soil moisture probe affected by hydrogen from various sources. *Water Resour Res*, **48**.

Franz, T. E., and Coauthors, 2013c: Ecosystem-scale measurements of biomass water using cosmic ray neutrons. *Geophys Res Lett*, **40,** 3929-3933.

GmbH, s., 2010: Digital Elevation Model 10 without anthropogenic landforms.

Gu, Y., and D. S. Oliver, 2007: An iterative ensemble Kalman filter for multiphase fluid flow data assimilation. *Spe J*, **12,** 438-446.

Han, X., H. J. H. Franssen, C. Montzka, and H. Vereecken, 2014: Soil moisture and soil properties estimation in the Community Land Model with synthetic brightness temperature observations. *Water Resour Res*, **50,** 6081-6105.

Han, X., H. J. H. Franssen, R. Rosolem, R. Jin, X. Li, and H. Vereecken, 2015: Correction of systematic model forcing bias of CLM using assimilation of cosmic-ray Neutrons and land surface temperature: a study in the Heihe Catchment, China. *Hydrol. Earth Syst. Sci.*, **19,** 615-629.

Han, X., and Coauthors, 2016: Simultaneous Soil Moisture and Properties Estimation for a Drip Irrigated Field by Assimilating Cosmic-ray Neutron Intensity. *J Hydrol*.

Han, X. J., H. J. H. Franssen, X. Li, Y. L. Zhang, C. Montzka, and H. Vereecken, 2013: Joint Assimilation of Surface Temperature and L-Band Microwave Brightness Temperature in Land Data Assimilation. *Vadose Zone J*, **12**.

Hastings, W. K., 1970: Monte-Carlo Sampling Methods Using Markov Chains and Their Applications. *Biometrika*, **57,** 97-&.

Hawdon, A., D. McJannet, and J. Wallace, 2014: Calibration and correction procedures for cosmic-ray neutron soil moisture probes located across Australia. *Water Resour Res*, **50,** 5029-5043.

Hendrick, L. D., and R. D. Edge, 1966: Cosmic-Ray Neutrons near Earth. *Phys Rev*, **145,** 1023-&.

Hendricks Franssen, H. J., and W. Kinzelbach, 2008: Real-time groundwater flow modeling with the Ensemble Kalman Filter: Joint estimation of states and parameters and the filter inbreeding problem. *Water Resour Res*, **44**.

Houser, P. R., W. J. Shuttleworth, J. S. Famiglietti, H. V. Gupta, K. H. Syed, and D. C. Goodrich, 1998: Integration of soil moisture remote sensing and hydrologic modeling using data assimilation. *Water Resour Res*, **34,** 3405-3420.

Huisman, J. A., S. S. Hubbard, J. D. Redman, and A. P. Annan, 2003: Measuring Soil Water Content with Ground Penetrating Radar: A Review. *Vadose Zone J*, **2,** 476-491.

Hunt, B. R., E. J. Kostelich, and I. Szunyogh, 2007: Efficient data assimilation for spatiotemporal chaos: A local ensemble transform Kalman filter. *Physica D*, **230,** 112-126.

Hurkmans, R., C. Paniconi, and P. A. Troch, 2006: Numerical assessment of a dynamical relaxation data assimilation scheme for a catchment hydrological model. *Hydrol Process*, **20,** 549-563.

Jackson, T. J., and T. J. Schmugge, 1989: Passive Microwave Remote-Sensing System for Soil-Moisture - Some Supporting Research. *Ieee T Geosci Remote*, **27,** 225-235.

Jackson, T. J., and Coauthors, 1999: Soil moisture mapping at regional scales using microwave radiometry: The Southern Great Plains Hydrology Experiment. *Ieee T Geosci Remote*, **37,** 2136-2151.

Jackson, T. J., and Coauthors, 2004: Vegetation water content mapping using Landsat data derived normalized difference water index for corn and soybeans. *Remote Sens Environ*, **92,** 475-482.

Jagdhuber, T., I. Hajnsek, A. Bronstert, and K. P. Papathanassiou, 2013: Soil Moisture Estimation Under Low Vegetation Cover Using a Multi-Angular Polarimetric Decomposition. *Ieee T Geosci Remote*, **51,** 2201-2215.

Jonard, F., L. Weihermuller, K. Z. Jadoon, M. Schwank, H. Vereecken, and S. Lambot, 2011: Mapping Field-Scale Soil Moisture With L-Band Radiometer and Ground-Penetrating Radar Over Bare Soil. *Ieee T Geosci Remote*, **49,** 2863-2875.

Jung, M., and Coauthors, 2010: Recent decline in the global land evapotranspiration trend due to limited moisture supply. *Nature*, **467,** 951-954.

Kalman, R. E., 1960: A New Approach to Linear Filtering and Prediction Problems. *Transaction of the ASME—Journal of Basic Engineering*.

Kelleners, T. J., D. A. Robinson, P. J. Shouse, J. E. Ayars, and T. H. Skaggs, 2005: Frequency dependence of the complex permittivity and its impact on dielectric sensor calibration in soils. *Soil Sci Soc Am J*, **69,** 67-76.

Kemna, A., A. Binley, A. Ramirez, and W. Daily, 2000: Complex resistivity tomography for environmental applications. *Chem Eng J*, **77,** 11-18.

Kerr, Y. H., 2007: Soil moisture from space: Where are we? *Hydrogeol J*, **15,** 117-120.

Kerr, Y. H., and Coauthors, 2012: The SMOS Soil Moisture Retrieval Algorithm. *Ieee T Geosci Remote*, **50,** 1384-1403.

Kohli, M., M. Schron, M. Zreda, U. Schmidt, P. Dietrich, and S. Zacharias, 2015: Footprint characteristics revised for field-scale soil moisture monitoring with cosmic-ray neutrons. *Water Resour Res*, **51,** 5772-5790.

Korres, W., T. G. Reichenau, and K. Schneider, 2013: Patterns and scaling properties of surface soil moisture in an agricultural landscape: An ecohydrological modeling study. *J Hydrol*, **498,** 89-102.

Koster, R. D., and Coauthors, 2004: Regions of strong coupling between soil moisture and precipitation. *Science*, **305,** 1138-1140.

Kuczera, G., and E. Parent, 1998: Monte Carlo assessment of parameter uncertainty in conceptual catchment models: the Metropolis algorithm. *J Hydrol*, **211,** 69-85.

Kumar, S. V., R. H. Reichle, K. W. Harrison, C. D. Peters-Lidard, S. Yatheendradas, and J. A. Santanello, 2012: A comparison of methods for a priori bias correction in soil moisture data assimilation. *Water Resour Res*, **48**.

Kurtz, W., H. J. H. Franssen, and H. Vereecken, 2012: Identification of time-variant river bed properties with the ensemble Kalman filter. *Water Resour Res*, **48**.

Kurtz, W., G. W. He, S. J. Kollet, R. M. Maxwell, H. Vereecken, and H. J. H. Franssen, 2016: TerrSysMP-PDAF version 1.0): a modular high-performance data assimilation framework for an integrated land surface-subsurface model. *Geosci Model Dev*, **9,** 1341-1360.

Lambot, S., L. Weihermuller, J. A. Huisman, H. Vereecken, M. Vanclooster, and E. C. Slob, 2006: Analysis of air-launched ground-penetrating radar techniques to measure the soil surface water content. *Water Resour Res*, **42**.

Lawrence, D. M., and A. G. Slater, 2008: Incorporating organic soil into a global climate model. *Clim Dynam*, **30,** 145-160.

Lee, J. H., 2014: Spatial-Scale Prediction of the SVAT Soil Hydraulic Variables Characterizing Stratified Soils on the Tibetan Plateau from an EnKF Analysis of SAR Soil Moisture. *Vadose Zone J*, **13**.

Liu, J. J., I. Fung, E. Kalnay, J. S. Kang, E. T. Olsen, and L. Chen, 2012: Simultaneous assimilation of AIRS Xco(2) and meteorological observations in a carbon climate model with an ensemble Kalman filter. *J Geophys Res-Atmos*, **117**.

Loke, M. H., J. E. Chambers, D. F. Rucker, O. Kuras, and P. B. Wilkinson, 2013: Recent developments in the direct-current geoelectrical imaging method. *J Appl Geophys*, **95,** 135-156.

Lv, L., T. E. Franz, D. A. Robinson, and S. B. Jones, 2014: Measured and Modeled Soil Moisture Compared with Cosmic-Ray Neutron Probe Estimates in a Mixed Forest. *Vadose Zone J*, **13**.

McJannet, D., and Coauthors, 2014: Field testing of the universal calibration function for determination of soil moisture with cosmic-ray neutrons. *Water Resour Res*, **50,** 5235-5248.

Mcneill, J. D., 1980: Electromagnetic terrain conductivity measurement at low induction numbers. *Technical Note TN-6, Geonics Limited, Ontario*.

Metropolis, N., A. W. Rosenbluth, M. N. Rosenbluth, A. H. Teller, and E. Teller, 1953: Equation of State Calculations by Fast Computing Machines. *The Journal of Chemical Physics*, **21,** 1087-1092.

Miyoshi, T., and M. Kunii, 2012: The Local Ensemble Transform Kalman Filter with the Weather Research and Forecasting Model: Experiments with Real Observations. *Pure Appl Geophys*, **169,** 321-333.

Montzka, C., V. R. N. Pauwels, H. J. H. Franssen, X. J. Han, and H. Vereecken, 2012: Multivariate and Multiscale Data Assimilation in Terrestrial Systems: A Review. *Sensors-Basel*, **12,** 16291-16333.

Montzka, C., M. Canty, R. Kunkel, G. Menz, H. Vereecken, and F. Wendland, 2008: Modelling the water balance of a mesoscale catchment basin using remotely sensed land cover data. *J Hydrol*, **353,** 322-334.

Montzka, C., H. Moradkhani, L. Weihermuller, H. J. H. Franssen, M. Canty, and H. Vereecken, 2011: Hydraulic parameter estimation by remotely-sensed top soil moisture observations with the particle filter. *J Hydrol*, **399,** 410-421.

Montzka, C., J. P. Grant, H. Moradkhani, H. J. H. Franssen, L. Weihermuller, M. Drusch, and H. Vereecken, 2013: Estimation of Radiative Transfer Parameters from L-Band Passive Microwave Brightness Temperatures Using Advanced Data Assimilation. *Vadose Zone J*, **12**.

Moradkhani, H., K. L. Hsu, H. Gupta, and S. Sorooshian, 2005a: Uncertainty assessment of hydrologic model states and parameters: Sequential data assimilation using the particle filter. *Water Resour Res*, **41**.

Moradkhani, H., S. Sorooshian, H. V. Gupta, and P. R. Houser, 2005b: Dual state-parameter estimation of hydrological models using ensemble Kalman filter. *Adv Water Resour*, **28,** 135-147.

Niu, G. Y., and Coauthors, 2011: The community Noah land surface model with multiparameterization options (Noah-MP): 1. Model description and evaluation with local-scale measurements. *J Geophys Res-Atmos*, **116**.

Njoku, E. G., 1977: Theory for Passive Microwave Remote-Sensing of near-Surface Soil-Moisture. *J Geophys Res*, **82,** 3108-3118.

Nordrhein-Westfalen, G. D., 2009: Informationssystem Bodenkarte 50, 1:50000.

Nurmi, J., 1999: The storage of logging residue for fuel. *Biomass Bioenerg*, **17,** 41-47.

Oehmichen, K., and Coauthors, 2011: Inventurstudie 2008 und Treibhausgasinventar Wald. Johann Heinrich von Thünen-Institut Bundesforschungsinstitut für Ländliche Räume, Wald und Fischerei.

Oglesby, R. J., and D. J. Erickson, 1989: Soil-Moisture and the Persistence of North-American Drought. *J Climate*, **2,** 1362-1380.

Oleson, K., and Coauthors, 2013: Technical description of version 4.5 of the Community Land Model (CLM). *NCAR Technical Note NCAR/TN-503+STR***,** 420.

Oleson, K. W., and G. B. Bonan, 2000: The effects of remotely sensed plant functional type and leaf area index on simulations of boreal forest surface fluxes by the NCAR land surface model. *J Hydrometeorol*, **1,** 431-446.

Pauwels, V. R. N., A. Balenzano, G. Satalino, H. Skriver, N. E. C. Verhoest, and F. Mattia, 2009: Optimization of Soil Hydraulic Model Parameters Using Synthetic Aperture Radar Data: An Integrated Multidisciplinary Approach. *Ieee T Geosci Remote*, **47,** 455-467.

Pelowitz, D. B., 2005: MCNPX user's manual, version 5, Rep. LA-CP-05-0369LA-CP-05-0369.

Penny, S. G., E. Kalnay, J. A. Carton, B. R. Hunt, K. Ide, T. Miyoshi, and G. A. Chepurin, 2013: The local ensemble transform Kalman filter and the running-in-place algorithm applied to a global ocean general circulation model. *Nonlinear Proc Geoph*, **20,** 1031-1046.

Qu, W., H. R. Bogena, J. A. Huisman, and H. Vereecken, 2013: Calibration of a Novel Low-Cost Soil Water Content Sensor Based on a Ring Oscillator. *Vadose Zone J*, **12**.

Qu, W., H. R. Bogena, J. A. Huisman, G. Martinez, Y. A. Pachepsky, and H. Vereecken, 2014: Effects of Soil Hydraulic Properties on the Spatial Variability of Soil Water Content: Evidence from Sensor Network Data and Inverse. *Vadose Zone J*, **13**.

Reichle, R. H., 2008: Data assimilation methods in the Earth sciences. *Adv Water Resour*, **31,** 1411-1418.

Reichle, R. H., D. B. McLaughlin, and D. Entekhabi, 2002a: Hydrologic data assimilation with the ensemble Kalman filter. *Mon Weather Rev*, **130,** 103-114.

Reichle, R. H., J. P. Walker, R. D. Koster, and P. R. Houser, 2002b: Extended versus ensemble Kalman filtering for land data assimilation. *J Hydrometeorol*, **3,** 728-740.

Reichle, R. H., S. V. Kumar, S. P. P. Mahanama, R. D. Koster, and Q. Liu, 2010: Assimilation of Satellite-Derived Skin Temperature Observations into Land Surface Models. *J Hydrometeorol*, **11,** 1103-1122.

Reigber, A., and Coauthors, 2013: Very-High-Resolution Airborne Synthetic Aperture Radar Imaging: Signal Processing and Applications. *P Ieee*, **101,** 759-783.

Rhodin, A., F. Kucharski, U. Callies, D. P. Eppel, and W. Wergen, 1999: Variational analysis of effective soil moisture from screen-level atmospheric parameters: Application to a short-range weather forecast model. *Q J Roy Meteor Soc*, **125,** 2427-2448.

Robinson, D. A., S. B. Jones, J. M. Wraith, D. Or, and S. P. Friedman, 2003: A Review of Advances in Dielectric and Electrical Conductivity Measurement in Soils Using Time Domain Reflectometry. *Vadose Zone J*, **2,** 444-475.

Robinson, D. A., and Coauthors, 2008a: Soil moisture measurement for ecological and hydrological watershed-scale observatories: A review. *Vadose Zone J*, **7,** 358-389.

Robinson, D. A., and Coauthors, 2008b: Advancing process-based watershed hydrological research using near-surface geophysics: a vision for, and review of, electrical and magnetic geophysical methods. *Hydrol Process*, **22,** 3604-3635.

Rosenbaum, U., J. A. Huisman, A. Weuthen, H. Vereecken, and H. R. Bogena, 2010: Sensor-to-Sensor Variability of the ECH2O EC-5, TE, and 5TE Sensors in Dielectric Liquids. *Vadose Zone J*, **9,** 181-186.

Rosenbaum, U., and Coauthors, 2012: Seasonal and event dynamics of spatial soil moisture patterns at the small catchment scale. *Water Resour Res*, **48**.

Rosolem, R., W. J. Shuttleworth, M. Zreda, T. E. Franz, X. Zeng, and S. A. Kurc, 2013: The Effect of Atmospheric Water Vapor on Neutron Count in the Cosmic-Ray Soil Moisture Observing System. *J Hydrometeorol*, **14,** 1659-1671.

Rosolem, R., T. Hoar, A. Arellano, J. L. Anderson, W. J. Shuttleworth, X. Zeng, and T. E. Franz, 2014: Translating aboveground cosmic-ray neutron intensity to high-frequency soil moisture profiles at sub-kilometer scale. *Hydrol. Earth Syst. Sci.*, **18,** 4363-4379.

Satalino, G., F. Mattia, M. W. J. Davidson, T. Le Toan, G. Pasquariello, and M. Borgeaud, 2002: On current limits of soil moisture retrieval from ERS-SAR data. *Ieee T Geosci Remote*, **40,** 2438-2447.

Schaefer, G. L., M. H. Cosh, and T. J. Jackson, 2007: The USDA Natural Resources Conservation Service Soil Climate Analysis Network (SCAN). *J Atmos Ocean Tech*, **24,** 2073-2077.

Seneviratne, S. I., D. Luthi, M. Litschi, and C. Schar, 2006: Land-atmosphere coupling and climate change in Europe. *Nature*, **443,** 205-209.

Seneviratne, S. I., and Coauthors, 2010: Investigating soil moisture–climate interactions in a changing climate: A review. *Earth-Science Reviews*, **99,** 125-161.

Sheets, K. R., and J. M. H. Hendrickx, 1995: Noninvasive Soil-Water Content Measurement Using Electromagnetic Induction. *Water Resour Res*, **31,** 2401-2409.

Sheffield, J., and E. F. Wood, 2008: Global trends and variability in soil moisture and drought characteristics, 1950-2000, from observation-driven Simulations of the terrestrial hydrologic cycle. *J Climate*, **21,** 432-458.

Shi, Y. N., K. J. Davis, F. Q. Zhang, C. J. Duffy, and X. Yu, 2014: Parameter estimation of a physically based land surface hydrologic model using the ensemble Kalman filter : A synthetic experiment. *Water Resour Res*, **50,** 706-724.

——, 2015: Parameter estimation of a physically-based land surface hydrologic model using an ensemble Kalman filter: A multivariate real-data experiment. *Adv Water Resour*, **83,** 421-427.

Shrestha, P., M. Sulis, M. Masbou, S. Kollet, and C. Simmer, 2014: A Scale-Consistent Terrestrial Systems Modeling Platform Based on COSMO, CLM, and ParFlow. *Mon Weather Rev*, **142,** 3466-3483.

Shukla, J., and Y. Mintz, 1982: Influence of Land-Surface Evapo-Transpiration on the Earths Climate. *Science*, **215,** 1498-1501.

Shuttleworth, J., R. Rosolem, M. Zreda, and T. Franz, 2013: The COsmic-ray Soil Moisture Interaction Code (COSMIC) for use in data assimilation. *Hydrol Earth Syst Sc*, **17,** 3205-3217.

Siebert, S., P. Doll, J. Hoogeveen, J. M. Faures, K. Frenken, and S. Feick, 2005: Development and validation of the global map of irrigation areas. *Hydrol Earth Syst Sc*, **9,** 535-547.

Simmer, C., and Coauthors, 2015: MONITORING AND MODELING THE TERRESTRIAL SYSTEM FROM PORES TO CATCHMENTS The Transregional Collaborative Research Center on Patterns in the Soil-Vegetation-Atmosphere System. *B Am Meteorol Soc*, **96,** 1765-1787.

Song, X. H., L. S. Shi, M. Ye, J. Z. Yang, and I. M. Navon, 2014: Numerical Comparison of Iterative Ensemble Kalman Filters for Unsaturated Flow Inverse Modeling. *Vadose Zone J*, **13**.

Sun, Y., Z. Hou, M. Huang, F. Tian, and L. R. Leung, 2013: Inverse modeling of hydrologic parameters using surface flux and runoff observations in the Community Land Model. *Hydrol Earth Syst Sc*, **17,** 4995-5011.

Temimi, M., and Coauthors, 2014: Soil Moisture Retrieval Using Ground-Based L-Band Passive Microwave Observations in Northeastern USA. *Vadose Zone J*, **13**.

Topp, G. C., J. L. Davis, and A. P. Annan, 1980: Electromagnetic Determination of Soil-Water Content - Measurements in Coaxial Transmission-Lines. *Water Resour Res*, **16,** 574-582.

Ulaby, F. T., P. C. Dubois, and J. vanZyl, 1996: Radar mapping of surface soil moisture. *J Hydrol*, **184,** 57-84.

Vereecken, H., L. Weihermuller, F. Jonard, and C. Montzka, 2012: Characterization of Crop Canopies and Water Stress Related Phenomena using Microwave Remote Sensing Methods: A Review. *Vadose Zone J*, **11**.

Vereecken, H., J. A. Huisman, H. Bogena, J. Vanderborght, J. A. Vrugt, and J. W. Hopmans, 2008: On the value of soil moisture measurements in vadose zone hydrology: A review. *Water Resour Res*, **44**.

Vereecken, H., and Coauthors, 2014: On the spatio-temporal dynamics of soil moisture at the field scale. *J Hydrol*, **516,** 76-96.

Vereecken, H., and Coauthors, 2016: Modeling Soil Processes: Review, Key Challenges, and New Perspectives. *Vadose Zone J*, **15**.

Verhoest, N. E. C., H. Lievens, W. Wagner, J. Alvarez-Mozos, M. S. Moran, and F. Mattia, 2008: On the soil roughness parameterization problem in soil moisture retrieval of bare surfaces from synthetic aperture radar. *Sensors-Basel*, **8,** 4213-4248.

Villarreyes, C. A. R., G. Baroni, and S. E. Oswald, 2011: Integral quantification of seasonal soil moisture changes in farmland by cosmic-ray neutrons. *Hydrol Earth Syst Sc*, **15,** 3843-3859.

——, 2014: Inverse modelling of cosmic-ray soil moisture for field-scale soil hydraulic parameters. *Eur J Soil Sci*, **65,** 876-886.

Vrugt, J. A., H. V. Gupta, W. Bouten, and S. Sorooshian, 2003: A Shuffled Complex Evolution Metropolis algorithm for optimization and uncertainty assessment of hydrologic model parameters. *Water Resour Res*, **39**.

Vrugt, J. A., C. G. H. Diks, H. V. Gupta, W. Bouten, and J. M. Verstraten, 2005: Improved treatment of uncertainty in hydrologic modeling: Combining the strengths of global optimization and data assimilation. *Water Resour Res*, **41**.

Vrugt, J. A., C. J. F. ter Braak, C. G. H. Diks, B. A. Robinson, J. M. Hyman, and D. Higdon, 2009: Accelerating Markov Chain Monte Carlo Simulation by Differential Evolution with Self-Adaptive Randomized Subspace Sampling. *Int J Nonlin Sci Num*, **10,** 273-290.

Waldhoff, G., 2012: Enhanced land use classification of 2009 for the Rur catchment. TR32DB.

Wen, X. H., and W. H. Chen, 2006: Real-time reservoir model updating using ensemble Kalman Filter with confirming option. *Spe J*, **11,** 431-442.

Whan, K., J. Zscheischler, R. Orth, M. Shongwe, M. Rahimi, E. O. Asare, and S. I. Seneviratne, 2015: Impact of soil moisture on extreme maximum temperatures in Europe. *Weather and Climate Extremes*, **9,** 57-67.

Wigneron, J. P., A. Chanzy, J. C. Calvet, and W. Bruguier, 1995: A Simple Algorithm to Retrieve Soil-Moisture and Vegetation Biomass Using Passive Microwave Measurements over Crop Fields. *Remote Sens Environ*, **51,** 331-341.

Wu, C. C., and S. A. Margulis, 2011: Feasibility of real-time soil state and flux characterization for wastewater reuse using an embedded sensor network data assimilation approach. *J Hydrol*, **399,** 313-325.

——, 2013: Real-Time Soil Moisture and Salinity Profile Estimation Using Assimilation of Embedded Sensor Datastreams. *Vadose Zone J*, **12**.

Yang, Z. L., and Coauthors, 2011: The community Noah land surface model with multiparameterization options (Noah-MP): 2. Evaluation over global river basins. *J Geophys Res-Atmos*, **116**.

Zacharias, S., and Coauthors, 2011: A Network of Terrestrial Environmental Observatories in Germany. *Vadose Zone J*, **10,** 955-973.

Zeng, X. B., and M. Decker, 2009: Improving the Numerical Solution of Soil Moisture-Based Richards Equation for Land Models with a Deep or Shallow Water Table. *J Hydrometeorol*, **10,** 308-319.

Zreda, M., D. Desilets, T. P. A. Ferre, and R. L. Scott, 2008: Measuring soil moisture content non-invasively at intermediate spatial scale using cosmic-ray neutrons. *Geophys Res Lett*, **35**.

Zreda, M., W. J. Shuttleworth, X. Zeng, C. Zweck, D. Desilets, T. Franz, and R. Rosolem, 2012: COSMOS: the COsmic-ray Soil Moisture Observing System (vol 16, pg 4079, 2012). *Hydrol Earth Syst Sc*, **17,** 1065-1066.

Zupanski, D., and M. Zupanski, 2006: Model error estimation employing an ensemble data assimilation approach. *Mon Weather Rev*, **134,** 1337-1354.

Publications in international peer-reviewed journals

Baatz, R., H. R. Bogena, H. J. H. Franssen, J. A. Huisman, C. Montzka, and H. Vereecken (2015), An empirical vegetation correction for soil water content quantification using cosmic ray probes, *Water Resour Res*, *51*(4), 2030-2046.

Baatz, R., H. Bogena, H. J. Hendricks-Franssen, J. A. Huisman, W. Qu, C. Montzka, and H. Vereecken (2014), Calibration of a catchment scale cosmic-ray probe network: A comparison of three parameterization methods, *J Hydrol*.

Baatz, R., Hendricks Franssen, H.-J., Han, X., Hoar, T., Bogena, H. and Vereecken, H. (2016). Evaluating the value of a network of cosmic-ray probes for improving land surface modeling. Hydrol. Earth Syst. Sci. Discuss., doi:10.5194/hess-2016-432.

Bogena, H. R., J. A. Huisman, R. Baatz, H. J. H. Franssen, and H. Vereecken (2013), Accuracy of the cosmic-ray soil water content probe in humid forest ecosystems: The worst case scenario, *Water Resour Res*, *49*(9), 5778-5791.

Borchard, N., M. Schirrmann, C. von Hebel, M. Schmidt, R. Baatz, L. Firbank, H. Vereecken, and M. Herbst (2015), *Spatio-temporal drivers of soil and ecosystem carbon fluxes at field scale in an upland grassland in Germany*, 84-93 pp.

Iwema, J., R. Rosolem, R. Baatz, T. Wagener, and H. R. Bogena (2015), Investigating temporal field sampling strategies for site-specific calibration of three soil moisture-neutron intensity parameterisation methods, *Hydrol Earth Syst Sc*, *19*(7), 3203-3216.

Korres, W., et al. (2015), Spatio-temporal soil moisture patterns - A meta-analysis using plot to catchment scale data, *J Hydrol*, *520*, 326-341.

Acknowledgements

The herein presented research was undertaken from April 2011 to July 2014 in the research group Stochastic Analysis of Terrestrial Systems at the Institute of Bio- and Geosciences Agrosphere (IBG-3), Forschungszentrum Jülich GmbH. The research was support by the SFB-TR32 ‘‘Patterns in Soil–Vegetation–Atmosphere Systems: Monitoring, Modelling and Data Assimilation’’ funded by the Deutsche Forschungsgemeinschaft (DFG).

First, I thank Prof. Dr. Harrie-Jan Hendricks Franssen for his scientific guidance, advice and enthusiastic commitment throughout the process of conducting this research. I am grateful to him for introducing me to the scientific communities of terrestrial modeling and data assimilation. Also I thank him for suggesting the stay at NCAR, Boulder, Colorado, which brought me into contact with great people in a great environment. I thank Prof. Dr. Harry Vereecken for providing a highly professional environment with highly supportive benefits throughout the three years at the IBG-3. I thank Dr. Heye Bogena for his expert advice throughout the PhD project, for encouraging and enabling me to participate in the setup and analysis of several cutting edge environmental monitoring technologies. I thank Prof. Dr. Sascha Oswald and Prof. Dr. Rafael Rosolem for many helpful critics and suggestions to further improve different chapters of this work, and for agreeing to read and review my dissertation.

I gratefully acknowledge and thank

- Tim Hoar for sharing his knowledge, advice and high motivation, for hosting me at NCAR, Boulder, Colorado, and making my stay at NCAR a lasting experience.
- Sander Huisman for his support, advices and helpful suggestions that brought part of this work to completion.
- Xujun Han for working with me on the implementation of the CLM-COSMIC-LETKF framework.
- The cosmic-ray community, Darin Desilets, Marek Zreda, Trenton Franz, Gabriele Baroni and Martin Schrön for many open discussions, suggestions, and critics that enabled and increased the value of this work.
- Daniel Dolfus, Martina Klein, Bernd Schilling, Marius Schmidt, and Ansgar Weuthen for their technical support with CRPs and SoilNet.
- My colleagues and friends at the IBG-3 for their constant encouragement, fruitful discussions and motivation.

I thank my family for their love, encouragement and constant support.

Band / Volume 349
Modellbasierte Ansteuerung räumlich ausgedehnter Aktuator- und Sensornetzwerke in der Strömungsregelung
M. Dück (2016), XIII, 153 pp
ISBN: 978-3-95806-193-4

Band / Volume 350
TRENDS 2015 – Transition to Renewable Energy Devices and Systems
ed. by D. Stolten and R. Peters (2016), 200 pp
ISBN: 978-3-95806-195-8

Band / Volume 351
Dual Phase Oxygen Transport Membrane for Efficient Oxyfuel Combustion
M. Ramasamy (2016), VIII, 136 pp
ISBN: 978-3-95806-196-5

Band / Volume 352
Transport, co-transport, and retention of functionalized multi-walled carbon nanotubes in porous media
M. Zhang (2016), VII, 112 pp
ISBN: 978-3-95806-198-9

Band / Volume 353
Untersuchungen zur Luftqualität in Bad Homburg
C. Ehlers, D. Klemp, C. Kofahl, H. Fröhlich, M. Möllmann-Coers und A. Wahner (2016), IV, 93 pp
ISBN: 978-3-95806-199-6

Band / Volume 354
Herstellung thermisch gespritzter Schichten mit optimierten Spannungseigenschaften
M. Mutter (2016), VI, 142, VII-XXII, xxvi pp
ISBN: 978-3-95806-200-9

Band / Volume 355
Entwicklung selbstheilender Wärmedämmschichten
D. Koch (2016), X, 120 pp
ISBN: 978-3-95806-201-6

Band / Volume 356
Betriebsstrategien für Brenngaserzeugungssysteme zur Anwendung in HT-PEFC-Hilfsstromaggregaten
D. Krekel (2017), IX, 265 pp
ISBN: 978-3-95806-203-0

Band / Volume 357
Korrosion metallischer Bipolarplatten in Hochtemperatur-Polymerelektrolyt-Brennstoffzellen
V. Weißbecker (2017), viii, 194 pp
ISBN: 978-3-95806-205-4

Band / Volume 358
Realistic Bandwidth Estimation in the Theoretically Predicted Radionuclide Inventory of PWR-UO2 Spent Fuel Derived from Reactor Design and Operating Data
I. Fast (2017), XI, 129 pp
ISBN: 978-3-95806-206-1

Band / Volume 359
Light Trapping by Light Treatment – Direct Laser Interference Patterning For the Texturing of Front Contacts in Thin-Film Silicon Solar Cells
T. Dyck (2017), vi, 172, XI pp
ISBN: 978-3-95806-208-5

Band / Volume 360
Interface and Topography Optimization for Thin-Film Silicon Solar Cells with Doped Microcrystalline Silicon Oxide Layers
C. Zhang (2017), VII, 156 pp
ISBN: 978-3-95806-209-2

Band / Volume 361
Calibration and large-scale inversion of multi-conguration electromagnetic induction data for vadose zone characterization
C. von Hebel (2017), ix, 123 pp
ISBN: 978-3-95806-210-8

Band / Volume 362
Process-based modelling of regional water and energy fluxes taking into account measured neutron intensities by cosmic-ray probes
R. Baatz (2017), xvi, 135 pp
ISBN: 978-3-95806-211-5

Energie & Umwelt /
Energy & Environment
Band / Volume 362
ISBN 978-3-95806-211-5